Genetic and functional analyses of the developing asymmetric zebrafish habenula.

Renato Gomes Da Silva Martinho

University College London

Department of Cell and Developmental Biology

PhD Supervisors:

Professor Stephen Wilson, Dr Isaac Bianco, Dr Ana Faro

A thesis submitted for the degree of

Doctor of Philosophy

February 2019

DECLARATION

I, Renato Gomes da Silva Martinho, confirm that the work presented in this thesis is my own. Where information has been derived from other sources, I confirm that this has been indicated in the thesis.

Abstract

The vertebrate brain develops anatomical and functional left-right asymmetries in localised regions, without affecting the laterality of the surrounding structures. To understand how brain laterality develops, we studied the development of robust habenular asymmetries in larval zebrafish. The left and right dorsal habenulae (dHb) have different sizes, asymmetric patterns of gene expression and establish distinct afferent and efferent connections. Although we are beginning to understand the molecular pathways that establish these asymmetries, the pathways underlying formation of the habenular progenitors remains largely elusive. Also, despite several habenular gene expression patterns being broadly asymmetric, there are no habenular markers for smaller habenular neuronal subpopulations in 4 dpf zebrafish. Lastly, we still need to investigate the importance of habenular asymmetry for its correct function and normal behaviour. This thesis aims to tackle these three gaps in habenular asymmetry research.

To do so, we first characterised the *A66*^{u757} mutant, which develops a smaller and symmetric habenula. The causative mutation is in the *rerea* gene, which encodes a co-regulator of nuclear receptors that modulates the expression of *fgf8*. In line with this, the pattern of *fgf8* expression is expanded in the diencephalon of mutants, and the parapineal is malformed, as observed in other FGF signalling mutants. Lastly, we show that the habenular phenotype of these mutants is concomitant with a delay in the formation of habenular progenitors.

Second, to understand which neuronal subpopulations compose the zebrafish habenula at 4 dpf, we developed a protocol to obtain habenular single cells for RNA sequencing. Cells collected from the left and right nuclei still express habenular genes in an asymmetric fashion. However, to increase the number of collected cells, we harvested GFP-positive cells from a transgenic line that expresses GFP in the dHb and in the olfactory organ. Consequently, we sequenced 586 cells, which were separated into dHb, ventral habenula and olfactory organ clusters. However, due to the relatively small number of sequenced cells, we did not manage to discriminate subpopulations of the dHb. We propose optimisation steps that will allow us to finish this work.

Lastly, to study the role of habenular asymmetry in behaviour, we tested two habenular mutants in an operant learning paradigm, through the ROAST

assay. We show that wild-type and left-isomerised dHb mutant larvae learn to terminate an aversive stimulus by changing the direction of a stereotypical aversive-heat-response. Despite not finding differences between these mutants and wild-types, we did not exclude the role of the habenula in this assay and propose future research to further test this function.

Impact Statement

In this work, I present new information about the formation of habenular progenitors. Understanding this step of habenular development will be important for understanding how a seemingly symmetric region of the brain is able to interpret the environmental molecular signals to become asymmetric. Moreover, it may elucidate the developmental steps that are hindered in certain human diseases, such as Autism, where brain asymmetry is altered (Herbert *et al.*, 2004; Wittling *et al.*, 2009; Carper *et al.*, 2016). Also, studying the function of the Rerea/Atrophin2 protein, which is truncated in a habenular mutant used in our study, may have an impact in understanding symptoms of Dentatorubral–pallidoluysian atrophy disease. This disease is caused by an expansion of a CAG trinucleotide repeat encoding polyglutamine in the Atrophin1 protein, which increases its affinity to Rerea and affecting its normal function (Yanagisawa *et al.*, 2000). Therefore, understanding the impact of the *rerea* mutation on the development of the brain and of its laterality, may help us understand the mechanisms that are affected in this disease.

I also describe development of a protocol that will help us characterise the neuronal subpopulations of the habenula of 4 dpf zebrafish. The final aim of this work will be to build a map of genetic markers that define the subpopulations of the habenula of zebrafish. This will create a database where researchers will be able to identify genes that are expressed in the habenula at 4 dpf and, consequently, mutations that may affect the development of this structure. Furthermore, we will be able to provide a comprehensive identification of the habenular populations that are missing in several mutants in comparison to wild-types. This will ultimately help understand behavioural phenotypes caused by the absence of specific habenular subpopulations.

Lastly, I describe the establishment of a high-throughput behavioural task that tests the capacity of larvae zebrafish to modulate their behaviour in response to an aversive heat-stimuli. This assay will allow us to assess if habenular asymmetry has a role in this behaviour. If it does, we will be able to include this assay in a pipeline for molecular, anatomical and functional characterisation of habenular asymmetry mutants. This will be an important way of quickly assessing the differences between brain asymmetry, and other central nervous system mutants, carrying mutations that may be linked to neurological syndromes and diseases in humans.

Acknowledgements

This work is the result of the efforts of many, many people. I may have had a big role in it, it is my PhD after all, but none of this would have happened without my family's belief in who I would become, my supervisors' scientific vision, or my friends' wisdom, both in and outside the lab. For that I am eternally grateful!

In chronological order, I have to thank GABBA, the Portuguese PhD programme that opened the doors to where I completed my thesis. Thanks to them I got the PhD grant from the Fundação para a Ciência e a Tecnologia, which funded my six months in Porto and, later, a major part of my stay in UCL, London, where I developed this thesis at.

Thank you, Steve, for seeing in me the potential of becoming your PhD student. Thank you for giving me the opportunity of working with such wonderful people that make yours, and the First Floor Fish groups, the best I could ever want to be part of. I also have to thank Elena, for presenting me to the world of behaviour studies in zebrafish and for giving me the starting tools of this work. And thank you, Isaac, for the scientific discussions and for having me in your lab meetings. I truly believe that I have grown a lot thanks to them and that without your input I would have been indefinitely stuck in the many traps of zebrafish behaviour.

I also want to acknowledge everyone from the fish facility with special thanks to Heather who always had an incredible patience for my short memory! And, right next to them, the guys-from-stores, Michael, Onyi and Emeka, who always have a smile and a joke ready for anyone who needs a bit of joy! To Debbie a very special thank you for managing PhD bureaucracy! From outside our department, to Ayad who thought me everything I know about FAC-sorting. I also want to thank Steven Harvey, who kickstarted me in the single-cell sequencing field, and was our collaborator for the DeTCT method, and to Tatjana Sauka-Spengler who was our collaborator for the 10x Genomics approach.

Lastly (kind off, not really), THANK YOU to everyone from the first floor. More than colleagues and bosses you were and will forever be my scientific family, the ones who are responsible for a big part of my success! I will never forget the little and the big things that you have done for me. Sabine for grabbing me to join the group lunches (since day one!); Jason for the logic problem discussions; Anya for all the funny comments (eeeeeh!) and for our moments as PhD reps; Declan for one of the best laughs anyone can bring out of me; Anukampa for saving me from my archnemesis: bureaucracy; Pedro for his lovely bacalhau à brás; Eirinn for the immense help with the sequencing data (and the parties… yes, and the board games!); Sumi for her incredible sympathy; Gaia for her fights for our rights; Gareth for his unexpected jokes; Claudia for always visiting us; Kate

for her beautiful images; Tom for the most amazing unknown facts (I swear he knows things that people are still going to invent. Probably Declan will invent them); Lisa for the birthday parties I never missed apart from this year ☹; Asaph for his hidden knowledge; Paride for his sudden football moves (auff!); Kasia for her support of our PhD rep work!; Barbara for always checking in on how I am; Masa for always arriving in the lab before me when I try to arrive early (thank you for the company); Diz for knowing everything without giving anything away (zebrafish neuron cell culture was a thing before anyone knew zebrafish neuron cell culture was a thing); Chintan for his great behavioural research insights (thank you SO MUCH for helping me with the corrections); Hannah who amazingly always has time to help in the lab; Hande for getting done what has to be done; and, finally, to Vanessa to whom I owe a big THANK YOU for the fundamental help you gave me while establishing the 10x Genomics approach in Tatjana's lab, and now for being this huge source of knowledge and friendliness! (I hope I didn't forget anyone… I really tried not to… oh dear… I will remember someone important after I print this, won't I?).

During my time in the lab I also had the pleasure of supervising the work of three incredible students, Benjamin, Olaf and Aysha. I hope you have learned with me as much as I have learned from you. Thank you for your curiosity and your hard work.

I had to save one paragraph for five very special women that made my life in the lab, and out of it, so much better and funnier. First, MK, the bearer of my child, you make my days so much better! Please don't ever stop being like you are! Then, Ingrid who taught me to live Life at its best, whilst keeping everything at a perspective. I still cannot believe you left, I miss you A LOT! (buying flight tickets now…). Shannaynayyyy, you are the representation of strength and perseverance! I am ever so glad for knowing you and I'm counting the seconds for our celebratory dinner… not for my thesis, but for when you create the most successful research institute in the world! I'll be waiting for the invite, thank you! And Joanna, you are one of the most special people I have met during my time in the lab. It is incredibly amazing the moments we shared! I could have never wished for a better friend than you, so thank you for being my friend and for being there when I most needed! And lastly, but never the least (none of them are), Ana, who became a sudden supervisor, and a very close friend! Thank you for all your help, in the lab, in my thesis, for correcting the silliest mistakes, but mostly for reminding me how much I love teaching and how much I want to become a teacher. I am ever so grateful to you and for the friendship we built! I hope you already know that.

Then, the surprise of my life: Yaz. You have come up out of nowhere, and now can't even imagine a life without you. I am really happy that serendipity has brought us

together. I cannot thank you enough for being there for me every step of the way of this thesis and for whatever comes next! You make me happy!

And finally, I saved the last lines for my family. The London family, today and forever my kids, Ruth and Nico. Thank you for being part of the best, funniest, wildest, *incrediblest* moments of my life! For you I have only four words: TOYST! Cookie, cookie, cookie! And, of course, my Portuguese family and friends. In the end of the day, all of this is for you, as you are responsible for making the pillars that support who I am today. You all know how much I love you, since we decided a long time ago to make it clear every single day (no regrets). I am happy to have grown around you. If there is any luck in the world, then I could not be luckier!

CONTENTS

TABLE OF FIGURES

LIST OF TABLES

ABREVIATIONS

AreaX	crossing of medial and lateral habenula neurons (mouse)
acTub	acetylated tubulin
CO2	carbon dioxide
DeTCT	Differential Expression Transcript Counting Technique
dHb	dorsal Habenula
dHbL	lateral subdomain of the dorsal habenula (zebrafish)
dHbM	medial subdomain of the dorsal habenula (zebrafish)
dIPN	dorsal Interpeduncular Nucleus (zebrafish)
dpf	days post fertilization
EmT	*Eminentia Thalami*
FAC-sorting	Fluorescence-Activated Cell Sorting
FEC	facial ectoderm
FGF	Fibroblast Growth Factor
fMRI	functional Magnetic Resonance Imaging
GFP	Green Fluorescent Protein
hpf	hours post fertilization
iIPN	intermediate Interpeduncular Nucleus (zebrafish)
ImnSys	Immune System (cluster)
IPN	Interpeduncular Nucleus
LPM	lateral plate mesoderm
MHB	mid-hindbrain boundary
MHbCd	dorsal-central subdomain of the medial habenula (rat)
MHbCv	central-ventral subdomain of the medial habenula (rat)
MHbD	dorsal domain of the medial habenula (mouse)
MHbI	inferior subdomain of the medial habenula (rat)

MHbIf	intermediate field of the medial habenula (mouse)
MHbS	superior subdomain of the medial habenula (rat/mouse)
MHbVc	central-ventral subdomain of the medial habenula (mouse)
MHbVL	lateral-ventral subdomain of the medial habenula (rat)
MHbVl	lateral-ventral subdomain of the medial habenula (mouse)
MHbVm	medial-ventral subdomain of the medial habenula (mouse)
NR	nuclear receptor
OB	olfactory bulbs
OO	Olfactory Organ (cluster)
P	pineal
pp	parapineal
qPCR	qPCR
RA	retinoic acid
ROAST	Relief Of Aversive Stimulus by Turn
scRNA-seq	single cell RNA sequencing
SktDev	Skeleton Development (cluster)
SMART-Seq2	Switching Mechanism at 5’ End of RNA Template Sequencing 2
SV2	synaptic vesicle glycoprotein 2
TRP	transient receptor potential channels
vENT	ventral entopeduncular nucleus
vHb	ventral Habenula (zebrafish)
vIPN	ventral Interpeduncular Nucleus (zebrafish)
VTA	Ventral Tegmental Area

CHAPTER 1.

INTRODUCTION

The vertebrate brain is mostly symmetric between the left and right hemispheres. However, it is now known that not all functions that develop in one hemisphere have a contralateral counterpart. To understand how these asymmetries develop, scientific research has focused on the development of the habenula of zebrafish (*Danio rerio)*. The habenulae, together with the pineal and parapineal, comprise a structure called the epithalamus. Within this complex, both the habenula and the parapineal develop conspicuous asymmetries, already evident in embryonic and larval stages. Along with increased genetic versatility and the quick reproduction rate of zebrafish, this species has become an ideal model organism to study brain asymmetry development.

In this chapter, we will review the recent findings made to elucidate the mechanisms involved in establishing habenular asymmetry. In addition to this, we will describe the neuronal structure and function of the habenula, in order to further unravel how asymmetry plays a role in behaviour.

1.1. Human brain asymmetries

Brain asymmetry is thought to have evolved to specialise one hemisphere to perform certain functions, while the other hemisphere carries out others (Vallortigara and Rogers, 2005). The interest in brain asymmetries dates to 1860, when Paul Broca described a patient with acquired aphasia (the inability to produce or understand spoken words) due to a lesion on the left temporal lobe (Dronkers *et al.*, 2007). Broca's area, as it was coined, was seen as responsible for semantic processing, while its contralateral domain is related with the interpretation of the tone and inflections of spoken words (Sacks, 1986; Flinker *et al.*, 2015).

Although the true mechanism establishing this asymmetry remains elusive, further discoveries of human brain laterality were made serendipitously. In the 1940s, Dr. William P. van Wagenen pioneered corpus callosotomies of patients in order to stop otherwise untreatable epilepsy (Mathews, Linskey and Binder, 2008; Wolman, 2012) . By severing these white matter tracts, an aberrant signal originating in one hemisphere was prevented from potentiating and spreading to the contralateral one and, thus, from causing seizures. However, subsequent studies identified that these patients, though cognitively and emotionally intact, exhibited other irregular behavioural traits (Andersen *et al.*, 1996). For example, in the seminal studies performed by Sperry, when images were only shown to the left visual field of these patients, they exhibited a reduced ability to verbally describe what they saw (Sperry, 1968). Today, functional magnetic resonance imaging has consolidated these findings by identifying the brain regions responsible for language processing and production in the left hemisphere, and the face recognition and visuospatial processing to be right dominant functions (Frost *et al.*, 1999; Schuster *et al.*, 2017).

Further studies investigating the same phenomenon identified that, nevertheless, left-handed patients were able to draw the image that was presented to their left eye (Baynes *et al.*, 1998). This was reminiscent of another well-known example of brain asymmetry which is reflected in lateralised hand preference. The vast majority of humans have a dominant hand for fine motor movements which, in about 90% of the population, is the right one (Raymond *et al.*, 1996). Neuroimaging studies revealed a correlation between handedness and asymmetric white matter connections, particularly in the dorsal branch of the superior longitudinal fasciculus, an area responsible for visuospatial integration and motor planning (Gutwinski *et al.*, 2011; Howells *et al.*, 2018). Furthermore, the language-related temporal cortex (where Broca's and Wernicke's[1] areas are located) is

[1] The Wernicke's area plays a role in supporting language comprehension and speech production (Binder, 2015). Like the Broca's area, it is predominantly found in the left hemisphere of right-handed individuals.

morphologically more lateralised in right-handed than left-handed individuals (Steinmetz *et al.*, 1991; Catani *et al.*, 2007).

Despite the current ease by which human brain functions can be assessed and morphological brain asymmetries can be described, understanding how these develop on a molecular and at a neuronal circuit level has proven a challenge. Therefore, researchers have turned their attention towards the study of brain regions that exhibit overt asymmetries in animal models. In this field, within vertebrates, the focus of research has been on the most conserved and conspicuously asymmetric brain structure: the habenula (Concha and Wilson, 2001).

1.2. The habenula

The habenula is a well conserved brain structure, present in the epithalamus of virtually all vertebrates (Concha and Wilson, 2001; Stephenson-Jones *et al.*, 2012). Mammalian habenula studies focus mainly on its function due to its role in linking the limbic forebrain to the monoaminergic centres in the midbrain and hindbrain (Bianco and Wilson, 2009). For instance, functional magnetic resonance imaging (fMRI) studies of the human habenula revealed that, when active, it inhibits the reward pathway (Ullsperger and von Cramon, 2003). The habenula has also been shown to activate during noxious electric or thermal stimuli, and also before the stimuli are given, when the patient has cues anticipating it (Furman and Gotlib, 2016; Liu *et al.*, 2017). Moreover, the same is observed in non-human primate and rodent studies, and the direct activation of the mouse habenula elicits aversion-like responses (Matsumoto and Hikosaka, 2007; Lammel *et al.*, 2012; Stephenson-Jones *et al.*, 2016).

The general morphology of the habenula in mammals consists of a lateral and a medial domain, one on each side of the brain (Andres, von Düring and Veh, 1999). However, despite humans having a bigger lateral domain on the left side of the brain, the habenula does not show overt structural asymmetries in the majority of mammals, (Ahumada-Galleguillos, Lemus, D??az, *et al.*, 2017). In lower vertebrates, however, habenular asymmetries are more conspicuous, with one of such examples being found in the zebrafish (Concha and Wilson, 2001). Like mammals, the habenula in zebrafish consists of two nuclei (Amo *et al.*, 2010). However, these are classically identified as dorsal and ventral habenulae (dHb and vHb), which are homologs of the mammal's medial and lateral habenula, respectively (Amo *et al.*, 2010).

Contrary to what is observed in the human lateral habenula, it is the dHb of zebrafish that shows the most clear asymmetries (Figure 1.1.A and 1.1.B) (Concha *et al.*, 2000; Gamse *et al.*, 2005). Morphologically, the left dHb is bigger and has more elaborated

neuropils than the right (Concha *et al.*, 2000; Colombo *et al.*, 2013). In addition to this, specific genes display asymmetric ratios of expression within the dHb nuclei, such as the *potassium channel tetramerisation domain containing 12.1* (*kctd12.1)* and *12.2 (kctd12.2)*, which led to the subdivision of the dorsal habenula domain into lateral (dHbL) and medial (dHbM) subdomains, respectively (Gamse *et al.*, 2005). Following the differential expression of these specific genetic markers, the dHbL and dHbM subdomains are asymmetrically distributed between the left and the right epithalamus: the dHbL is bigger on the left nucleus, while the dHbM is bigger on the right.

Further asymmetries can be seen in the afferent and efferent projections of the dHb (Figures 1.1.A, 1.1.A'' and 1.1.B). For instance, dHbL neurons, mostly enriched in the left side, project to the dorsal and intermediate interpeduncular nucleus (dIPN and iIPN, respectively), while dHbM neurons, enriched in the right, project to the ventral IPN (vIPN) (Aizawa *et al.*, 2005; Bianco *et al.*, 2008). Also, the mitral cells of the olfactory bulbs project to the right dHbL, while the parapineal (a leftwards positioned structure of the epithalamus) and the *Eminentia thalami* (EmT) project to the left dHb (Concha *et al.*, 2000; Gamse, 2003; deCarvalho *et al.*, 2013; Turner *et al.*, 2016; Zhang *et al.*, 2017). Concordantly, these asymmetric projections reflect in the dHb neuronal activity: light stimuli activates more neurons of the left dHb, whereas the right nucleus shows more activation upon olfactory stimuli (Dreosti *et al.*, 2014).

The optical transparency, ease of genetic manipulation and robust habenular asymmetries makes the zebrafish the ideal model organism to study the molecular pathways involved in the development of brain laterality. The following sections will discuss how these asymmetries are believed to develop, which molecular pathways are involved, and the importance of these asymmetries for the correct function of the habenula.

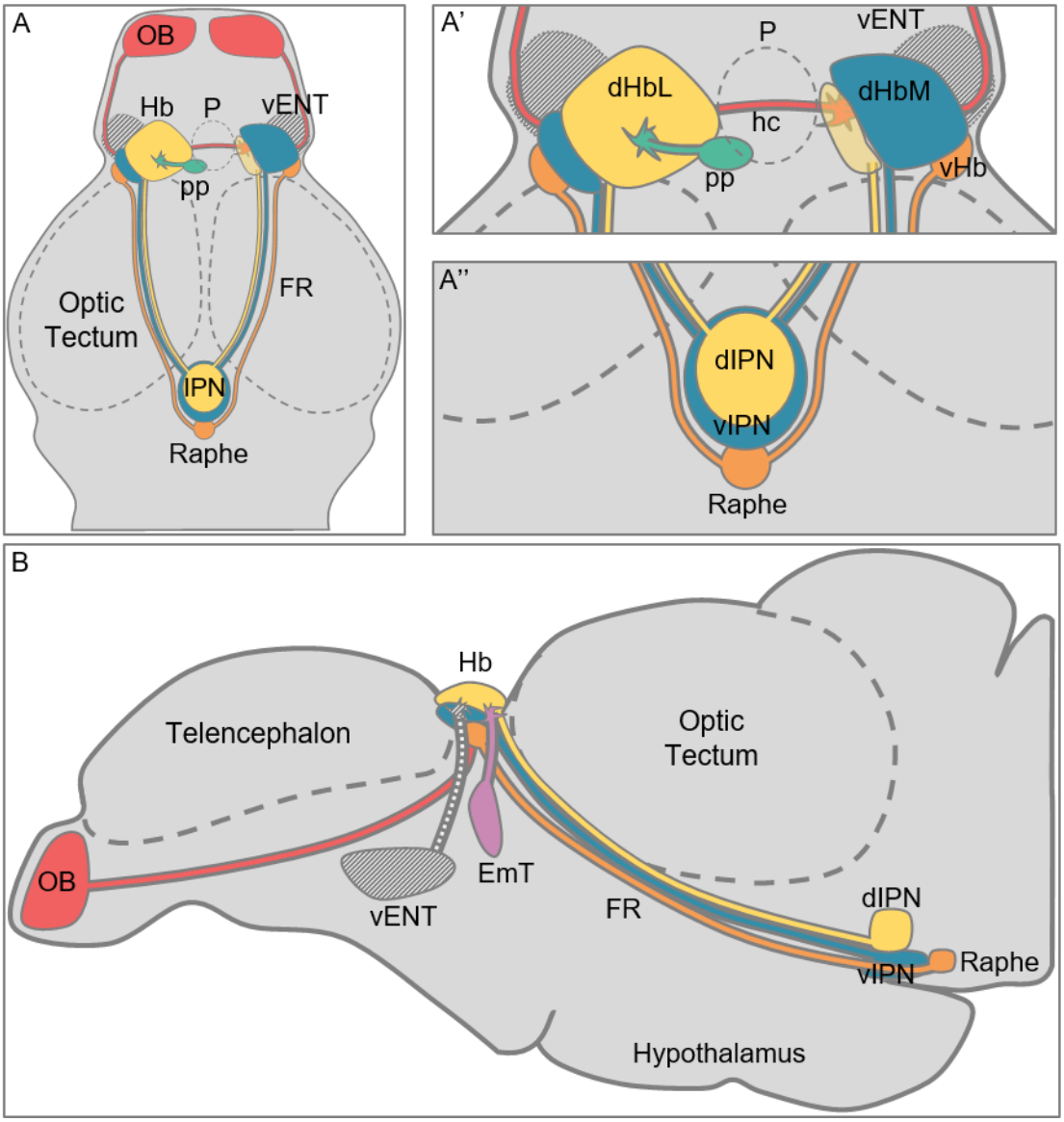

Figure 1.1 Habenula Circuitry of Danio rerio. (A) Schematic representation of the dorsal view of the brain of a 4 dpf wild-type zebrafish larva. **(A')** Schematic detail of the dorsal view of the epithalamus of a 4 dpf wild-type zebrafish larva. **(A'')** Schematic detail of the dorsal view of the midbrain IPN and Raphe of a 4 dpf wild-type zebrafish larva. **(B)** Schematic representation of the lateral view of the brain of a 4 dpf wild-type zebrafish larva. **Description:** The habenula (Hb) consists of two nuclei, one in each side of the brain. Each nucleus consists of three different domains: the symmetric ventral habenula (vHb, orange), the lateral dorsal habenula (dHbL, yellow), which is bigger in the left nuclei, and the medial dorsal habenula (dHbM, blue) that is bigger in the right. dHbL neurons project to the dorsal interpeduncular nucleus (dIPN, yellow), the dHbM projects to the ventral IPN (vIPN, blue), and the vHb projects to the Raphe nuclei (Raphe, orange). All habenular axons reach the midbrain targets through the Fasciculus Retroflexus (FR). Between both habenular nuclei is the pineal (P, dotted line) and the parapineal (pp, green). The parapineal is ventroposterior to the pineal and slightly

towards the left side, and only projects to the left dHbL. The ventral Entopeduncular Nucleus (vENT, stripped) is ventrally positioned to the habenula, and to the *Eminentia Thalami* (EmT, purple in B). Although not depicted, the vENT projects to both nuclei but the EmT only projects to the left dHb. The mitral cells of the olfactory bulbs (OB, red) only project to the right dHbL. The projections of the left OB reach the habenula through the habenular commissure (hc).

1.3. The development of the zebrafish dorsal habenula

The development of the zebrafish dHb starts in the diencephalon at 24 hours post fertilisation (hpf) from a seemingly symmetric pool of habenular progenitors (Dean *et al.*, 2014). However, the dHb subsequently starts developing asymmetrically as two neurogenic waves, the first at 32 hpf and the second at 48 hpf, respectively promote differential neurogenesis in the left and right habenular progenitors (Aizawa *et al.*, 2007). These neurogenic waves are thought to integrate with molecular signals from the left-migrating parapineal in order to form a fully asymmetric dHb, since the parapineal migration is required for the specification of more dHbL in the left nucleus than the right (Concha *et al.*, 2003; Gamse, 2003; Hüsken *et al.*, 2014). Once its molecular asymmetries are defined, the dHb continues its development by establishing anatomical asymmetries at the level of dendritic and axonal elaboration (Bianco *et al.*, 2008; Colombo *et al.*, 2013). This section aims to discuss the research carried out to unravel the aforementioned molecular mechanisms that lead to the formation of an asymmetric dHb in zebrafish.

1.3.1. The formation of dHb progenitors.

The first sign that the dHb is being formed happens at 24 hpf, when the expression of *developing brain homeobox 1b* (*dbx1b)* marks the formation of the habenular progenitors (Figure 1.2) (Dean *et al.*, 2014). The *dbx1b*-positive cells consist of a pool of proliferative cells from which dHb committed neurons will be formed (Dean *et al.*, 2014). As will be discussed in a later section of this chapter, the timely fine-tuning of the ratio of habenular progenitors that keep proliferating to those starting neurogenesis is very important for the establishment of asymmetries (Aizawa *et al.*, 2007). Thus, delaying or accelerating neurogenesis will affect this ratio and form an aberrant habenula (Itoh *et al.*, 2003; Aizawa *et al.*, 2007; Doll *et al.*, 2011).

The differentiation of the habenular progenitors into dHb neurons occurs in a lateromedial direction (Figure 1.2.A[1] to 1.2.A[5]) (Dean *et al.*, 2014; Roberson and Halpern, 2017a). During early development, the expression of *dbx1b* is ventromedially positioned, while the differentiated, *ELAV like neuron-specific RNA binding protein 3* (*elavl3*)

expressing neurons occupy the most dorsolateral domain (Figure 1.2.A[4] and 1.2.A[5]) (Roberson and Halpern, 2017a). Between these two subgroups, there are all the cells that are transitioning from the habenular progenitor stage to fully differentiated dHb neurons, which express the *chemokine (C-X-C motif), receptor 4b* gene (*cxcr4b)* in combination with either *dbx1b* or *elavl3* (Roussigné *et al.*, 2009; Dean *et al.*, 2014; Roberson and Halpern, 2017a). From this, a molecular pattern is established where one can map the different cell populations depending on what biomarkers are expressed, from the medioventral habenular progenitor cells to the dorsolateral dHb neurons.

The misspecification of the habenular progenitors has direct consequences on the formation of the dHb, but the consequences are not always straightforward. In the *Wnt ligand secretion mediator (wls)* mutants, the WNT pathway is downregulated and this delays the formation of *dbx1b* cells specifically in the epithalamus up to 27 hpf (Figures 1.2.C[1] to 1.2.C[5]) (Kuan *et al.*, 2015). The consequence is an extremely reduced dHb which, nevertheless, maintains its asymmetries. This contrasts with other Wnt pathway mutants in which asymmetry is disrupted (see below).

The Fibroblast Growth Factor (FGF) pathway also affects the specification of the habenular progenitor cells. Mutants for *fibroblast growth factor 8* (*fgf8)* do not express *dbx1b* in the dorsal diencephalon at 24 or 28 hpf (Figures 1.2B[1] to 1.2.B[2]) (Dean *et al.*, 2014). Although its expression was not shown to increase in later timepoints, the formation of a small pair of dHb nuclei allows the speculation that the habenular progenitors are formed (Regan *et al.*, 2009). Interestingly, drug inactivation of FGF signalling between 28 and 56 hpf abolishes the expression of *dbx1b.* Nevertheless, its expression in the dorsal diencephalon is recovered 12 hours after removing FGF signalling inactivators (Dean, Gamse and Wu, 2018). This suggests that FGF activity is required for the onset and maintenance of the *dbx1b*-positive habenular progenitors, throughout habenular development (Dean, Gamse and Wu, 2018). Unfortunately, there are no studies of *fgf8* inactivation in later stages of development, to understand if it would still affect the *dbx1b*-positive habenular progenitors that still exists until 30 dpf (Roberson and Halpern, 2017a).

One of the most puzzling examples of a mutant with no expression of *dbx1b* is the *mediator complex subunit 12* (*med12)* mutant (Wu *et al.*, 2014). In *med12* mutants, *dbx1b* is absent in the habenula up to 2 dpf. However, this leads to the formation of two habenula-like clusters of cells that do not express any habenular markers (Wu *et al.*, 2014). There has been no full explanation for this phenotype other than the possibility of Med12 mediating the timely expression of *dbx1b* and this mechanism failing in the mutant (Wu *et al.*, 2014). However, such a late formation of pHb could delay the start of neurogenesis until after the second neurogenic wave and lead to the formation of

neurons with character distinct to those formed in the first two neurogenic waves. To further understand this phenomenon and thus, how the Hb develops in zebrafish, the molecular signals involved during these instances of neurogenesis in the dHb need to be investigated.

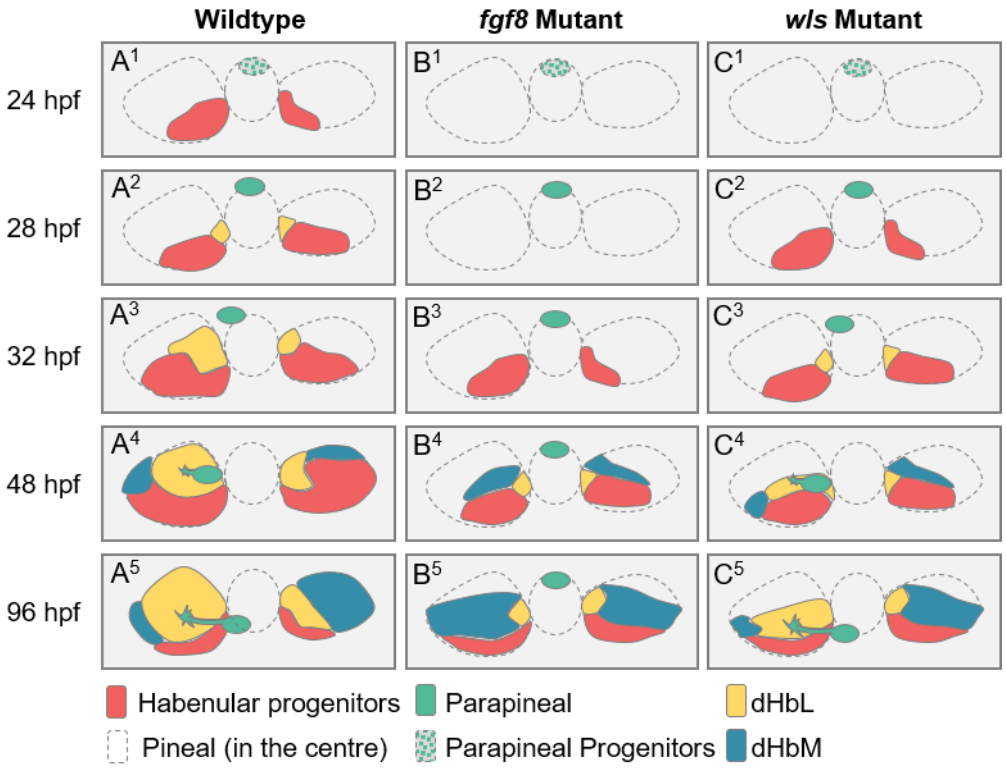

Figure 1.2 Habenula development in wild-type, *fgf8* mutant and *wls* mutant larvae. (A^1 to A^5) Schematic representation of the dorsal view of the epithalamus of a wild-type zebrafish between 24 and 96 hpf. (A^1) In wild-type zebrafish, the expression of *dbx1b* starts at 24 hpf and defines the habenular progenitor cell pool (red). At this point, the parapineal is not differentiated (grey with green dots, parapineal progenitors) but cells at the most anterior domain of the pineal complex (dotted line) constitute the parapineal anlage. (A^2) At 28 hpf the habenular progenitor pool has expanded, and a few medial cells start neurogenesis in what will become dHbL neurons (yellow). At this point, the parapineal primordium (green) starts delaminating from the pineal complex. (A^3) At 32 hpf more habenular progenitor cells enter neurogenesis and commit to become dHbL neurons and the parapineal has started migrating toward the left side. (A^4) At 48 hpf there is a larger dHbL domain in the left habenula than in the right. The majority of cells that start neurogenesis at this point will become dHbM neurons (blue). The parapineal organ has migrated to the left and starts elaborating axonal projections to the left dHbL. (A^5) By 96 hpf, overt habenular asymmetries are established. Most cells in both nuclei have differentiated into dHb neurons, but there still is a pool of habenular progenitors in the ventromedial domain of the habenula. The parapineal is ventral and posterior to the

pineal and only projects to the left dHbL. **(B[1] to B[5])** Schematic representation of the dorsal view of the epithalamus of a mutant zebrafish with abolished FGF signalling activity between 24 and 96 hpf. (B[1] to B[3]) In *fgf8* mutants there is no expression of *dbx1b* at least until 28 hpf. The parapineal progenitors are committed to become parapineal cells but fail to delaminate and migrate to the left side. (note: expression of *dbx1b* was not shown in the fgf8 mutant at 32 hpf. However, it is represented here as a hypothesis based on the fact of a dHb structure being formed at later timepoints in this mutant background). (B[4] and B[5]) The delay in the formation of an habenular progenitor pool drives the formation of small habenulae. Furthermore, since *fgf8* mutation results in an impaired parapineal migration, the left dHb develops with a right dHb character. **(C[1] to C[5])** Schematic of the dorsal view of the epithalamus of a mutant zebrafish with abolished WNT signalling activity between 24 and 96 hpf. (C[1] to C[3]) In *wls* mutants the expression of *dbx1b* is delayed until 27 hpf, but the parapineal is correctly specified and migrates to the left side. Despite the delay in the formation of habenular progenitors, neurogenesis starts at 32 hpf. (C[4] and C[5]) The delay in the formation of habenular progenitors results in the formation of small habenular nuclei. However, since the parapineal still migrates to the left side, left-right asymmetries are still present in the habenula of this mutant.

1.3.2. The dHb neurogenic waves.

After the habenular progenitor cell pool is specified, neurogenesis is quickly biased towards the left side, and by 32 hpf more cells have started neurogenesis on the left than on the right nucleus (Aizawa *et al.*, 2007; Roussigné *et al.*, 2009). This is called the first wave of habenular neurogenesis and its asymmetry is imposed by the leftwards activation of nodal (Roussigné *et al.*, 2009). Then, at 48 hpf, the second wave of neurogenesis peaks, when the number of neurogenic cells in the right nucleus increases to numbers closer to those found in the left nucleus (Aizawa *et al.*, 2007). After these two neurogenic waves, neurogenesis reduces and becomes symmetric, but does continue (Aizawa *et al.*, 2007).

The importance of these two neurogenic waves is that cells that differentiate during the first wave mostly express *kctd12.1* at 4 dpf and, therefore, develop a dHbL character (Aizawa *et al.*, 2007). Conversely, more neurons resulting from the second wave express *kctd12.2* (medial dHb). After the second neurogenic wave, there is a trend for most cells to become of the dHbM type on both sides. Therefore, due to these neurogenic waves, the left habenula consists of more dHbL neurons, while the right habenula consists of more dHbM neurons.

Although the factors that drive differentiation in each wave are still unknown, alterations in the timing of neurogenesis has a direct impact on habenular asymmetry (Aizawa *et al.*, 2007; Dean, Gamse and Wu, 2018). Defective Notch signalling results in excessive early neurogenesis, which drives the depletion of the habenular progenitor pool, and the formation of a left-isomerized dHb (Itoh *et al.*, 2003; Aizawa *et al.*, 2007). Further validating this concept, the mutation of the *sec61 translocon alpha 1 subunit* (*sec61a1)* also causes the habenular progenitors to start neurogenesis earlier and the development of a left-isomerized dHb (Doll *et al.*, 2011). However, alterations that cause hyperactivation of Notch lead to a delay in habenular neurogenesis. This will ultimately results in the formation of right-isomerized dHb (Aizawa *et al.*, 2007).

Nodal related genes, such as *nodal-related 2* (*ndr2*, former *cyclops*), *lefty1* and *paired like homeodomain transcription factor 2* (*pitx2*), are expressed in the left side of the developing epithalamus of zebrafish from as early as 18 hpf (Michael R. Rebagliati *et al.*, 1998; Concha *et al.*, 2000). The lateralised expression of these Nodal related genes drives habenular asymmetric neurogenesis via an FGF-dependent way (Roussigné *et al.*, 2009). Without asymmetric expression of nodal related genes*, fgf8* is expressed symmetrically in the habenular progenitors, rather than being more expressed on the right side (Dean, Gamse and Wu, 2018). Since FGF signalling delays neurogenesis, the lower amounts of FGF on the left side of wild-type larvae allows neurogenesis to start first in that side than in the right (Lahti *et al.*, 2011; Dean, Gamse and Wu, 2018).

1.3.3. The parapineal controls dHb asymmetry

In parallel to the habenular development, another epithalamic structure also develops asymmetries at this developmental time window: the pineal complex, which includes the medially positioned pineal organ and its leftward positioned accessory organ, the parapineal (P and pp, respectively, in Figures 1.1.A and 1.1.A'; dotted line and green structure in 1.2.A[1-5]). The parapineal is a small structure that consists of less than twenty cells which delaminate from the anterior domain of the pineal (Concha *et al.*, 2003). Around 27 hpf, the parapineal starts migrating leftwards and, by 4 dpf, it is positioned ventroposterior to the pineal (Concha *et al.*, 2003; Roussigné *et al.*, 2018). The presence of a parapineal and its migration are required for the development of the dHbL character (Concha *et al.*, 2003; Gamse, 2003; Bianco *et al.*, 2008; Regan *et al.*, 2009). Thus, misspecification of PP cells affects habenular laterality.

One way in which parapineal specification is controlled is via *med12* (Wu *et al.*, 2014). This mediator is important for the timely expression of *T-box 2b* (*tbx2b)*, without which parapineal cells would be misspecified and dispersed ventrally to the pineal (Snelson *et al.*, 2008; Wu *et al.*, 2014). Without a working parapineal, both habenulae develop a right

dHb character, which suggests that this is the default state of habenular development (Concha *et al.*, 2003; Gamse, 2003; Bianco *et al.*, 2008; Snelson *et al.*, 2008). On the other hand, the formation of too many parapineal cells has the opposite effect on habenular asymmetry: when the Nodal target, *pitx2c,* is knocked down by morpholino injection, the number of parapineal cells increases by half, and the dHb becomes left-isomerized (Garric *et al.*, 2014). Interestingly, by ablating the excess number of parapineal cells of *pitx2c*-morphants, it was possible to rescue the habenular phenotype, suggesting the exact number of parapineal cells is paramount to the correct elaboration of epithalamic asymmetries (Garric *et al.*, 2014).

The current theory is that the default developmental programme of dHb cells is biased towards the medial character and that parapineal cells are likely to counteract this programme and promote dHbL fate (Hüsken *et al.*, 2014). This mechanism probably involves the parapineal inhibition of the Wnt pathway, since mutants with hyperactive Wnt signalling have right-isomerised habenulae, and mutants with hypoactive Wnt signalling have left-isomerised habenulae, independently of the presence of a parapineal (Carl *et al.*, 2007; Hüsken *et al.*, 2014). The wild-type parapineal is located on the left side of most embryos, and thus more neurons on this side acquire a dHbL fate, while neurons in the right become dHbM (Concha *et al.*, 2003; Gamse, 2003; Gamse *et al.*, 2005; Viswanath *et al.*, 2014). Moreover, given that most neurons of the first neurogenic wave become dHbL and that only early parapineal ablations affect the development of dHb asymmetries, this function of the parapineal must happen during the first neurogenic wave (Aizawa *et al.*, 2007; *Lekk, I., Wilson, S.W., unpublished results*).

Another way that parapineal cells specification is mediated is through the FGF pathway. At 20 hpf, *fgf8* is only medially expressed in the anterior epithalamus, partially covering the anterior pineal anlage (Regan *et al.*, 2009). In its absence, the parapineal is smaller and does not migrate from the midline (Regan *et al.*, 2009; Clanton, Hope and Gamse, 2013). This combined with the delay in habenular progenitor formation (see section 1.3.1.) drives the formation of a small symmetric habenula in *fgf8* mutants. However, providing an external source of Fgf8 is enough to trigger parapineal migration, as this has been shown to rely on the activation of the FGF pathway in a few parapineal “leading” cells (Regan *et al.*, 2009; Roussigné *et al.*, 2018).

Despite triggering parapineal migration, the FGF pathway does not determine its laterality. The leftwards positioning of the parapineal in more than 90% of wild-type embryos is determined by the leftwards expression of Nodal related genes in the epithalamus (M R Rebagliati *et al.*, 1998; Concha *et al.*, 2000). The Nodal signalling pathway has been known for controlling the establishment of overall left-right asymmetries in the developing embryo, since it is only activated on the left side of the

lateral plate mesoderm (LPM) (Michael R. Rebagliati *et al.*, 1998; Long, Ahmad and Rebagliati, 2003; Baker, Holtzman and Burdine, 2008). In the epithalamus, both its inactivation and its bilateral activation randomizes the direction of parapineal migration and, accordingly, of habenular laterality (Concha *et al.*, 2000; Gamse *et al.*, 2005; Inbal *et al.*, 2007).

The lateralised Nodal signalling in the LPM promotes its own activation in the epithalamus. For instance, the loss of *southpaw* (*spw*), a nodal related gene that is only expressed in the LPM, results in the loss of *ndr2, lefty1 and pitx2* in the epithalamus (Long, Ahmad and Rebagliati, 2003; Gamse *et al.*, 2005). However, there are other molecular mechanisms that specifically control the Nodal pathway in the left epithalamus, without affecting its activity in the LPM. One such signalling cascade is the Wnt pathway which controls the expression of Nodal related genes, specifically in the diencephalon (Carl *et al.*, 2007). Hyperactivating the Wnt pathway leads to bilateral expression of *lefty1* and *pitx2* in the epithalamus without affecting the left expression of *spw* in the LPM (Carl *et al.*, 2007). However, when the Wnt pathway is downregulated and its effect over the Nodal pathway is alleviated, the expression of these nodal related genes is normal in the epithalamus, due to the influence of the leftwards Nodal activity in the LPM (Hüsken and Carl, 2013; Hüsken *et al.*, 2014).

1.3.4. Habenular anatomical asymmetries.

In larvae zebrafish the left dHb is bigger and has broader neuropils than the right dHb (Concha *et al.*, 2000; Taylor *et al.*, 2011; Colombo *et al.*, 2013; Lee *et al.*, 2014). Whilst the size asymmetry is a direct consequence of neurogenesis starting first on the left side, the dendritic arbor elaboration results from a later developmental step. This asymmetry is, in part, controlled by the negative interaction between the Kctd12 proteins and Unc-51 like autophagy activating kinase 2 (Ulk2) (Taylor *et al.*, 2011; Lee *et al.*, 2014). Ulk2 promotes neuropil elaboration and is initially expressed symmetrically in the epithalamus. However, probably due to a stronger interaction between Kctd12.2 than Kctd12.1 and Ulk2, Ulk2 activity is strongly inhibited in the right dHb, while in the left side Ulk2 is able to promote the elaboration of dendritic arbors (Taylor *et al.*, 2011; Lee *et al.*, 2014).

In parallel, *dishevelled associated activator of morphogenesis 1a* (*daam1a)*, which codes a Wnt-related protein and is asymmetrically expressed in the left dHb, increases the elaboration of the habenular dendrites and axons (Colombo *et al.*, 2013). Both dHb nuclei project to the IPN, in the midbrain, through the Fasciculus Retroflexus (FR) and the terminal arbor morphology of left and right dHb axons is quite distinct (Aizawa *et al.*, 2005; Bianco *et al.*, 2008). The axons from the left dHb, which express more *daam1a,*

extend to a higher dorsoventral depth of the IPN and produce more branches than the axons originating from the right dHb (Bianco *et al.*, 2008; Colombo *et al.*, 2013).

The asymmetric projection of the dHb to the IPN is not limited to the axonal morphology. Neurons that express *kctd12.1* mainly project to the dorsal and intermediate IPN, while the *kctd12.2* neurons project to the ventral IPN (Aizawa *et al.*, 2005; Bianco *et al.*, 2008). The asymmetric representation of *kctd12* neurons in the dHb creates an effect called, "laterotopic projection*",* in which the left and right dHb projections are topographically represented in a dorsoventral pattern in the IPN (Aizawa *et al.*, 2005). This is partially explained by another asymmetrically expressed gene, *neuropilin 1 a (nrp1a)*, which is only present in neurons of the left dHb (Kuan *et al.*, 2007). Nrp1a is a transmembrane glycoprotein and coreceptor of the Sema domain, immunoglobulin domain (Ig), short basic domain, secreted, (semaphorin) 3D (Sema3D), an axon guidance molecule that is expressed along the FR. So, *nrp1a* expressing neurons, are guided to the dorsal IPN, through the gradient of Sema3D (Kuan *et al.*, 2007). However, no equivalent receptor-chemoattractant pair was yet found for the right dHb.

A recent study showed that the aforementioned *cxcr4b*, a gene expressed in cell transitioning from habenular progenitors to dHb neurons, is also involved in the guidance of the dHb axons to the IPN (Roberson and Halpern, 2017b). The *cxcr4b* gene encodes a chemokine receptor and, its ligand, *cxcl12a* is expressed caudally to the habenula. Mutating *cxcr4b* or *cxcl12a* results in the dHb axons projecting anteriorly, rather than to the IPN (Roberson and Halpern, 2017b). Therefore, despite the downregulation of the transcription of *cxcr4b* upon the full differentiation of dHb neurons, basal levels of the Cxcr4b protein are kept to correctly guide the axonal projections to the IPN (Roberson and Halpern, 2017a).

1.3.5. Habenular development after 4 dpf

At 4 dpf, zebrafish larvae still express the progenitor habenular marker *dbx1b* in the most ventromedial portion of the dHb (Roberson and Halpern, 2017a). This expression is maintained at least until 30 dpf and the number of neurons increases from an average of 400 cells at 4 dpf, to about 1500 cells at 10 dpf (Satija *et al.*, 2015; Roberson and Halpern, 2017a). Therefore, despite dHb asymmetries being well defined by 4 dpf, this structure's development does not stop at this time point.

At 10 dpf, a population of habenular neurons still expresses *tubulin, beta 5 (tubb5)*, a gene that is a marker of immature neurons (Breuss *et al.*, 2012; Pandey *et al.*, 2018). This goes in line with the number of habenular neurons increasing to 8,000 in fully matured zebrafish. Furthermore, four new habenular sub-populations are formed between 10 dpf and 1 year old zebrafish: one in the dHb and three in the vHb (Pandey

et al., 2018). Interestingly, all populations are predicted to occupy a more ventromedial position of the habenula, next to *dbx1b*-expressing cells (Roberson and Halpern, 2017a; Pandey *et al.*, 2018). Nevertheless, since there is no evidence of habenular asymmetry development during these later timepoints, studies of habenular asymmetry are usually focused in the embryonic and larval developmental stages.

1.4. The neuronal subpopulations of the habenula

The overt asymmetric features of the zebrafish habenula led to an increased interest in finding genes that define neuronal populations that are asymmetrically present in this structure. In addition to this, the important role that the habenula plays in mammals with regards to depression and substance abuse disorders (namely nicotine addiction), led to an increasing interest in understanding which type of neurons constitute the habenula of rodents. In order to achieve this, increasingly larger scale studies have focused on the identification and characterisation of the neuronal subpopulations that constitute the habenula of rodents and zebrafish.

1.4.1. Habenular subpopulations in rodents

The first characterisation of habenular neuronal types was done in rats and was purely based on topographic, morphologic and cytochemical criteria (Andres, von Düring and Veh, 1999). This work found 10 domains in the lateral habenula and 5 domains in the medial habenula, which were later topographically correlated with the habenular domains that constitute the mouse habenula (Andres, von Düring and Veh, 1999; Wagner, Stroh and Veh, 2014). Additional studies partially corroborated these results through the *in silico* analysis of gene expression in the mouse habenula (Wagner, French and Veh, 2016). A database containing information about the expression of more than 20,000 genes in the mouse brain, revealed that gene expression in the lateral habenula does not follow the previously stated anatomical boundaries, whereas the medial habenula does (Wagner, French and Veh, 2016).

It was discovered that three of the five medial habenular domains are clearly labelled by the expression of the *WNT Inhibitory Factor 1* (*Wif1)*, *Cubilin* (*Cubn)* and *Somatostatin Receptor 4* (*Sstr4)*, with *Myosin XVI (Myo16)* spanning the other two domains (Wagner, Stroh and Veh, 2014). Moreover, the molecular study identified a new domain characterised by the co-expression of *Adenylate Cyclase Activating Polypeptide 1* (*Adcyap1)*, *Cholinergic Receptor Nicotinic Alpha 3 Subunit* (*Chrna3),* and *Tumour Protein P53 Inducible Protein 11 (Trp53i11)*. On the other hand, gene expression patterns in the lateral habenula do not follow the characterised subdomain boundaries. For instance, *ELMO Domain Containing 1* (*Elmod1)* is expressed in the whole lateral

habenula; while the *Extracellular Leucine Rich Repeat and Fibronectin Type III Domain Containing 1* (*Elfn1)* and the *Transmembrane Protein 163 (Tmem163)* genes are expressed in several domains of the lateral and medial habenulae. The GABAergic neuron marker *Glutamate Decarboxylase 2* (*Gad2)* is expressed in a lateral region of the lateral habenula, while the *Potassium Voltage-Gated Channel Subfamily A Regulatory Beta Subunit 2* (*Kcnab2)* is in a medial region of the lateral habenula. Lastly, the serotonergic receptor 5-*Hydroxytryptamine Receptor 2C* (*Htrc2)* and the *Cholinergic Receptor Muscarinic 2* (*Chrm2)* are expressed in a punctate pattern between *Gad2* and *Kcnab2* (Wagner, French and Veh, 2016).

The specific subdomains of the medial habenula also have localised neurotransmitter expression (Figure 1.3.A and 1.3.B). In the rat, the superior medial habenula (MHbS) is mainly glutamatergic; the dorsal-central medial habenula (MHbCd) expresses both glutamate and substance P; and the lateral-ventral (MHbVL), central-ventral (MHbCv) and inferior (MHbI) sub-nucleus medial habenula are both cholinergic and glutamatergic (Figure 1.3.A) (Aizawa *et al.*, 2012). Although this correlation was only established for a few domains in the mouse habenula, its homology with the rat habenula allows to predict the types of neurons that constitute each of these domains (Figure 1.2.B). Nevertheless, the high regionalisation of neurotransmitters in the medial habenula suggests that each of its domains carries out highly specialised functions, with regards to behaviour.

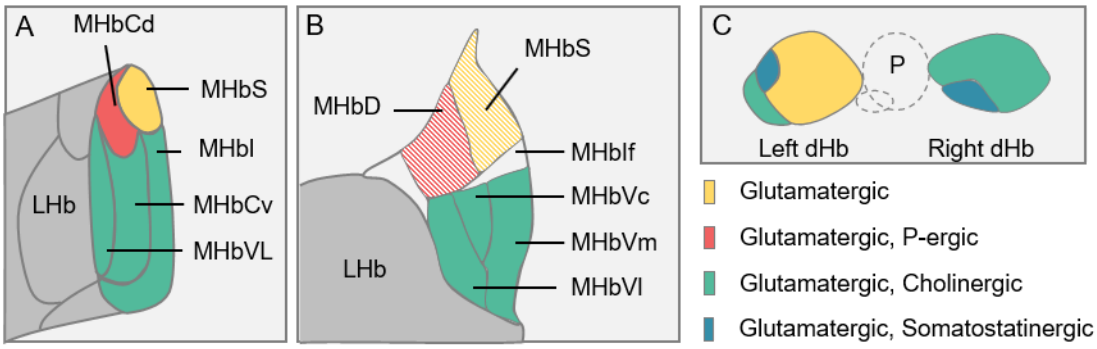

Figure 1.3 Habenula neurotransmitter map. (A) Schematics of the neurotransmitter expression pattern in the rat medial habenula. The superior sub-nucleus of the medial habenula (MHbS) has glutamatergic neurons (yellow). The neurons of the dorsal-central sub-nucleus of the medial habenula (MHbCd) are glutamatergic and Substance P-ergic (red). The lateral-ventral, central-ventral and inferior sub-nucleus of the medial habenula (MHbVL, MHbCv and MHbI, respectively) consist of glutamatergic, cholinergic neurons (green). **(B)** Schematics of the neurotransmitter expression pattern in the mouse medial habenula. Given the homology between rat and mouse habenula nuclei, the superior sub-nucleus of the medial habenula (MHbS) is expected to have glutamatergic neurons (striped yellow), while the neurons of the dorsal sub-nucleus of the medial habenula

(MHbD) are expected to be glutamatergic and Substance P-ergic (striped red). The lateral-ventral, central-ventral and medial-ventral sub-nucleus of the medial habenula (MHbVl, MHbVc and MHbVm, respectively) consist of glutamatergic and cholinergic neurons (green). There is no information about the neuron types in the intermediate field of the medial habenula (MHbIf) or the Area X (which consist of lateral and medial habenula neurons). **(C)** Schematics of the neurotransmitter expression pattern in the zebrafish medial habenula. The majority of neurons in the left dHb are solely glutamatergic. A subset of the lateral dHb are glutamatergic and somatostatinergic (blue) but, there are more of these neurons in the right nucleus. The remaining neurons are glutamatergic and cholinergic (green), which are also more represented in the right nucleus. The schemes in this figure were based in figures from (Aizawa *et al.*, 2012; deCarvalho *et al.*, 2014; Wagner, French and Veh, 2016)

1.4.2. Habenular subpopulations in zebrafish

It is accepted that the vHb of zebrafish is the homologue of the mammalian lateral habenula, and the zebrafish dHb the homologue of rodents' medial habenula (Amo *et al.*, 2010). This correlation was established because the vHb projects to the raphe nuclei and expresses *protocadherin 10* (*pcdh10a)* like the lateral habenula of mammals (Amo *et al.*, 2010). However, current evidence shows that genes such as *gad2*, a marker of GABAergic neurons expressed in the lateral habenula of mice, are actually expressed in the dHb of zebrafish, suggesting that this correlation may need to be further dissected (Wagner, French and Veh, 2016; Pandey *et al.*, 2018). Currently, a detailed comparison between the neuronal populations that constitute the habenulae in rodents and zebrafish is limited, given the lack of a public database of the zebrafish habenular gene expression. Nevertheless, this gap is closing as many studies have now attempted to characterise in depth the neuronal composition of zebrafish's habenula (Pandey *et al.*, 2018).

The zebrafish dHb is classically defined by the expression of genes such as *guanine nucleotide binding protein (G protein), gamma 8* (*gng8)* and *anoctamin 2* (*ano2),* while the vHb is defined by *muscleblind-like splicing regulator 3* (*mbnl3)*, *amine oxidase, copper containing 1* (*aoc1)* or *kiss-1 metastasis suppressor* (*kiss1)* (Thisse and Thisse, 2004; Amo *et al.*, 2010; deCarvalho *et al.*, 2013, 2014; Lupton *et al.*, 2017). Due to the small size of the vHb, there have been no attempts to dissect the neuronal subpopulations of this region, however, the same does not apply to the dHb.

Apart from expressing *kctd12.1,* the dHbL subdomain is also defined by the expression of *neuronal pentraxin 2a* (*nptx2a)* and the *kctd12.1*-expressing dHbM by *pou class 4 homeobox 1* (*pou4f1*, former *brn3a)* (Aizawa *et al.*, 2005; Agetsuma *et al.*, 2010; Doll *et al.*, 2011). Due to the asymmetric distribution of these two subdomains in the left and

right dHb, the *kctd12.1* and *kctd12.2* genes became the most commonly used markers for left and right dHb, respectively. However, asymmetric expression is not limited to medial and lateral markers of the dHb. For example, the *nrp1a* gene is only expressed in the left dorsal nucleus, while *potassium channel tetramerisation domain containing 8* (*kctd8)* is enriched in the right (Kuan *et al.*, 2007; Garric *et al.*, 2014).

An obvious approach towards understanding the role of asymmetry for habenular function was to characterise the neurotransmitters expressed by dHb neurons. At 4 dpf, virtually all dHb neurons are glutamatergic, as seen by the broad expression of the *solute carrier family 17 member 6b (slc17a6b,* former *vglut2a*) (Figure 1.3.C) (deCarvalho *et al.*, 2014). A fraction of these – mostly in the right dHbM – are also cholinergic (expressing *solute carrier family 18 member 3b* (*slc18a3b*, former *vachtb*) and *choline O-acetyltransferase b* (*chatb)* (Hong *et al.*, 2013; deCarvalho *et al.*, 2014). A subset of the dHbL neurons express *somatostatin 1, tandem duplicate 1* (*sst1.1*), however, there are more *sst1.1* neurons in the right nucleus (deCarvalho *et al.*, 2014). Moreover, while a subpopulation of substance P (*tachykinin 1*, *tac1*) expressing neurons is only observed in adults, *tachykinin 3a* (*tac3a*; a neurotransmitter of the family of substance P) is expressed in neurons of the right dHb of 4 dpf larvae (Biran *et al.*, 2012; deCarvalho *et al.*, 2014). Lastly, at 10 dpf, it is also predicted that 2 to 3 neurons are GABAergic in the dHb (Pandey *et al.*, 2018). Altogether, despite the asymmetric expression of most neurotransmitter markers, the dHb of zebrafish is likely to send excitatory, rather than inhibitory projections to the IPN.

A recent study sequenced single-cells of the habenula of 10 dpf larvae and found that the whole vHb consists of one homogenous subpopulation of neurons expressing *kiss1,* while the dHb consists of 14 different neuronal subpopulations (Pandey *et al.*, 2018). Two dHb clusters are enriched in the right dHb, which are defined by the genes *caveolae associated protein 4b (cavin4b,* former *murcb)* and *adrenoceptor beta 2, surface a (adrb2a*). Four are left-enriched and defined by *adcyap1a*, *protein phosphatase 1, regulatory (inhibitor) subunit 1C (ppp1r1c)*, *protocadherin 7b* (*pcdh7b)* and *wingless-type MMTV integration site family, member 7Aa* (*wnt7aa*). The posterior dHb can be subdivided in four symmetric regions (defined by *cerebellin 2b precursor* (*cbln2b)*, *copine IVa* (*cpne4a)*, *5-hydroxytryptamine (serotonin) receptor 1A a* (*htr1aa)* and *sry (sex determining region Y)-box 1a* (*sox1a))*. Three of the found subpopulations are represented by very few cells and do not have a specific pattern. Lastly, there is still a population of immature neurons, expressed in the medial ventral region, defined by *tubulin, beta 5* (*tubb5b*) (Pandey *et al.*, 2018).

The evidence of the numerous subpopulations of the dHb of zebrafish shows how little we know about its true function. The high variety and number of neuron types in such a small structure suggests that the habenula must play a role in many different behaviours.

1.5. Habenula Function

Despite the many studies investigating the role of the habenula in behaviour modification, its true function still is somewhat elusive. Counterintuitively, this is due to the habenula being implicated in many behaviours. Altogether, the habenula was shown to be part of the circadian timekeeping, sleep, addiction, fear, anxiety and depression, among others (Aizawa *et al.*, 2013; Amo *et al.*, 2014; Velasquez, Molfese and Salas, 2014; Facchin, Duboue and Halpern, 2015; Baño-Otálora and Piggins, 2017). However, what seems to connect all these behaviours, is habenular control over the dopaminergic and serotonergic reward system. In this section, we will describe what is known about the function of the zebrafish habenula and how asymmetry affects this function.

1.5.1. dHb activity in zebrafish.

In zebrafish, dHb functional studies have focused on its asymmetric character. The *Eminentia thalami*, which receives inputs from the retina, mostly projects to the left dHb and, indeed, light stimuli activates more cells from this nucleus (Hendricks and Jesuthasan, 2007; Dreosti *et al.*, 2014; Zhang *et al.*, 2017). Likewise, the mitral cells of the olfactory bulbs only project to the right habenula, and most habenular neurons that are activated by olfactory stimuli are found in the right epithalamus (Dreosti *et al.*, 2014; Turner *et al.*, 2016).

More recently, it was shown that the right dHb is asymmetrically activated by heat stimuli and by carbon dioxide (CO_2) (Haesemeyer *et al.*, 2018; Koide, Yabuki and Yoshihara, 2018). Although both nuclei are activated by these noxious stimuli, the right dHb is activated first, upon the application of the stimuli while the left side has a delayed response that is highly increased at the end of the stimuli (Haesemeyer *et al.*, 2018; Koide, Yabuki and Yoshihara, 2018). It is not fully understood how sensory projections to the habenula drive heat and CO_2 asymmetric activation of the dHb. That said, this response may be driven by activation of transient receptor potential channels (TRP), as they are implicated in eliciting a noxious response upon exposure to heat or high levels of CO_2 in mammals (Wang, Chang and Liman, 2010; Julius, 2013). Thus, it is reasonable to assume that the habenula plays a crucial role in modulation of behaviour upon exposure of aversive stimuli.

1.5.2. The habenula signals negative reward

Studies on the connectivity of the habenula of mammals have strongly suggested that the habenula is involved in the reward signalling pathway. In rats, medial habenula primary inputs originate from the limbic system, specifically in the stria medullaris (Herkenham and Nauta, 1977; Qin and Luo, 2009). In addition to this, many monoaminergic afferents have also been identified from the dopaminergic inputs of the interfascicular nucleus of the Ventral Tegmental Area (VTA), the noradrenergic signals from the *locus coeruleus* and the mesencephalic raphe in the midbrain (Herkenham and Nauta, 1977; Phillipson and Pycock, 1982; Gottesfeld, 1983). With regards to efferent projections, the habenula of both mammals and fish have projections to the IPN, which then go on to terminate in the raphe nuclei (Herkenham and Nauta, 1977; Carlson, Noguchi and Ellison, 2001; Aizawa *et al.*, 2005; McCallum *et al.*, 2012). There have also been studies showing that the medial habenula has projections to the pineal gland and lateral habenula (Rønnekleiv and Møller, 1979).

According to the pattern of habenular connectivity in humans, primates and rodents, the lateral habenula is activated in response to negative stimuli and their associated cues (Matsumoto and Hikosaka, 2007, 2009a; Agetsuma *et al.*, 2010; Stephenson-Jones *et al.*, 2016; Liu *et al.*, 2017). This activation is modulated by a subdomain of the *globus pallidus interna*, that projects to the habenula and is activated by negative stimuli (Hong and Hikosaka, 2008, 2013; Stephenson-Jones *et al.*, 2016). In zebrafish, the homolog of the *globus pallidus*, the ventral entopeduncular nucleus (vENT), projects to the ventral and dorsal habenula (Amo *et al.*, 2014; Turner *et al.*, 2016). However, unlike some other afferent projections, both habenular nuclei receive inputs from the vENT.

In zebrafish, ablating the vHb or the left dHb prevents zebrafish from learning the association between a cue and the shock that follows it (Lee *et al.*, 2010; Amo *et al.*, 2014; Lupton *et al.*, 2017). On the other hand, an aversive concentration of bile salts increases the neuronal activity of the right dHb which, consequently, promotes avoidance behaviours (Krishnan *et al.*, 2014). However, the dHb does not seem to be solely important for the expression of aversive behaviours. For instance, the left dHb responds to mild electric stimuli (aversive stimuli) but in this context is needed to promote swimming after the refractory period that follows a shock (Duboué *et al.*, 2017). Moreover, despite the majority of studies showing an habenular activation in response to aversive stimuli, contradictory results showed that lesioning the left dHb impairs zebrafish light preference behaviours (Zhang *et al.*, 2017). Also, associating the side of an arena with the optogenetic activation of the left dHb promoted a preference behaviour for that side of the arena (Zhang *et al.*, 2017). Therefore, despite the many studies suggesting the importance of the habenula to signal the negative-value of a stimulus, we

still do not hold a full understanding of its function. Nevertheless, all studies seem to indicate that the habenular asymmetry in zebrafish plays an important role in its function.

1.5.3. The role of the habenula in depression and nicotine addiction

The crucial role the habenula plays in normal brain function has made it a potential target for many of the symptoms seen in neurological syndromes and diseases in humans, such as depression. Many rodent studies, as well as analyses in humans, have shown that lateral and medial habenular hyperactivity is strongly correlated with depression (Caldecott-Hazard, Mazziotta and Phelps, 1988; Liu *et al.*, 2017). Depression models in rats have revealed increased metabolic activity in both habenulae, as well as the IPN, along with decreased metabolic activity in the VTA, basal ganglia and amygdala (Shumake, Edwards and Gonzalez-Lima, 2003). This suggests that the development of the severity of symptoms in depression may be caused by an increasing hyperactivation of the habenula in face of negative events. Given the habenular connectivity, this hyperactivity suppresses the dopaminergic and serotonergic signals, thus, promoting affective symptoms such as anhedonia, reduced affection and reduced appetite (reviewed in Yang, Wang, Hu, & Hu, 2018). In line with this, deep brain stimulation to suppress habenular activity induces the remission of severe depression symptoms (Sartorius and Henn, 2007; Sartorius *et al.*, 2010).

The habenula also plays a critical role in nicotine addiction. Through genetic and proteomic analyses, the medial habenula has been shown to express high levels of nicotinic acetylcholine receptors (nAChRs). It is estimated that 90-100% of the neurons in the medial habenula express α3, α4, α5, β2, and/or β4 nAChR subunits, which have been strongly implicated in the addictive properties of nicotine (Sheffield, Quick and Lester, 2000; Salas *et al.*, 2009; Hong *et al.*, 2013). Through the influence of the dopaminergic system via the IPN and VTA, the habenula may modulate the reinforcing properties of nicotine and, upon abstinence of nicotine, play a role in withdrawal symptoms by altering dopaminergic signals to the nucleus accumbens (Salas *et al.*, 2009; McCallum *et al.*, 2012; Shih, McIntosh and Drenan, 2015).

In line with this, rats at the peak of nicotine withdrawal show increased depressive behaviour and cognitive deficits in a reversal learning paradigm, which may be due to hyperactivity of the habenula (Jackson *et al.*, 2017). Moreover, zebrafish in low concentrations of nicotine perform better in a choice task between a good and bad outcome chamber, while high concentrations impair performance (Levin and Cerutti, 2009). It is thought that low levels of nicotine are able to increase basal levels of habenular activation, promoting aversion to nicotine and limit its intake (Fowler *et al.*, 2011). However, the increased basal activation also promotes efficient responses to

negative stimuli, thus increasing performance in reversal learning tasks (Zuo *et al.*, 2016). On the other hand, high concentrations of nicotine have a stronger effect directly in the ventral tegmental area, which increases dopamine and positive-reward-like symptoms, thus, promoting addiction (Zuo *et al.*, 2016).

1.6. Aims of the Thesis

The habenula of zebrafish has proved to be a great model to dissect the molecular mechanisms that drive the development of brain left-right asymmetries, but many details regarding its development and its function remain elusive to this day.

We now have a clearer picture of how signalling pathways such as Nodal, FGF and Wnt interplay during the epithalamic development to control the asymmetric timing of neurogenesis and cell-fate allocation that lead to the elaboration of habenular asymmetries. However, there is still a gap in the understanding of the molecular steps controlling the specification and maintenance of habenular progenitors. Recent studies have identified some of the markers that are expressed by this population of cells which allowed researchers to show that FGF and Wnt pathways control its timely formation. However, it remains unclear how these pathways modulate the transcriptional profile that ultimately commits a cell to become a habenular progenitor.

Furthermore, the medial habenula of rodents and the dHb of zebrafish consist of several well-defined groups of neurons. These neurons are virtually all glutamatergic, but a big proportion is also somatostatinergic, P-ergic or cholinergic. Moreover, the characterisation of the 10 dpf zebrafish habenula has shown that it consists of, at least, 15 subpopulations of habenular neurons. However, studies of habenular asymmetry mutants are performed at much earlier timepoints, the latest being at 4 dpf, and we do not know if this neuronal variability is already present at this timepoint or if it arises later. In order to further understand this process, we would need to have a comprehensive map of the neuronal subpopulations that constitute the zebrafish habenula at 4 dpf, along with the molecular markers that can define them.

Lastly, the habenula has been shown to play a role in the elaboration of certain behavioural outputs. For instance, in zebrafish, the acquisition of a response to a light that predicts an aversive stimulus is dependent on the dHb. This, and many other works with humans, primates and rodents, suggest that the habenula signals during negative experiences, which is essential for learning tasks. However, this correlation has never been established in larvae zebrafish or to the habenular asymmetry.

With the aim of tackling some of the gaps in the knowledge of habenular asymmetry development, habenular neuronal composition and the function of this structure during behaviour, I set out to do the following:

1. Characterise the habenular development of a zebrafish mutant with reduced and symmetric habenular nuclei;

2. Identify the subpopulation of neurons that constitute the dorsal habenula of 4 dpf zebrafish;

3. Study the importance of habenular asymmetry for the normal behaviour of zebrafish larvae during a reversal learning paradigm.

CHAPTER 2.

DEVELOPMENT OF HABENULAR PROGENITORS IS REGULATED BY THE NUCLEAR RECEPTOR CO-REGULATOR REREA.

2.1. INTRODUCTION

From *Caenorhabditis elegans* to *Homo sapiens,* functional and structural asymmetries are consistently present in the central nervous system of animals (Gamse, 2003; Poole and Hobert, 2006; Spring *et al.*, 2010; Concha, Bianco and Wilson, 2012; Ahumada-Galleguillos, Lemus, Díaz, *et al.*, 2017). However, we still lack a full picture of the molecular mechanisms that drive the elaboration of these asymmetries during embryonic development. The transparency of the zebrafish embryo and its amenability to genetic manipulation combined with its overt habenular asymmetries, makes it the perfect subject to study the development of brain asymmetries (Gamse *et al.*, 2005). The habenula of zebrafish is an epithalamic structure that consists of two nuclei, one on each side of the brain, separated by the pineal and the left habenula projecting parapineal (Gamse *et al.*, 2005). Although the ventral domain of the habenula (vHb) does not show evidence of being asymmetric, the left dorsal habenula (dHb) is bigger and has more elaborated neuropil than the right one (Colombo *et al.*, 2013). Moreover, by 4 days post fertilization (dpf) gene expression, and afferent and efferent connections are different between the left and right dHb (Gamse *et al.*, 2005). Therefore, studies of habenular development in zebrafish are at the core of brain asymmetry research.

Forward genetics has played a vital role in dissecting the molecular pathways that regulate epithalamic asymmetries. In our group and others, zebrafish mutant lines were generated through a random ENU-induced mutagenesis (N-Ethyl-N-nitrosourea) approach, and screened for habenular asymmetry defects by whole-mount *in situ* hybridization (WISH) with a probe for *kctd12.1* (Hüsken *et al.*, 2014). This is possible because the *kctd12.1* gene is expressed in the dorsal lateral habenular neurons (dHbL) which are found in greater proportion in the left epithalamus of wild-type zebrafish (Gamse, 2003).

Using this experimental design, several novel dHb asymmetry mutants have been thoroughly characterised including mutants with right dHb isomerism (t-*box 2b* (*tbx2b)* mutants), left dHb isomerism (*paired-like homeodomain 2 (pitx2), transcription factor 7 like 2 (tcf7l2)* and *sec61 translocon alpha 1 subunit (sec61a1)* mutants), with unspecified dHb (*mediator complex subunit 12* (*med12)* mutant), or with small habenular nuclei (*fibroblast growth factor 8a (fgf8a)* and *Wnt ligand secretion mediator (wls)* mutants*)* (Snelson *et al.*, 2008; Regan *et al.*, 2009; Doll *et al.*, 2011; Garric *et al.*, 2014; Hüsken *et al.*, 2014; Wu *et al.*, 2014; Kuan *et al.*, 2015). Altogether, these studies revealed the importance of different signalling pathways (such as Wnt, FGF and Nodal) for the establishment of epithalamic asymmetries.

In *wls, fgf8* and *med12* mutants, the formation and specification of the habenular progenitors is defective (Regan *et al.*, 2009; Dean *et al.*, 2014; Kuan *et al.*, 2015). In *wls* mutants, the downregulation of Wnt delays the expression of the habenular progenitor marker *dbx1b*, from 24 hpf to 27 hpf, rendering the 4 dpf dHb smaller than in siblings (Beretta *et al.*, 2013; Kuan *et al.*, 2015; Roberson and Halpern, 2017a). Likewise, mutants for *fgf8a* do not express *dbx1b* at 24 hpf or 28 hpf (Dean *et al.*, 2014). However, at 4 dpf, a small and symmetric dHb is formed, which suggests that the formation of habenular progenitors is delayed rather than abrogated (Regan *et al.*, 2009; Dean *et al.*, 2014; Dean, Gamse and Wu, 2018). Lastly, in *med12* mutants, the FGF pathway is inactivated through a not well understood mechanism (Wu *et al.*, 2014). This inactivation is concurrent with a delayed expression of *dbx1b* until 2 dpf, which ultimately results in the dHb cells not being specified at 4 dpf (Wu *et al.*, 2014). Taken together, these results point to the importance of the FGF and Wnt pathways in the formation of the habenular progenitors and, consequently, for the correct formation of the dHb.

In this chapter, we will describe a novel mutant with defective habenular development. As will be described, we believe that the mutation is in the *arginine-glutamic acid dipeptide (RE) repeats a* (*rerea*) gene. *rerea* encodes a coregulator of nuclear receptors (NRs) (Plaster *et al.*, 2007; Vilhais-Neto *et al.*, 2010). NRs are a family of transcription factors which are activated by liposoluble ligands, such as steroid-hormones or retinoic acid (RA) (Sever and Glass, 2013). Once active, NRs regulate gene expression by forming complexes with coregulators, and histone acetyltransferases (HATs) or deacetylases (HDACs) (Sever and Glass, 2013). The coregulator Rerea forms complexes with NRs such as the Chicken ovalbumin upstream promoter-transcription factor (COUP-TF), the T-cell leukaemia homeobox 1 (Tlx1), and the Retinoic Acid Receptor (RAR) (Wang *et al.*, 2006; Plaster *et al.*, 2007; Vilhais-Neto *et al.*, 2010).

Rere (the murine homolog of *rerea*) mutant mice display asymmetric somite formation due to a decrease in RA signalling on the right side of the presomitic mesoderm, accompanied by an ectopic expansion of *Fgf8* (Vilhais-Neto *et al.*, 2010). In the zebrafish *rerea*^{ru622} mutant*, fgf8* expression is increased at 24 hours post-fertilization (hpf) in the presumptive diencephalon, mid-hindbrain boundary and optic vesicles (Asai *et al.*, 2006). This mutant and *rerea*^{tb210} mutants show defects in the optic vesicles, pharyngeal arches and in the most anterior part of the head, thus being originally named *babyface*. However, no phenotype was previously described in the dHb of these mutants.

In this study, we characterised a novel ENU-induced mutant, the *A66*^{u757}, displaying a reduced dHb domain when compared to siblings. The presumptive causative lesion in this line results in an early stop codon within the *rerea* coding frame which affects the last 158 amino acids of the coding protein. Homozygous *A66*^{u757} mutants show a

compromised formation of the most anterior head structures and a defective otic vesicle. Moreover, despite the altered morphology of the olfactory bulbs, in the anterior forebrain, mitral cells still send efferent projections asymmetrically to the right dhb of mutants, as previously described for wild-types (Miyasaka *et al.*, 2009). On the other hand, both the development and asymmetric projections of the parapineal of mutants are compromised. Lastly, the formation of habenular progenitors is delayed in mutants and preceded by an expansion of the *fgf8* expression in the diencephalon and otic vesicles.

2.2. RESULTS

2.2.1. *A66^{u757}* mutants have a reduced dHb

To identify genes with a role in the development of habenular asymmetry, the progeny of lines carrying ENU-induced mutations was screened by WISH for habenular asymmetry defects (Hüsken *et al.*, 2014). We isolated the *u757* mutation which, in approximately 25% of the progeny of a sibling pair mating, led to the reduced expression pattern of *kctd12.1* in both dHb nuclei of 4 dpf larvae (Figures 2.1.C and 2.1.C'). However, this reduction was more drastic on the left side (Figures 2.1.C and 2.1.C').

To further understand the extent by which habenular asymmetry is affected in *A66^{u757}* mutants, we performed WISH for a dorsal medial habenula marker (dHbM), the *potassium channel tetramerization domain containing 12.2* (*kctd12.2*) (Gamse *et al.*, 2005). While the expression pattern of *kctd12.2* became broader on the left dHb, in the right dHb it was restricted to the most posterior region (Figures 2.1.D and 2.1.D'). These results suggest that the mutation in *A66^{u757}* affects the development of both dHb nuclei. Concordantly, the expression pattern of the dHb marker *gng8* (Figures 2.1.E, 2.1.E') and of the vHb marker *KiSS-1 metastasis-suppressor* (*kiss1*) (Figures 2.1.F and 2.1.F') were greatly reduced in both habenulae of mutants (Amo *et al.*, 2010; deCarvalho *et al.*, 2014). In sum, the *u757* mutation causes a reduction of both dHb nuclei in comparison with siblings. Moreover, the small dHb is concurrent with a great reduction of the dHbL subdomain on both sides, and an increase of the dHbM domain on the left side, reducing its asymmetry.

To assess whether the defects observed were brain-specific, and considering viscera asymmetry is often compromised in habenular mutants, we performed WISH for a liver (*fatty acid binding protein 1a, liver*; *fabp1a)* and a pancreas (*serine protease 1*; *prss1*) markers to look for alterations in the morphology and/or laterality of these organs (Figures 2.1.B and 2.1.B') (Biemar *et al.*, 2001a; Her *et al.*, 2003). In *A66^{u757}* mutants, albeit smaller, both organs were correctly positioned along the left-right axis (Figures 2.1.B and 2.1.B'). These results suggest that the *u757* mutation affects habenular and visceral development, but not the viscera asymmetry.

Since *A66^{u757}* mutants displayed a reduction of the size of some viscera organs, we sought to understand if there were other developmental defects in this background. At 5 dpf, *A66^{u75}* mutants do not inflate the swim bladder, the pectoral fins are underdeveloped, and the anterior-most part of the head is reduced (Figures 2.1.A, 2.1.A' and Supplementary Figure 2.1.C to 2.1.E'). Moreover, at 4 dpf, mutants have smaller otoliths and about a third of these show an open choroid fissure in at least one of the eyes (Figures 2.1.A, 2.1.A', and Supplementary Figure 2.1.A to 2.1.B').

Given that anterior structures in the head of mutants are reduced in comparison to siblings, the observed reduction of the dHb could be a consequence of compromised forebrain development. To further understand how the anatomy of the brain is affected in *A66*^{u757} mutants, we performed immunohistochemistry (IHC) to reveal the general morphology of axons (acetylated tubulin, acTub) and neuropil (synaptic vesicle glycoprotein 2, SV2) (Concha *et al.*, 2000; Turner *et al.*, 2016). When compared with siblings, only two brain regions showed major alterations in *A66*^{u757} mutants: the habenula and the olfactory bulbs (OBs; Figures 1G to 1J'). The neuropil domains of the dHb were smaller in mutants than in siblings, and the neuropil was more symmetric (Figures 1G to 1J'). The OBs were significantly reduced, and the olfactory bulb fissure was not well defined in mutants (Asterisk in Figures 2.1.H and 2.1.J').

Taken together, these results suggest that the *u757* mutation affects the development of several structures in the embryo, but that in the brain it primarily disrupts the development of dorsal forebrain structures, namely the dHb and OBs.

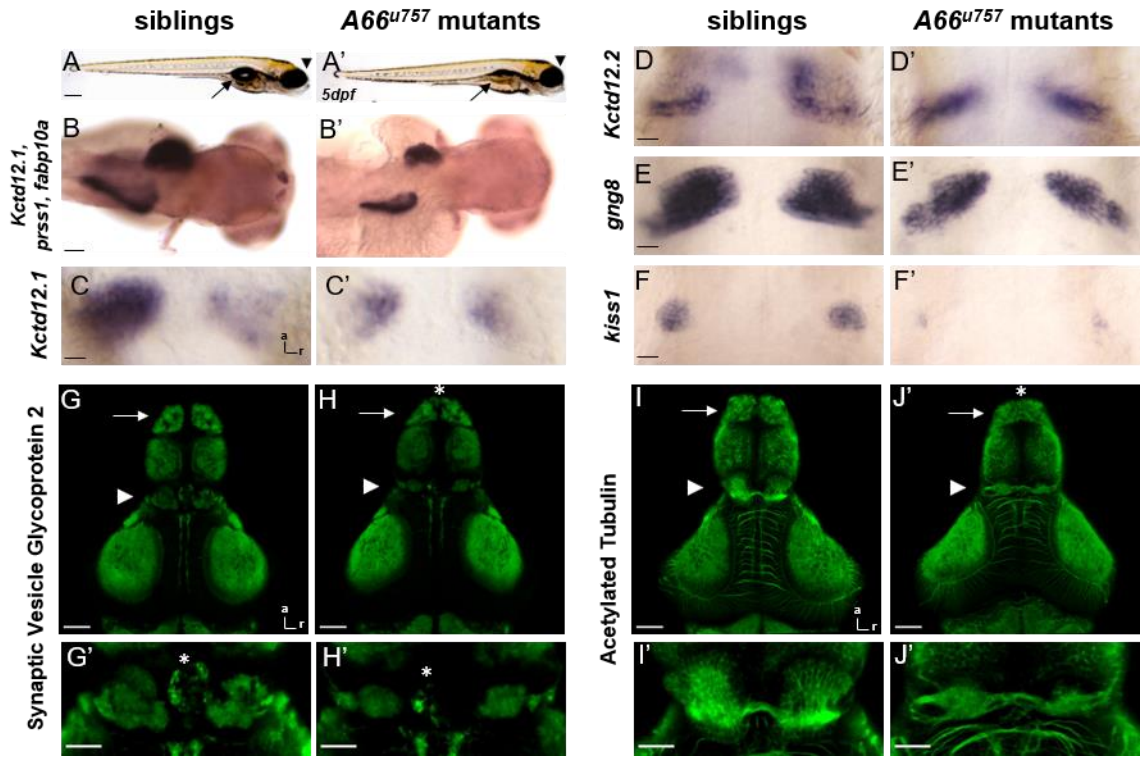

Figure 2.1. The A66u757 mutant fails to break habenular symmetry. (A-A') Lateral view of *A66*^{u757} mutant and sibling zebrafish larvae at 5dpf. **(B-B')** Dorsal view of *A66*^{u757} mutants and siblings at 4dpf, stained by WISH for markers of dHbL neurons (*kctd12.1*), liver (*fabp10a*, on the left side of the body) and pancreas (*prss1*, on the right side of the body). **(C-F')** Dorsal view of the epithalamus of *A66*^{u757} mutants and siblings at 4dpf, stained by WISH for markers of dHbL neurons (*kctd12.1*) **(C-C')**, dHbM neurons (*kctd12.2*) **(D-D')**, pan-dHb neuron marker (*gng8*) **(E-E')**, and the vHb (*kiss1*) **(F-F')**. **(G)**

and (H) Dorsal view of the midbrain and forebrain of *A66*^{u757} mutants and siblings at 4dpf, stained by IHC to reveal details of neuropil (Synaptic Vesicle 2, SV2). **(G') and (H')** Magnification of the epithalamus region of figures (G) and (H), respectively. **(F-F')**. **(I) and (J)** Dorsal view of the midbrain and forebrain of *A66*^{u757} mutants and siblings at 4dpf, stained by IHC to reveal details of axonal tracts (Acetylated Tubulin, AcTub). **(I') and (J')** Magnification of the epithalamus region of figures (I) and (J), respectively. Legend: a, anterior; r, right. Scale bar: (A-A') 500 µm; (B-B') 250 µm; (C-F') 25 µm; (G-H') 60 µm; (I-J') 30 µm.

2.2.2. u757 mutants have a nonsense mutation in the *rerea* gene

To determine the genetic lesion driving the habenular defects in *A66*^{u757} *embryos*, we performed RNA-sequencing–based mutation mapping of phenotype-sorted mutants (Supplementary Figure 2.3). This sequencing experiment was done in 2 biological replicates (from two independent generations), with 3 technical replicates per biological replicate, for each phenotype.

Pairs of heterozygous mutants were mated, and mutant progeny were selected based on their habenular phenotype at 4 dpf. To visualise the habenular phenotype *in vivo*, we used the *Et*(*gata2a:eGFP*)^{pku588} transgene. *Et(gata2a:eGFP)*^{pku588} is an enhancer trap line, predominantly expressing GFP in neurons of the dHbL (Hüsken *et al.*, 2014). Like *kctd12.1*, the transgene is enriched in the left side of the epithalamus of wild-type embryos at this stage (Figure 2.2.A). As predicted from our previous results, *A66*^{u757} mutants show reduction or absence of GFP-expressing cells in the dHb, whilst still being expressed in other region of the brain (Figure 2.2.A' and Supplementary Figure 2.1).

ENU-mediated mutagenesis creates single nucleotide polymorphisms (SNPs) (de Bruijn, Cuppen and Feitsma, 2009). Therefore, we compared the values of homozygosity of SNP variants (i.e. not previously annotated in the zebrafish reference genome 10, GRCz10) between siblings and mutants (Supplementary Figure 2.3). Here we identified the Linkage Group 23 as the one bearing the mutation. In both biological replicates, we could identify the same regions of LG23 with a high homozygosity index in mutants, while these are significantly lower in siblings (Figure 2.2.B).

An allele with a recessive SNP mutation following Mendelian inheritance has to be present in both alleles of the gene in mutants. However, it will only be present in one third of the total alleles of siblings (i.e. two out of three siblings are heterozygotes and each one carries one copy of the mutated allele, while there are six alleles in total – two from wild-types and four from heterozygotes) (Supplementary Figure 2.2). However, to

account for sample contamination due to *in vivo* screening errors, we performed the analysis to SNPs present in more than 90% of mutants and in 20-40% of siblings (Figure 2.2.B and Table 2.1). Out of these SNPs, only 13 were present in both biological replicates of the *u757* mutant line, and only 5 were in a coding sequence: 1 in the gene *myosin, heavy chain 7B, cardiac muscle, beta b (myh7bb)*; 1 in the gene *noc2-like nucleolar associated transcriptional repressor* (*noc2l)*; and 3 in the *rerea*.

The SNP in *myh7bb* causes a synonymous mutation, which is unlikely to lead to a phenotype, while the one in *noc2l* leads to a missense mutation predicted to be tolerated *in silico* (Table 2.1). Lastly, two of the SNPs identified in the *rerea* gene lead to a synonymous mutation, while the third one is a nonsense mutation in exon 18 of 21 (Figures 2.2.C to 2.2.C'' and Table 2.1). The identified 4122, cytosine to thymine mutation in *rerea* is predicted to result in a truncated protein, with loss of 158 amino acids in the C-terminus of the protein. This alteration is more likely to lead to a protein disruption than any of the remaining candidates, given it predictably abrogates a conserved atrophin domain of the Rerea protein (Plaster *et al.*, 2007).

Rerea is a transcription coregulator that consists of 5 conserved domains: the Bromo adjacent homology (BAH), the Egl-27 and MTA1 homology 2 (ELM2), the SWI3/ADA2/N-CoR/TFIII- B (SANT), the Gata zinc-finger (GATA) and the Atrophin domains (Plaster *et al.*, 2007). Together, the first four domains resemble those found in the Metastasis Associated 1 Family Member 2 (Mta2), a protein that scaffolds a repressive chromatin remodelling complex (Bowen *et al.*, 2004; Shen *et al.*, 2007). However, the function of the atrophin domain, which is affected in the *A66*^{u757} mutant, remains elusive. Nevertheless, Rerea was shown to inhibit the expression of *fgf8* in zebrafish (Plaster *et al.*, 2007). Given that *fgf8* is involved in the formation of the dHb, the mutation in the *rerea* gene of *A66*^{u757} mutants is a strong candidate to affect the development of the dHb.

To confirm that partial loss of the atrophin domain of Rerea would lead to a habenular development phenotype, we attempted to generate a second *rerea* mutant allele by a CRISPR-Cas9 approach to target the exon 18 of this gene (Hsu, Lander and Zhang, 2014). Screening for *indels* with High-Resolution Melt Analysis, we identified F0 fish with mutations in the targeted region, however, further sequencing proved that the F1 progeny did not carry any mutations (data not shown) (Samarut, Lissouba and Drapeau, 2016).

To further assess if loss of Rerea in zebrafish would affect habenular development, we knocked-down the expression of *rerea* using a morpholino approach. Although *rerea* knock-down successfully mimicked the head phenotype observed in *A66*^{u757} mutants, and lower penetrance defects such as closer otoliths and coloboma, morphants failed to

show any detectable habenular phenotype, as ascertained by in vivo screening of morpholino injected *Et(gata2a:eGFP)*^{pku588} fish (Supplementary figure 2.4 and data not shown). The lack of habenular phenotype in *rerea* morphants could be explained by the fact that the late mutation in the gene only leads to a partial loss of function of the protein (see discussion).

In spite of these negative results, we performed phenotypic analysis of embryos genotyped by KASP for the 4122 C>T *rerea* SNP. This experiment confirmed that embryos carrying two copies of the predicted *rerea* mutation show full penetrance of the aforementioned habenular phenotype (data not shown).

Taken together, these results strongly suggest that the 4122 C>T SNP found in exon 18 of *rerea* is likely to be the causative lesion that leads to loss of habenular asymmetry in *A66*^{u757}. We will, therefore, refer to this novel mutant line as *rerea*^{u757} from hereafter.

Table 1.1. The rerea gene has a predicted nonsense mutation. Table with the values obtained after mRNA sequencing and SNP analysis. The SIFT (Sorting Intolerant From Tolerant) algorithm was used to calculate if the *noc2l* missense mutation was tolerated (i.e. if the amino acid alteration was deleterious (SIFT < 0.05) or not (SIFT ≥ 5).

Location (GRCz10)	Gene Name / Genomic Region	Reference/Altered Nucleotide	Frequency of altered nucleotide in Mutants	Frequency of altered nucleotide in Siblings	Affected Genic Region	Consequence	SIFT
14,477,732	**Intergenic region**	A/G	1.00	0.21	N.A.	N.A.	N.A.
18,821,212	**myh7bb**	G/A	0.94	0.32	exon	Synonymous Variant	N.A.
20,222,275	**usp19**	A/T	1.00	0.25	intron	N.A.	N.A.
22,996,506	**rerea**	A/G	0.98	0.29	exon	Synonymous Variant	N.A.
22,996,575	**rerea**	C/T	0.95	0.28	exon	Synonymous Variant	N.A.
22,997,005	**rerea**	C/T	0.94	0.21	exon	Stop Gained	N.A.
23,211,397	**noc2l**	C/A	0.93	0.26	exon	Missense Variant	Tolerated (0.18)
28,790,451	**Intergenic region**	C/A	0.93	0.33	N.A.	N.A.	N.A.
30,965,404	**Intergenic region**	T/C	0.96	0.33	N.A.	N.A.	N.A.
31,451,924	**Intergenic region**	T/C	1.00	0.36	N.A.	N.A.	N.A.
31,451,925	**Intergenic region**	G/T	1.00	0.36	N.A.	N.A.	N.A.
31,516,237	**eya4**	A/G	1.00	0.25	intron	N.A.	N.A.
31,516,252	**eya4**	T/A	1.00	0.20	intron	N.A.	N.A.

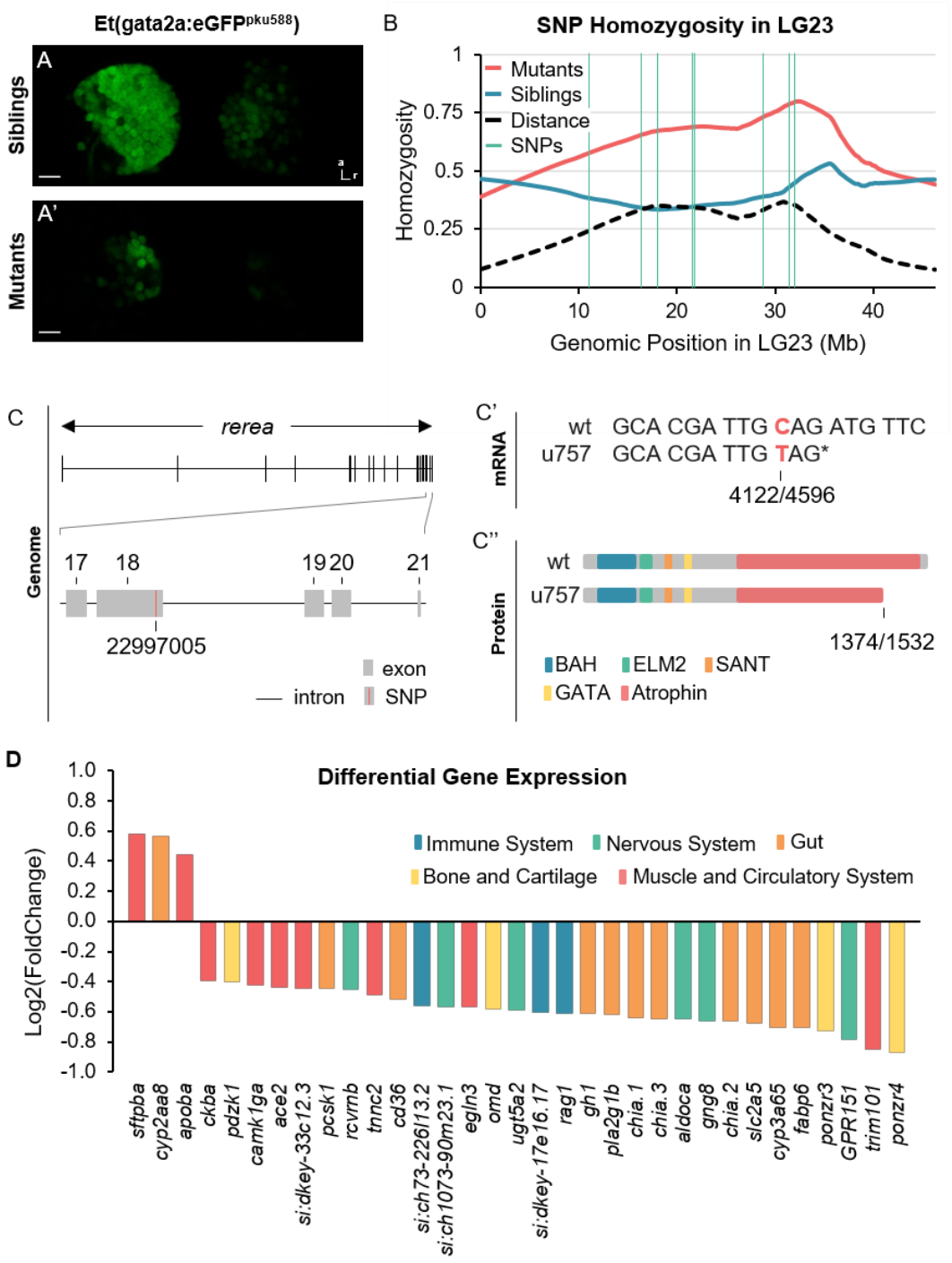

Figure 2.2. The u757 mutation maps to exon 18 of the rerea gene. (A-A') Dorsal view of the epithalamus of 4 dpf, *A66*^{u757} mutants carrying the transgene *Et(gata2a:eGFP)*^{pku588}, immuno-stained for GFP (green). Scale bar: 10 µm. Legend: a, anterior; r, right. **(B)** Homozygosity ratio of mutants (red) and siblings (blue) in the Linkage Group 23 (LG23), obtained from the frequency of new SNPs found by RNA-seq. The distance between both homozygosity ratios is in dashed (black). SNPs of interest (green) were found in more than 90% of mutants and between 20 and 40% of siblings in two distinct generations of the *u757* line. **(C)** Scheme of the *rerea* gene in the LG23 with a SNP mutation found in the exon 18 (out of 21) of *u757* mutants. **(C')** Scheme of the

SNP mutation in the *rerea* mRNA and of the consequent formation of an early stop codon. **(C'')** Scheme of the altered Rerea protein resultant of the early stop codon. The last 158 amino acids are not present in the mutated form and this only affects the Atrophin domain of the protein. **(D)** Genes being differentially expressed between siblings and mutants, colour-coded by the systems these are involved in. Positive values represent gene upregulation and negative values represent downregulation. (adjusted p-value < 0.05).

2.2.3. *rerea*$^{u757/u757}$ mutants show downregulation of dHb markers

Mapping the *u757* lesion through an RNA sequencing approach also allowed us to study the effect of this mutation on the expression levels of different genes (Figure 2.2.D). At 4 dpf, we could identify 3 genes that were significantly upregulated, while 30 genes were significantly downregulated in mutants (Figure 2.2.D, adjusted p-value < 0.05). All genes fell under one of five ontological categories: 11 genes were involved in gut development or function (1 of these was upregulated); 9 genes were involved in muscle or the circulatory system (2 of which were upregulated); 6 with the nervous system, 4 with bone and cartilage and 3 with the immune system.

In this experiment, we could identify the pan-dHb marker *gng8* as one of the most significantly downregulated genes in *u757* mutants (Figure 2D). Worth noting, the *G protein-coupled receptor 151* (*gpr151)*, a marker of medial dHb neurons, also was downregulated in *rerea*^{u757} mutants (Chou *et al.*, 2016). In fact, these findings are in line with our previous observation that all dHb fates are compromised in *rerea*^{u757} mutants and increase our confidence in the obtained RNA-sequencing data.

We also found that *recoverin b* (*rcvrnb)*, a marker of pineal photoreceptors, is downregulated in *rerea*^{u757} mutants, concordant with forebrain fates being affected in these fish (Schredelseker and Driever, 2018). Furthermore, the *proprotein convertase subtilisin/kexin type 1* (*pcsk1)* and the *phospholipase A2, group IB* (pancreas) *pla2g1b* genes, involved in the pancreas development, are also downregulated (Hama *et al.*, 2009; Tarifeño-Saldivia *et al.*, 2017). Additionally, the *plac8 onzin related protein 3* (*ponzr3)* and *4* (*ponzr4)* are involved in the development of the pharyngeal arches and are amongst the most downregulated genes in *rerea*^{u757} mutants (Bedell *et al.*, 2012). This result is in line with *rerea*^{tb210} mutants having pharyngeal arch development defects (Plaster *et al.*, 2007; Le Pabic, Ng and Schilling, 2014). However, *rerea*^{u757} mutants do not show major defects in the pharyngeal arches, as ascertained with Alcian Blue stain for chondrocytes (data not shown). As mentioned above, this could be explained by the different nature of the mutations found in the *rerea*^{tb210}, *rerea*^{ru622} and *rerea*^{u757}alleles.

2.2.4. dHb afferent and efferent connectivity is affected in *rerea*^{u757} mutants.

In zebrafish, a subset of mitral cells of the olfactory bulb (OB) project specifically to the right habenula (Figures 2.3.A, 2.3.A', 2.3.C and 2.3.C') (Miyasaka *et al.*, 2009). To assess if these projections were affected in rerea^{u757} mutants, we imaged embryos in the Tg(*lhx2a:GFP*)^{zf176Tg} background, a transgenic line that expresses GFP in the membrane of OB mitral cells (Figures 2.3.B, 2.3.B', 2.3.D and 2.3.D') (Miyasaka *et al.*, 2009). Consistent with previous results, the OB was reduced in mutants and the inter-olfactory bulb fissure was malformed (Figures 2.3.B and 2.3.B'). Additionally, in contrast with siblings, the mitral cells of rerea^{u757} mutants did not cross through the anterior commissure (arrows; Figures 2.3.B and 2.3.B'). However, mitral cells still projected to the right dHb, despite the axonal terminals being much smaller than in siblings (Figures 2.3.B, 2.3.B', 2.3.D and 2.3.D').

Zebrafish larvae with a smaller or absent parapineal or with parapineal axonal defects develop symmetric habenulae with right-side character (Snelson et al., 2008; Lekk I. and Wilson S.W. unpublished data). Since rerea^{u757} mutants show an increased expression of dHbM markers in the left epithalamus, we probed if their parapineal development was affected. To test this, we imaged rerea^{u757} mutants and siblings in the Tg(*foxd3:GFP;flh:GFP*)^{zf104,u711} background, which expresses GFP in the pineal complex from early developmental stages (Figure 4) (Concha *et al.*, 2003; Snelson, Burkart and Gamse, 2008). At 50 hpf, the parapineal of siblings (n=6/7) has delaminated from the pineal organ, had migrated to the left side of the pineal and elaborated a few projections towards the left dHb nucleus (Figure 2.4.A). In mutants, however, the parapineal was either absent (n=6/11) or migrated closer to the pineal than in siblings (n=5/11) (Figure 2.4.A' and 2.4.B'). Furthermore, parapineal projections were rarely visible in *rerea*^{u757} mutants (asterisk, Figure 2.4.A'). Additionally, the pineal organ was smaller than in siblings (Figures 2.4.A' and 2.4.B'). However, it was unlikely that the parapineal defects were due to a delay in development, since at this timepoint *rerea*^{u757} mutants already displayed differentiated pineal projecting neurons, as marked by SV2 (arrow, Figure 2.4.B). Rather, the pineal complex defects were likely a consequence of a dorsal diencephalon developmental defect in *rerea*^{u757} mutants.

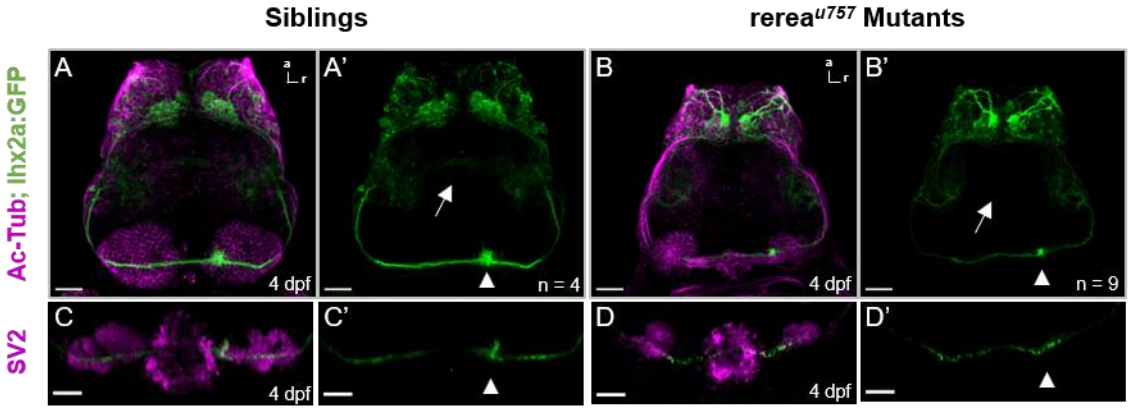

Figure 2.3. The projections from lhx2a-positive mitral cells of the olfactory bulb to the right habenula are defective in rereau757 mutants. (A-B') Dorsal view of the forebrain of 4dpf siblings and *rerea*^{u757} mutants carrying the transgene Tg(lhx2a:GFP)^{zf176Tg} immuno-stained for GFP (green) and acetylated tubulin (magenta). Arrows mark the anterior commissure and arrow heads mark the (putative) point of contact with the right habenula. **(C-D')** Dorsal detailed view of the epithalamus of 4 dpf siblings and *rerea* mutants carrying the transgene Tg(lhx2a:GFP)^{zf176Tg} immuno-stained for GFP (green) and synaptic vesicle glycoprotein 2 (SV2, magenta). Arrow heads mark the (putative) point of contact with the right habenula. Scale bar: 20 µm.

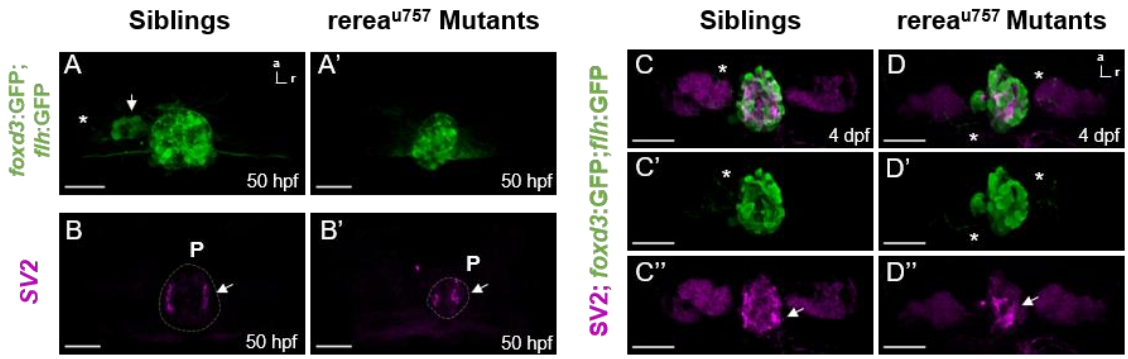

Figure 2.4. The development of the pineal complex is defective in rerea mutants. (A-A') Dorsal view of the epithalamus of 50 hpf *rerea*^{u757} mutants (n = 11) and siblings (n = 7) carrying the transgene Tg(*foxd3:GFP;flh:GFP*)^{zf104,u711} immuno-stained for GFP. Arrow points at the parapineal and the asterisk indicates the parapineal axons to the left habenula. In the mutant in (A'), no parapineal structure could be discerned from the pineal. **(B-B')** Dorsal view of the epithalamus of 50 hpf *rerea*^{u757} mutants (n = 3) and siblings (n = 1) immuno-stained for the Synaptic Vesicle Glycoprotein 2 (SV2, magenta). **(C-D'')** Dorsal view of the epithalamus of 4 dpf *rerea*^{u757} siblings (**C- C''**, n = 4) and mutants (**D-D''**, n = 7) carrying the transgene Tg(*foxd3:GFP;flh:GFP*)^{zf104,u711} immuno-

stained for GFP (green) and SV2 (magenta). Asterisks mark projections of the parapineal to the dHb and arrows mark the projecting neurons of the pineal. Legend: a, anterior; P, pineal; pp, parapineal; r, right; Scale bar: (A-B') 30 um; (C-D'') 20um.

To assess if the parapineal defects observed in *rerea*^{u757} mutants at 50 hpf persisted in later time points, we looked at the morphology of the pineal complex in siblings and mutants at 4 dpf. As previously described, the parapineal of 4 dpf siblings occupied a ventral leftwards position in relation to the pineal (n=4/4; Figure 2.4.C) (Bianco *et al.*, 2008). However, in *rerea*^{u757} mutants the parapineal cells were either undetectable (n=3/7, data not shown), dispersed (n=1/7, data not shown) or had failed to assume a more ventral position and remained on the left side of the pineal (n=3/7; Figure 2.4.D'). When a parapineal was present, its projections were found to targeted the left dHb (n=2/3) or both dHb nuclei (n=1/3; Figure 2.4.D'). Additionally, the pineal of mutants was often smaller or developed with an abnormal shape (Figures 2.4.D to 2.4.D''). Moreover, its projection neurons, which in siblings occupied the most lateral parts of the pineal, were ectopically positioned in mutants (Figures 2.4.C'' and 2.4.D'').

During development, both dHb sub-nuclei innervate the Interpeduncular Nucleus (IPN) (Bianco *et al.*, 2008). Neurons of the dHbL (enriched on the left side) project to the dorsal IPN (dIPN) and intermediate IPN (iIPN) while the dHbM neurons (enriched in the right side) project to the ventral IPN (vIPN) (Aizawa *et al.*, 2005; Gamse *et al.*, 2005; Kuan *et al.*, 2007). By labelling the left and right habenula nucleus with the lipophilic dyes DiI and DiD, respectively, we visualised projections from the left habenula to the dIPN, and projections from the right habenula to the vIPN of 4 dpf siblings (Supplementary Figures 2.4.A to 2.4.A'''). However, the precise labelling of the habenular nucleus of mutants was challenging due to its small size. Despite this limitation, we were able to successfully label the habenular efferent projections of one *rerea*^{u757} mutant in which both left and right habenulae projected to the vIPN (Supplementary Figures 2.4.B to 2.4.B''').

In summary, the projections from the mitral cells of the OB still project to the right dHb in *rerea*^{u757} mutants, despite the projections being greatly reduced. On the other hand, when present, the parapineal cells were found to target the left or both nuclei, and the axonal efferents from the dHb to the IPN seem to only target the vIPN in *rerea*^{u757} mutants. In this study we did not address whether this is a direct result of the mutation or a consequence of the dysregulation of gene expression from the small dHb nucleus of mutants.

2.2.5. dHb progenitor domains are reduced in *rerea*^{u757} mutants

The reduced number of differentiated dorsal habenular neurons observed at 4 dpf in *rerea*^{u757} mutants could be explained in one of three ways: a failure to specify dHb progenitors; a reduction in proliferation of these cells; or a failure in the differentiation of dHb neurons from the progenitor pool. To investigate if the habenular progenitor domain is correctly specdified in *rerea*^{u757} mutants, we examined the expression of *dbx1b*, a marker for dorsal habenula progenitors, at critical developmental time-points (Figure 2.5) (Dean *et al.*, 2014). In siblings, *dbx1b* was expressed in the presumptive diencephalon from 24 hpf (Figures 2.5A, 2.5.C and 2.5.C''). This expression domain was broader at 36 hpf (Figures 2.5.B', 2.5.D, 2.5.D''). Then, at 48 hpf, there was a residual domain of *dbx1b* expression in the medial ventricular area of the epithalamus, which corresponded to a pool of habenular progenitor cells that feed the habenular growth until late stages of development (Figures 2.5.B'', 2.5.E and 2.5.E'') (Roberson and Halpern, 2017a). However, in 24 hpf *rerea*^{u757} mutants, the habenular expression of *dbx1b* was markedly reduced, and sometimes undetectable (Figures 2.5.B, 2.5.F and 2.5.F''). Moreover, despite the *dbx1b* expression domain becoming broader in the presumptive habenula at 36 and 48 hpf, it was usually smaller than in siblings (Figures 2.5.D'', 2.5.E'', 2.5.G'' and 2.5.H''). Of note, the *dbx1b* expression in other brain regions of *rerea*^{u757} mutants remained comparable to siblings, suggesting a specific defect of the specification of habenular progenitors (Figures 2.5.A to 2.5.B''). These results suggest that the small dHb nuclei of *rerea*^{u757} mutants could be due to a reduced habenular progenitor domain.

To understand if the reduced habenular progenitor domain size was accompanied with a delay in habenular differentiation, we performed WISH for *cxcr4b*, a transient marker for newly generated habenula neurons (Figures 2.5.C to 2.5.H'') (Roberson and Halpern, 2017a). In siblings, expression of *cxcr4b* was visible in presumptive pineal cells at 24 hpf and very faintly in the left epithalamus (arrow; Figure 2.5.C'). At 36 hpf, the expression became stronger on both sides and by 48 hpf it became largely symmetric and encompassed all the dHb domain (Figures 2.5.D' and 2.5.E'). Moreover, at 48 hpf the expression was mutually exclusive from *dbx1b* in the most lateral portions of the habenular nuclei, presumably as cells progress from a progenitor to a differentiated dHb status (Figures 2.5.E to 2.5.E'').

As with siblings, in mutants the expression of *cxcr4b* was present in the presumptive pineal. However, pineal cells were more densely packed in *rerea*^{u757} mutants than what was observed in siblings (Figures 5C' and 5F'). Additionally, at this time point no expression was seen in the presumptive habenula. At 36 hpf, the *cxcr4b* expression became evident in the most lateral portions of the habenula anlage (arrow; Figure 5G'). Finally, like in siblings, at 48 hpf *cxcr4b* is expressed by most cells in the habenula

domain and is stronger in the lateral portion of the habenular nuclei, where *dbx1b* is less expressed (Figures 2.5.H to 2.5.H'). These results indicate that, despite the habenular progenitors' specification occurring later in *rerea*^{u757} mutants, by 48 hpf most cells have initiated neuronal differentiation – like in siblings. This suggests that the molecular mechanisms responsible for determining timing of habenula neurogenesis remains largely unaffected in *rerea*^{u757} mutants. Given the significantly smaller pool of habenular progenitors in mutants, and since neurogenesis onset is unaffected, the smaller habenular nuclei of *rerea*^{u757} mutants might be explained by a precocious depletion of the available pool of progenitor cells.

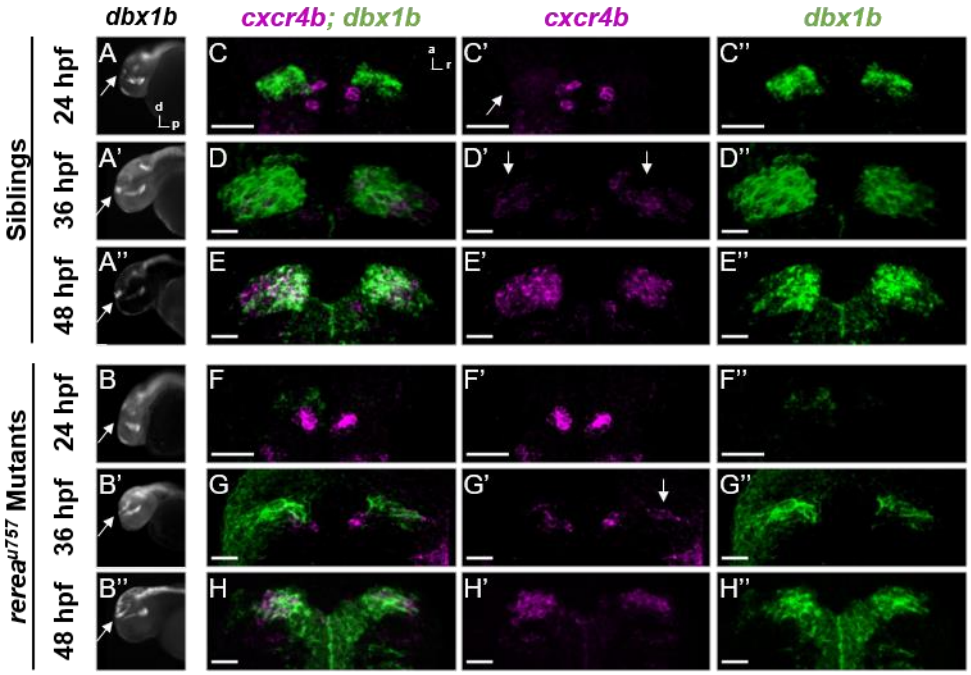

Figure 2.5. rereau757 mutants have a smaller pool of habenular progenitors. (A-A'') Lateral view of the head of 24, 36 and 48 hpf siblings, stained by WISH for *dbx1b* (white). Arrow marks the *dbx1b* expression in the epithalamus. **(B-B'')** Lateral view of the head of 24, 36 and 48 hpf *rerea*^{u757} mutants, stained by WISH for *dbx1b* (white). Arrow marks the *dbx1b* expression in the epithalamus. **(C-H'')** Dorsal view of the presumptive epithalamus of 24, 36 and 48 hpf (C-E'') siblings and (F-H'') *rerea*^{u757} mutants stained by WISH for *cxcr4b* (magenta) and *dbx1b* (green). Arrows mark the expression of cxcr4b in the presumptive habenula.

2.2.6. Expression of *fgf8* is broader in the presumptive diencephalon of *rerea*^{u757} mutants

The *rerea* gene has previously been shown to inhibit the FGF pathway through direct interaction with HDACs (Asai *et al.*, 2006; Plaster *et al.*, 2007). In the *rerea*^{ru622} mutant, there is an increase in *fgf8* expression at 24 hpf, which is observable by WISH as a broader pattern in the facial ectoderm (FEC), diencephalon and mid-hindbrain boundary (MHB) (Asai *et al.*, 2006). Also, these mutants show ectopic expression in the otic vesicles, where high levels of *fgf8* in the otic vesicle are only seen from 36 hpf in wild-type larvae (Reifers *et al.*, 1998). Since increased levels of *fgf8* expression delays expression of *dbx1b* in the epithalamus we sought to analyse its expression in *rerea*^{u757} mutants through WISH (Figure 2.6). At 24 hpf, siblings express *fgf8* in the FEC, presumptive diencephalon and in the MHB (Figures 2.6.A and 2.6.A'). At this time-point, *rerea*^{u757} mutants express *fgf8* in the FEC, diencephalon and MHB, similarly to siblings, but also show ectopic expression of *fgf8* in the otic vesicles (Figures 2.6.C to 2.6.D'). To further investigate any differences in the domain of expression of *fgf8* in the dorsal diencephalon, we performed fluorescent WISH and measured the volume and area of *fgf8* expression pattern. We found that the volume of *fgf8* expression was significantly increased in mutants when compared to siblings and that the area of expression showed a strong tendency to be increased (t-Test, $p<0.05$ for volume and $p=0.05$ for area; Figures 2.6.E and 2.6.E'). Together, these results suggest that the *fgf8* expression is increased in *rerea*^{u757} mutants at 24 hpf, a time point that can affect the development of the pineal complex and of the habenular progenitors.

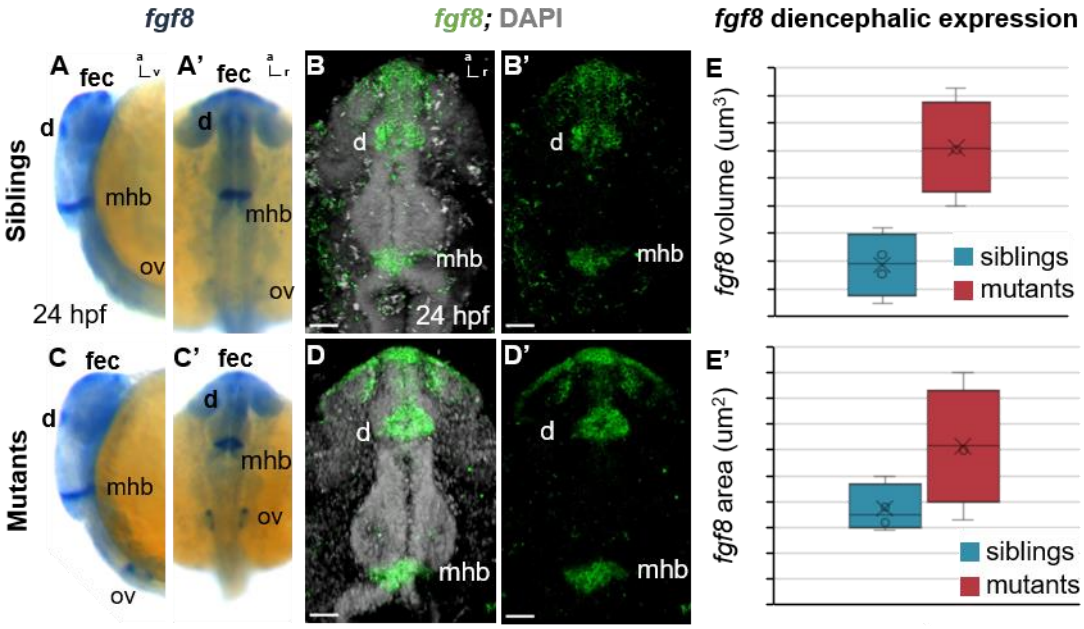

Figure 2.6. fgf8 expression is expanded in the diencephalon of rereau757 mutants. **(A-A')** Lateral (A) and dorsal (A') view of 24 hpf siblings stained by WISH for *fgf8* (dark blue). **(B-B')** Dorsal view of 24 hpf siblings stained by WISH for *fgf8* (green) and DAPI (grey). **(C-C')** Lateral (A) and dorsal (A') view of 24 hpf *rerea*^{u757} mutants stained by WISH for *fgf8* (dark blue). **(D-D')** Dorsal view of 24 hpf *rerea*^{u757} mutants stained by WISH for *fgf8* (green) and DAPI (grey). **(E-E')** Measurement of the *fgf8* expression (E) volume and (E') area in the presumptive diencephalon of siblings and *rerea*^{u757} mutants, as seen in (B') and (D'). t-Test: two sample assuming equal variances, p=0.00341 for volume and p=0.05068 for area. **Scale bar:** 50 um. **Legend: a**, anterior; **v**, ventral; **r**, right; **d**, presumptive diencephalon; **fec**, facial ectoderm; **mhb**, midbrain hindbrain boundary; **ov**, otic vesicle.

2.3. DISCUSSION

Forward genetic studies are a good approach to dissect new molecular pathways that affect habenular development. In this study, we have identified a novel mutation in the *rerea* gene, *rerea*^{u757}, which results in a truncated version of the Rerea protein. At 24 hpf, *rerea*^{u757} mutants have an expanded expression of *fgf8* in the diencephalon. We pose that this ectopic expression delays the specification of habenular progenitors, which ultimately leads to the formation of smaller dHb by 4dpf. Moreover, the dHb of *rerea*^{u757} mutants also develops a bigger dHbM than dHbL on both sides, possibly due to a delay of habenular progenitor specification combined with the malformation of the parapineal. In this section we will discuss how the *rerea*^{u757} mutation may be affecting *fgf8* expression, how this molecular interplay may affect the development of the habenula, and which further experiments will test our current hypothesis.

2.3.1. The *rerea*^{u757} mutant phenotype resembles habenular progenitor misspecification mutants

In *rerea*^{u757} mutants, the dHb and vHb domains are greatly reduced when compared with the habenula of siblings (Figure 2.1). This phenotype is likely to be a consequence of the delay in the formation of the habenular progenitors, as was demonstrated by the expression of *dbx1b* (Figure 2.5). This phenotype in *rerea*^{u757} mutants resembles that of *med12, fgf8* and *wls* mutants (Regan *et al.*, 2009; Dean *et al.*, 2014; Kuan *et al.*, 2015). However, in *med12* mutants, *dbx1b* is only detected at 48 hpf, while in *rerea*^{u757} mutants this expression is present at least from 36 hpf (Wu *et al.*, 2014). Moreover, at 4 dpf, the habenulae of *rerea*^{u757} mutants expresses dHb markers (Figure 2.1), whereas *med12* mutants do not (Wu *et al.*, 2014). Therefore, *med12* is probably unrelated to the mechanism that drives the habenular phenotype in *rerea*^{u757} mutants or is an exacerbated phenotype of the same pathway.

On the other hand, the *rerea*^{u757} mutant resembles the *wls* and *fgf8* mutants. In wls mutants, *dbx1b* expression is delayed to about 27 hpf, while in *fgf8* mutants, *dbx1b* is expressed after 28 hpf (Dean *et al.*, 2014; Kuan *et al.*, 2015). Also, both *wls* and *fgf8* mutants form a smaller habenula with reduced expression of dHb markers (Regan *et al.*, 2009; Kuan *et al.*, 2015). However, habenular asymmetry is preserved in *wls* mutants, while in *fgf8* mutants the dHb nuclei are usually symmetric because the parapineal cells do not migrate from the midline (Regan *et al.*, 2009; Kuan *et al.*, 2015). In resemblance to the *fgf8* mutant, the dHbL of *rerea*^{u757} mutants is smaller than in siblings, and both the formation and migration of the parapineal are defective (Figures 2.1 and 2.4). However, while in *fgf8* mutants there is downregulation of the FGF pathway, in the *rerea*^{u757} mutant there is a broadening of the *fgf8* expression pattern, which suggests that the FGF

pathway is actually hyperactivated (Figure 2.6) (Regan *et al.*, 2009; Dean, Gamse and Wu, 2018). These seemingly contradictory results were also seen in other *rerea* mutants (Asai *et al.*, 2006; Plaster *et al.*, 2007). In mice and zebrafish, Rerea was shown to repress *fgf8* expression (Plaster *et al.*, 2007; Vilhais-Neto *et al.*, 2010). However, in the zebrafish *rerea*^{ru622} mutants the expanded pattern of *fgf8* was concordant with increased mRNA levels of FGF-feedback-induced antagonists (Asai *et al.*, 2006). This suggests that in *rerea* mutants, the overexpression of *fgf8* triggers the expression of FGF antagonists to inhibit the pathway (Asai *et al.*, 2006). In fact, the injection of a morpholino to inhibit the FGF antagonist *interleukin 17 receptor D* (*il17rd*, formerly *sef*), recovered the wild-type development of the otic vesicle in *rerea*^{ru622} mutants (Asai *et al.*, 2006).

To test if the overexpression of *fgf8* in *rerea*^{u757} mutants leads to an inactivation of the FGF pathway during the critical timepoints for habenular progenitors and parapineal development, we propose three experiments. Firstly, we will perform quantitative PCR for *fgf8* and known FGF-feedback-induced antagonists (such as *il17rd* and *sprouty homolog 4*, *spry4*) between 24 hpf and 36 hpf, to see if these genes are upregulated in the *rerea*^{u757} mutant. Secondly, we will monitor the activity of the FGF pathway in the diencephalon of *rerea*^{u757} mutants between 24 and 36 hpf with the FGF reporter Tg(*dusp6:d2EGFP*)^{pt6} (Molina, Watkins and Tsang, 2007). In this reporter, a destabilised version of GFP is expressed under the control of the promotor of the *dual specificity phosphatase 6* (*dusp6*) gene, which is another FGF-feedback-induced antagonist of the pathway (Molina, Watkins and Tsang, 2007). This experiment will give specific information about the activity of the FGF pathway in the diencephalon of *rerea*^{u757} mutant larvae *in vivo*. Lastly, we will repeat the *il17rd* morpholino experiments in the *rerea*^{u757} mutants, to test if the downregulation of FGF antagonists recovers the epithalamic phenotype (Asai *et al.*, 2006).

2.3.2. Is the increased dHb symmetry driven by delayed habenular progenitor formation?

During neurogenesis of the wild-type dHb, most progenitors that differentiate at 32 hpf become dHbL neurons while those that differentiate at 48 hpf become dHbM neurons (Aizawa *et al.*, 2007). Since neurogenesis starts first on the left side then on the right, most left dHb neurons become dHbL while most right dHb neurons become dHbM (Aizawa *et al.*, 2007). Mutations that promote early neurogenesis of dHb cells, such as mutations that downregulate Notch signalling or drug-treatments that decrease, but do not abolish, FGF activity, lead to the symmetric formation of dHbL neurons in both habenular nuclei (Aizawa *et al.*, 2007). On the other hand, delaying neurogenesis, for example by hyperactivating Nodal or FGF signalling pathways, results in the formation of right-isomerized dHb (Itoh *et al.*, 2003; Aizawa *et al.*, 2007).

The decrease of the dHbL in both nuclei and the increase of dHbM in the left dHb of *rerea*^{u757} mutants suggests that most habenular progenitors start differentiating during the second neurogenic wave (Figure 1). Since in *rerea*^{u757} mutants, the habenular progenitors are formed later than in siblings, it is possible that there are fewer progenitor cells available to initiate neurogenesis at 32 hpf, and that most cells differentiate at 48 hpf (Figure 2.5). Supporting this hypothesis, is the expression of *cxcr4b* in *rerea*^{u757} mutants that is already present at 36 hpf and in most habenular cells at 48 hpf (Figure 2.5). Since *cxcr4b* is expressed in cells committed to become dHb neurons, this result suggests that it is not the timing of neurogenesis per se that is affected, but the availability of progenitor cells.

Thus, to understand when neurogenesis happens in *rerea*^{u757} mutants, we will perform Bromodeoxyuridine / 5-bromo-2'-deoxyuridine (BrdU) pulse-labelling experiments (Aizawa *et al.*, 2007). In this experiment, the aim is to mark all cells that stop dividing and started neuronal differentiation during the first (32 hpf) or second (48 hpf) waves of neurogenesis. This is achieved by a short period incubation of living larvae in a BrdU solution which only labels cells in M-phase (Hsu, 2015). Then, during development, the cells that keep proliferating (i.e. the habenular progenitors) dilute their BrdU content between daughter cells while differentiated cells keep high levels of BrdU (Hsu, 2015). This way, at 4 dpf, we can fate-map Hb progenitors that underwent final differentiation at the time of the given BrdU pulse time, by colocalising BrdU positive cells with dHbL or dHbM markers (Aizawa *et al.*, 2007).

To complement these results, we will also test when neurons are fully differentiated in the dHb. This can be achieved by detecting the expression of the neuronal marker ELAV like neuron-specific RNA binding protein 3 (Elavl3) in the presumptive diencephalon of *rerea*^{u757} mutants between 24 and 52 hpf (Colombo *et al.*, 2013).

Nevertheless, we have to bear in mind that the parapineal development is also affected in *rerea*^{u757} mutants, and this structure has a great impact on habenular asymmetry development (Concha *et al.*, 2003; Gamse, 2003; Bianco *et al.*, 2008). For instance, in *fgf8* mutants, the small symmetric habenula seems to be the result of effects of the FGF pathway in both the habenular formation and specification of habenular progenitors (Neugebauer and Yost, 2014). However, it is very likely that it is the combination of the parapineal-induced asymmetry cues with the asymmetric neurogenesis that drives dHb asymmetry. Therefore, both events seem to be essential for the formation of an asymmetric habenula and it may be impossible to separate them for this study.

2.3.3. The connectivity of the dHb of rerea^{u757} mutants suggests the preservation of some, but not all, diencephalic asymmetries.

In wild-type zebrafish, the mitral cells of the olfactory bulbs project to a specific subdomain of the right dHbL, which expresses the gene *family with sequence similarity 84 member B* (*fam84b*) (Miyasaka *et al.*, 2009; deCarvalho *et al.*, 2013). In *rerea*^{u757} mutants, despite the size and domain changes of the dHb, the mitral cells still project to the right dHb. Since in right-isomerized dHb mutants, *fam84b* is bilaterally expressed and mitral cells project to both habenular nuclei, this suggests that despite the reduction of dHbL in *rerea*^{u757} mutants, *fam84b* populations are still present on the right side (deCarvalho *et al.*, 2013). Although we did not test this hypothesis, it would be interesting to assess if this population is still restricted to the right dHb of *rerea*^{u757} mutants.

With the defective development of the parapineal in *rerea*^{u757} mutants it becomes difficult to understand if this structure is able to project correctly to the left dHb (Gamse, 2003). We did find two cases where the parapineal projected to the left dHb, but one of the mutants showed projections to both habenular nuclei (Figure 2.4). This is likely to be caused by the reduction of the left dHbL, to which the wild-type parapineal projects to (Figure 2.1) (Taylor *et al.*, 2011).

Due to the asymmetric representation of the dHbL and dHbM domains in the dHb of wild-type larvae, the left and right dHb nuclei send laterotopic projections to the dorsal and ventral IPN, respectively (Aizawa *et al.*, 2005; Gamse *et al.*, 2005; Kuan *et al.*, 2007; Bianco *et al.*, 2008). Despite the difficulties in labelling these projections due to the small habenula of *rerea*^{u757} mutants, we were successful in labelling the projections of one mutant larva. In this larva, very few axons reached the IPN, probably due to the smaller dHb nuclei consisting of less neurons (Supplementary figure 2.5). Moreover, since there was an increase in the population of dHbM and a reduction of dHbL neurons, most projections targeted the vIPN, as is expected of dHbM neurons of wild-type fish (Aizawa *et al.*, 2005; Gamse *et al.*, 2005; Bianco *et al.*, 2008). Despite obtaining the expected results, we need to increase the number of biological replicates to validate this result.

2.3.4. How would the *rerea*^{u757} mutation affect *fgf8* expression?

Rerea is a coregulator of nuclear receptors (NRs) (Plaster *et al.*, 2007; Vilhais-Neto *et al.*, 2010). Rerea works as a bridge between the NRs and Histone Acetyltransferases (HATs) to promote gene expression, or Histone Deacetylases (HDACs) to inhibit expression (Sever and Glass, 2013). COUP-TF and Tlx are NRs shown to interact with Rerea through a very conserved sequence of amino acids (ALRTLSEY) in the atrophin domain (Wang *et al.*, 2006). These NRs would be good candidates to control habenular development since both are expressed during early developmental stages in the dorsal

diencephalon of zebrafish (Bertrand *et al.*, 2007). However, the truncated Rerea protein of *rerea*^{u757} mutants still has the ALRTLSEY sequence, which makes it possible that the *rerea* mutation does not affect the interaction between these proteins (*in silico* observation, data not shown). Nevertheless, it is still possible that the loss of the last 158 amino acids disrupts the protein conformation and, therefore, the binding to these NRs. A possible future experiment, is to test if the Rerea protein of *rerea*^{u757} mutants interacts with COUP-TF and Tlx *in vivo* through protein extraction and co-immunoprecipitation (Liao *et al.*, 2003; Fu *et al.*, 2012). Moreover, it would be interesting to understand if the zebrafish Rerea protein interacts with the same NRs that its mammalian and drosophila homologs do (Zhang *et al.*, 2002; Vilhais-Neto *et al.*, 2010).

In mice, the Rere protein was shown to interact with the Retinoic Acid Receptors alpha and beta (RAR-alpha and RAR-beta) in a complex with COUP-TF and P300 to activate gene expression (Vilhais-Neto *et al.*, 2010). In zebrafish, there is no homolog of RAR-beta but there are two RAR-alphas, Raraa and Rarab (Samarut *et al.*, 2014). Mutations in *rarab* generate defects in the heart, otic vesicle, liver, pectoral fins and pharyngeal arches, all of which resemble the developmental defects of *rerea* mutants (Linville *et al.*, 2009; He *et al.*, 2011; Garnaas *et al.*, 2012; D'Aniello *et al.*, 2013). Moreover, both in mice and zebrafish, Retinoic Acid (RA) inhibits the FGF pathway (Zhao and Duester, 2009; Vilhais-Neto *et al.*, 2010; Cunningham *et al.*, 2013). Lastly, preliminary results from our group show that drug-induction of the RA pathway generates small habenulae and compromises the specification of the parapineal (Faro A. and Wilson S., unpublished results). Therefore, our current hypothesis is that Rerea regulates the expression pattern of *fgf8* through its interaction with Rarab and histone deacetylases or acetylases. Also, in *rerea*^{u757} mutants, the truncated protein possibly fails to interact with Rarab, thus failing to inhibit *fgf8*. Alike COUP-TF and Tlx, understanding if this interaction happens in zebrafish would be very informative for our research. Moreover, understanding how RA affects the habenular development of wild-type and *rerea*^{u757} mutants may help us dissect the mechanism through which this mutation affects the formation of habenular progenitors. We are planning on studying this by treating embryos with drug inhibitors of the RA pathway (such as diethylamino-benzaldehyde – DEAB) or through RA treatments (Hyatt *et al.*, 1992; Le, Dowling and Cameron, 2012). Also, once we find the suboptimal doses that do not exert any effect in the development of wild-type larvae, we will test if *rerea*^{u757} mutants are more, or less sensitive to changes in altered RA activity.

Despite the likelihood that the mutation in the *rerea* gene being causative of the habenular phenotype, we currently lack a formal proof of this. Despite the mutation being present in all larvae with a reduced habenula or increased *fgf8* expression, this could still be due to *rerea* being tightly linked to another mutation that is driving the habenular

phenotype (data not shown). Moreover, the injection of the *rerea* morpholino only drove non-habenular phenotypes (Supplementary Figure 2.4). However, the morpholino injection abolishes the transcription of the *rerea,* while the *rerea*^{u757} allele expresses a truncated form of the protein. This truncated form could still be functional but not interact with a few of the NRs that the wild-type version does (Zhang *et al.*, 2002; Plaster *et al.*, 2007; Vilhais-Neto *et al.*, 2010). Since we failed to create a new CRISPR-driven mutation in the *rerea* gene we will resort to assessing complementation to an existing *rerea* mutant, *rerea*^{sa1112}, which has a premature stop in exon 16 (out of 21). Thus, to understand if a truncated version of the Rerea protein is needed to drive the reduced habenula phenotype, we will screen *rerea*^{sa1112} homozygous mutants for habenular developmental defects. Moreover, if we find a phenotype in these fish, and to validate the *rerea*^{u757} mutation, we will screen hemizygous *rerea*$^{sa1112/u757}$ embryos for habenular developmental defects. We hope that, this way, we will be able to fully understand the role of the co-regulator Rerea in the habenular development.

2.4. SUPPLEMENTARY FIGURES

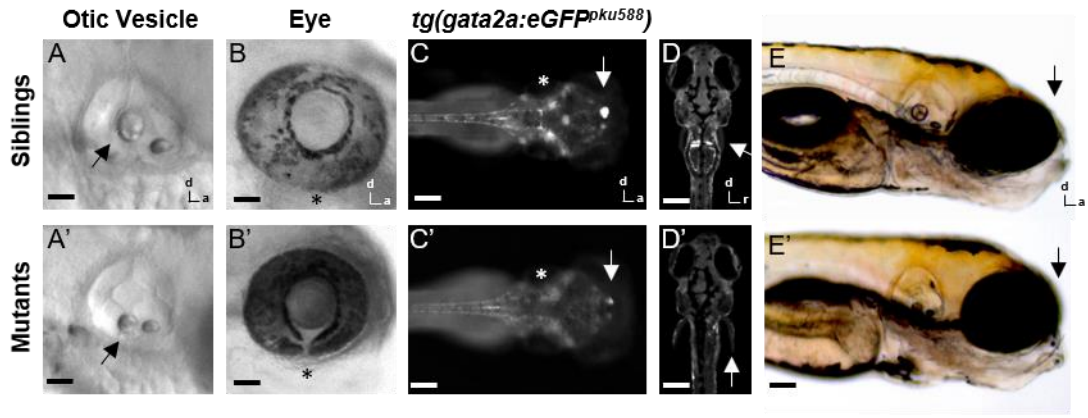

Supplementary Figure 2.1. The u757 mutants show reduced otoliths and low penetrance coloboma. **(A-A')** Lateral view of the otic vesicle of a 4 dpf, *A66*^{u757} mutant and sibling. The arrow is marking the misplacement and reduction of one of the otoliths. **(B-B')** Lateral view of the eye of a 4 dpf, u757 mutant and sibling. The asterisk is marking the position of the choroid fissure. **(C-C')** Dorsal view of a 4 dpf, u757 mutant and sibling, carrying the *Et*(*gata2a:eGFP*)^{pku588} transgene. The arrow is marking the position of the epithalamus. Asterisk marks a domain that still expresses GFP in the mutant. **(D-D')** Dorsal view of 5 dpf, *A66*^{u757} mutant and sibling. The arrow is marking the position of the pectoral fin, which in siblings is barely visible as it is positioned close to the body. The asterisk marks the swim-bladder. **(E-E')** Lateral view of the head of a 4 dpf, u757 mutant and sibling (zoomed of larvae in Figure 2.1.A and 2.1.A'). The arrow points to the reduced anterior head structures. Scale bar: (A-B') 20 µm; (C-C') 50 µm; (D-D') 70 µm; (E-E') 180 µm. Legend: a, anterior; d, dorsal; r, right.

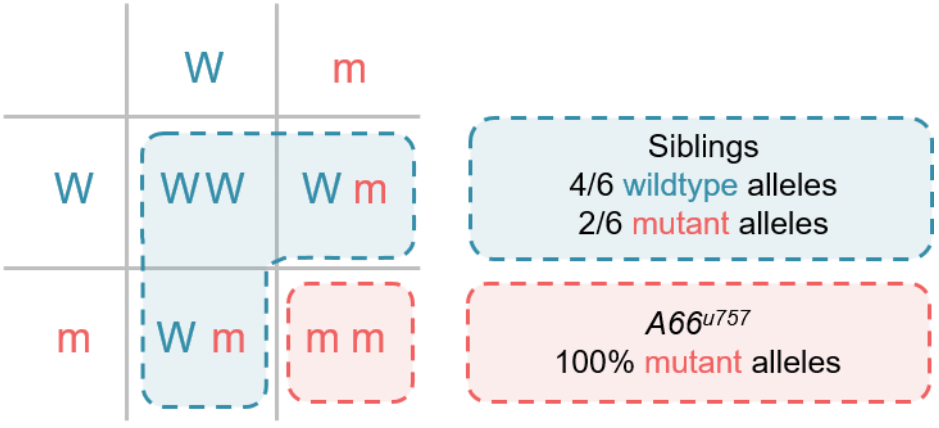

Supplementary Figure 2.2. Frequency of mutant alleles in A66u757 mutants and siblings. The progeny of a *A66*^{u757} sibling pair mating, carrying a copy of the wild-type (W) and mutant (m) allele of a gene, will either have two copies of the W allele (1/4 of the progeny), one copy of each allele (2/4 of the progeny), or two copies of the m allele

(1/4 of the progeny). Therefore, in a population that only consists of mutant larvae, all alleles will carry the mutation. In siblings, a third of the sequenced alleles will carry the mutation while two thirds will not (two m alleles for every 4 W alleles).

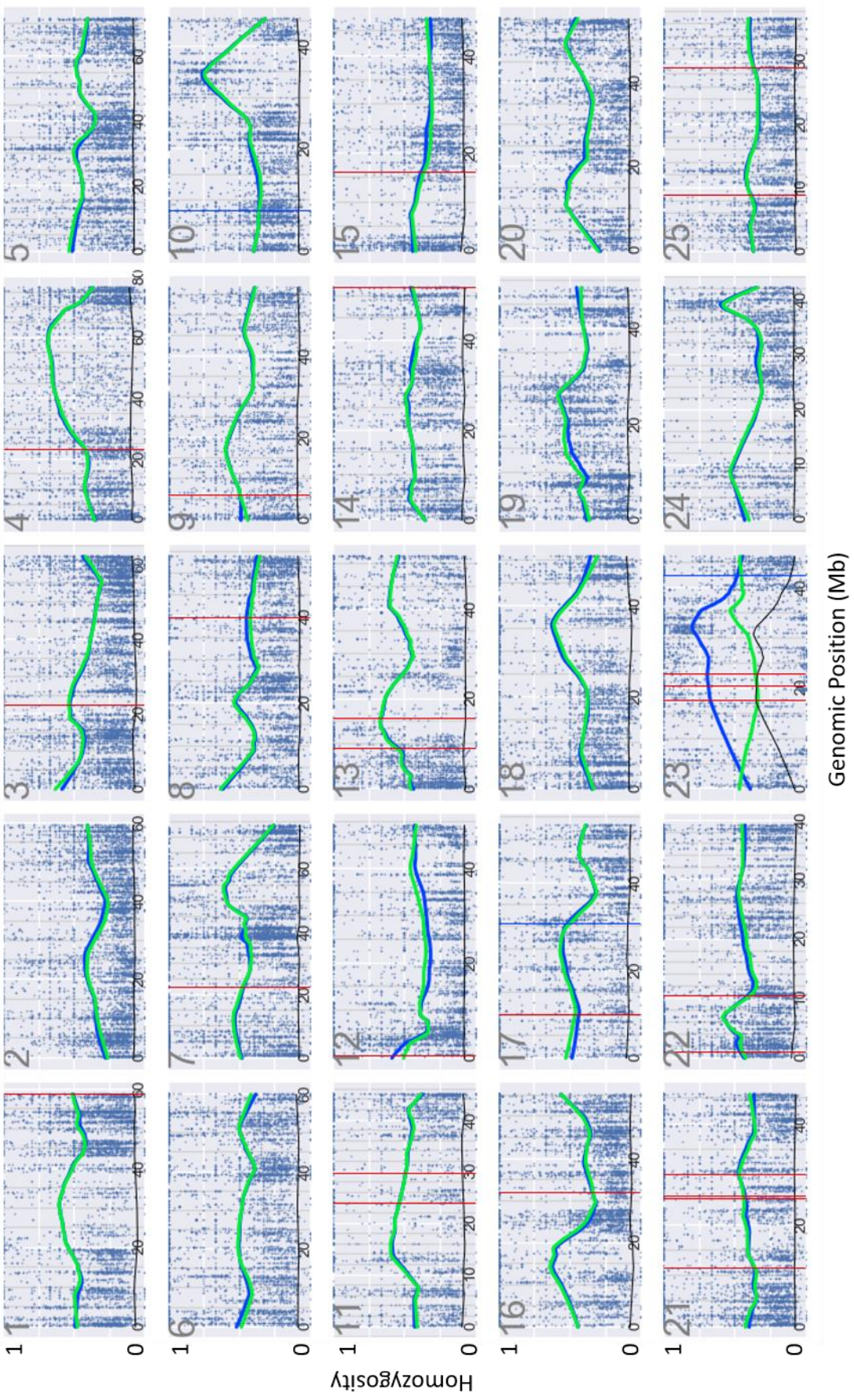

Supplementary Figure 2.3. Homozygosity ratio in all linkage groups of A66u757.
Homozygosity ratio of *rerea*^{u75} mutants (blue) and siblings (green) in all linkage groups,

obtained from the frequency of new SNPs found by RNA-seq. Blue dots represent the frequency each SNP was found in the population and red lines represent genes that were differentially expressed between siblings and mutants. Black line represents the homozygosity distance between *rerea*^{u757} mutants and siblings. **Definition: Homozygosity** is a value between 0 and 1, which measures the frequency of the most common allele (in this case, a SNP) in a genomic region of the population. For example, if a mutant SNP is present in 75% of the larvae, it has homozygosity 0.75. However, if it is present in 25% of the larvae, the homozygosity for that genomic region is still 0.75 because 75% of the population shares the same SNP, despite it being the WT allele. This measure will, therefore, show which regions are in linkage with the *u757* mutation and, therefore, reveal the probable location of the same.

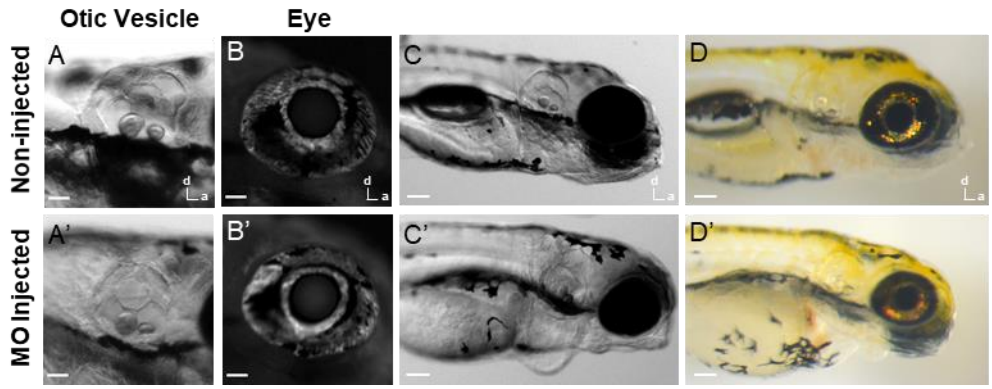

Supplementary Figure 2.4. The rerea morpholino injected larvae show u757-like phenotypes. (A-A') Lateral view of the otic vesicle of a 4 dpf, morpholino injected and non-injected larvae. **(B-B')** Lateral view of the eye of a 4 dpf, morpholino injected and non-injected larvae. **(C-D')** Lateral view of a 4 dpf, morpholino injected and non-injected larvae. Scale bar: (A-B') 50 µm; (C-D') 70 µm. Legend: a, anterior; r, right.

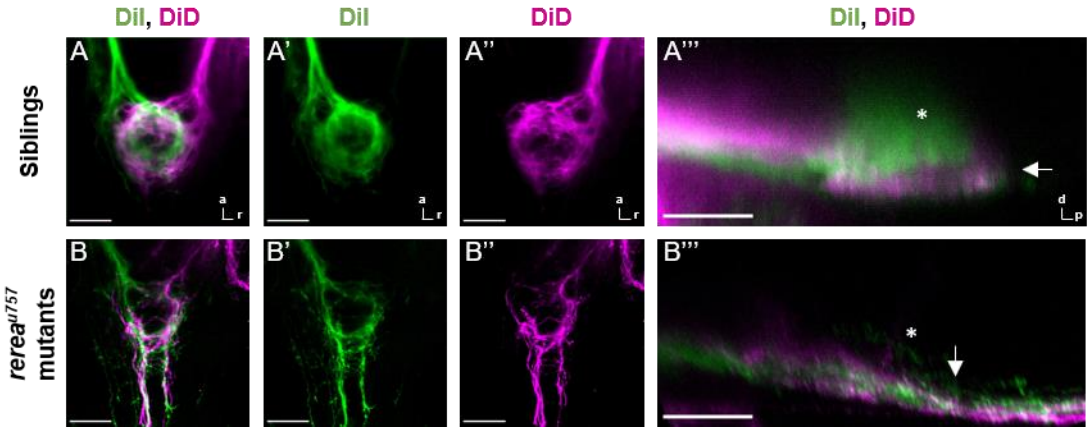

Supplementary Figure 2.5. The rereau757 mutants only project to the ventral IPN. (A-A'') Dorsal view of habenular projections to the IPN dyed with DiI (green, left dHb)

and with DiD (magenta, right dHb) in 4 dpf sibling. **(A’’’)** Lateral view of habenular projections to the IPN dyed with DiI (green, left dHb) and with DiD (magenta, right dHb) in 4 dpf sibling. Asterisk mark the dorsal IPN and the arrow marks the ventral IPN. **(B-B’’)** Dorsal view of habenular projections to the IPN dyed with DiI (green, left dHb) and with DiD (magenta, right dHb) in 4 dpf sibling. **(B’’’)** Lateral view of habenular projections to the IPN dyed with DiI (green, left dHb) and with DiD (magenta, right dHb) in 4 dpf sibling. Asterisk mark the dorsal IPN and the arrow marks the ventral IPN. Scale bar: 20 µm; Legend: a, anterior; d, dorsal; p, posterior; r, right.

CHAPTER 3.

DEVELOPMENT OF A PROTOCOL FOR SINGLE-CELL RNA SEQUENCING OF THE ZEBRAFISH DORSAL HABENULA.

3.1. INTRODUCTION

A full understanding of habenular neuronal cytoarchitecture and function can only be achieved through a thorough characterization of the molecular and anatomical composition of its neurons. Like many other brain structures, the habenula is known to consist of different neuronal types. Early morphological studies identified five different neuronal subpopulations in the rodent medial habenula, the homolog of the zebrafish dHb (Andres, von Düring and Veh, 1999; Wagner, Stroh and Veh, 2014). Later on, large scale molecular studies revealed that gene expression patterns follow these previously characterised habenular subdomains, supporting the hypothesis that these consist of subpopulations of neurons with different functions (Aizawa *et al.*, 2012; Wagner, French and Veh, 2016).

Similar approaches led to the discovery and characterisation of different habenular subdomains in zebrafish. In this organism, the habenula is broadly defined by the expression of *gng8,* which expresses in all dHb neurons and a subset of vHb cells (deCarvalho *et al.*, 2014). However, the dHb and vHb domains can be further divided by the expression of *ano2* and *kiss1,* respectively (Thisse and Thisse, 2004; Amo *et al.*, 2010; Lupton *et al.*, 2017). Moreover, the dHb is composed of the dHbL and dHbM domains which are characterised by the expression of *kctd12.1* and *kctd12.2*, respectively (Aizawa *et al.*, 2005; Doll *et al.*, 2011). Given the asymmetric development of the dHb, the characterization of its neuronal composition has been biased towards finding genes that are unilaterally enriched. The earliest examples are the expression patterns of *kctd12.1* and *kctd12.2* which are broader in the left and right dHb, respectively (Gamse, 2003; Gamse *et al.*, 2005). However, asymmetric gene expression patterns are not solely seen in markers of the dHbL and dHbM domains. The *nrp1a* gene is only expressed in the whole left dorsal nucleus, while *kctd8* and *solute carrier family 18 member 3a* (*slc18a3a*, former *vachta)* are enriched in the right (Kuan *et al.*, 2007; Hong *et al.*, 2013). However, like in mice, functional and transcriptome mapping studies show that the habenula is comprised of many more distinct neuronal subpopulations (deCarvalho *et al.*, 2014; Dreosti *et al.*, 2014; Jetti, Vendrell-Llopis and Yaksi, 2014; Wagner, French and Veh, 2016; Pandey *et al.*, 2018).

A recent study comparable in its goals to the one discussed in this chapter, characterised fifteen different habenular subpopulations in the dHb of 10 dpf and adult zebrafish (Pandey *et al.*, 2018). However, there is a lack of a transcriptome map at 4 dpf, a stage at which these asymmetries already are established and most habenular asymmetry development studies are performed. Moreover, the marker of habenular progenitors, *dbx1b*, is expressed in the most medio-ventral region of the 4 dpf larvae habenulae and the number of dHb neurons has a 3-fold increase between 4 and 10 dpf

(Roberson and Halpern, 2017a; Pandey *et al.*, 2018). This suggests that a great part of the 10 dpf dHb neurons are still being born at 4 dpf, and that these new neurons (and possibly new subdomains) are formed from the most medial region of the habenula.

The profiling of the cells that constitute a tissue provides vital information on its developmental origin and ultimate function (Satija *et al.*, 2015; Tan, Onichtchouk and Winata, 2016). With the development and optimization of single-cell RNA sequencing (scRNA-seq) techniques, such as the Differential Expression Transcript Counting Technique (DeTCT) and the 10x Genomics Technique, single-cell sequencing of whole tissues/organs has become accessible and relatively cheap (Collins *et al.*, 2015; Goodwin, McPherson and McCombie, 2016; Tan, Onichtchouk and Winata, 2016). In these techniques, rather than sequencing full transcripts, only a fragment of the 3' mRNA molecules is sequenced (Islam *et al.*, 2014; Collins *et al.*, 2015). These sequences are long enough to map the fragment to the genome, while freeing physical and computational space to sequence more transcripts and cells. Moreover, in both approaches, each transcript is marked with a Unique Molecular Identifier (UMI) (Kivioja *et al.*, 2012). By doing so, each sequenced read can be traced back to its mRNA of origin and absolute quantification of gene expression is possible (Kivioja *et al.*, 2012). Together, these optimisations made it feasible to compare the gene expression of up to 384 (DeTCT) or 10,000 single cells (10x Genomics) and to cluster them into subpopulations (Collins *et al.*, 2015; Pandey *et al.*, 2018).

In this work, we will describe two protocols optimised to obtain *gng8*-positive single cells of the habenula of 4 dpf larvae, for scRNA-seq through DeTCT or 10x Genomics. The developed protocols do not greatly affect the viability of the dissociated cells which still express habenular genes in an asymmetric fashion. Lastly, we will show that despite collecting fewer cells than expected through the 10x Genomics approach, these are clustered into different populations, two of those from the dHb and vHb.

3.2. RESULTS

3.2.1. FAC-sorted dHb cells from 4 dpf larvae express asymmetry habenula markers.

DeTCT allows for the characterization of the transcriptome of 384 cells at a time. With the aim of sequencing the RNA of dHb single-cells through DeTCT, a protocol that yielded no less than 384 dHb cells was optimised. The best approach at purifying a cell population is through Fluorescence-Activated Cell Sorting (FAC-sorting), a technique that selectively collects cells expressing a fluorophore, such as GFP. Therefore, a protocol was designed to obtain single-cells from the dHb of 4 dpf Tg(*gng8*:GFP) fry, in which GFP is expressed in all dHb neurons and in a subset of vHb neurons (Figures 3.1.A[1] and 3.1.B) (Dreosti, E., Wilson, S.W., unpublished). At 4 dpf, there are more GFP-positive cells in the left dHb than in the right (Figure 3.1.B). Therefore, if both nuclei were collected and dissociated together, there could be a bias towards sequencing more cells from the left nucleus. Moreover, the Tg(*gng8:GFP*) line has broad expression of GFP in the olfactory organ (data not shown). Given this, and taking into account the limited number of cells that can be sequenced by the DeTCT approach, the dHb nuclei were manually dissected and their cells dissociated and FAC-sorted separately in order to obtain a pure population of dHb cells (Figure 3.1.A[2] and Methods).

Dissociation of the dHb into single cells was performed by incubating the manually-dissected habenulae in a trypsin solution (Figure 3.1.A[3]). This, coupled with the pressure of FAC-sorting, could affect cell viability. Therefore, to control for viability, dissociated cells were incubated in the vital dye DAPI, which only permeates dying cells. Cells co-expressing DAPI and GFP were selectively sorted out by FAC-sorting. GFP-positive cells, on average, comprised of 0.4% of the total sorted population. Furthermore, of the GFP-sorted cells 95% from the left dHb and 98.6% from the right dHb were DAPI negative (Figure 3.1.C). This result suggested that the protocol was not compromising the viability of the vast majority of dHb cells.

Although most cells did not show signs of non-viability, this does not rule out transcriptome changes due to cellular stress. To understand if the collected cells maintained their habenular character, pools of left and right dHb cells collected by FAC-sorting were tested for the expression of *kctd12.1* and *kctd12.2* by quantitative PCR (qPCR). The results show that both pools of cells expressed these genes. Moreover, the expression levels respected the left-right origin of the cell pools: cells from the left dHb expressed higher levels of *kctd12.1* (a left habenular marker) and lower levels of *kctd12.2* (a right habenular marker) than the right dHb (Figure 3.1.D).

Altogether, these results suggest that the optimised protocol successfully purifies dHb cells from 4 dpf larvae, without greatly affecting their habenular character.

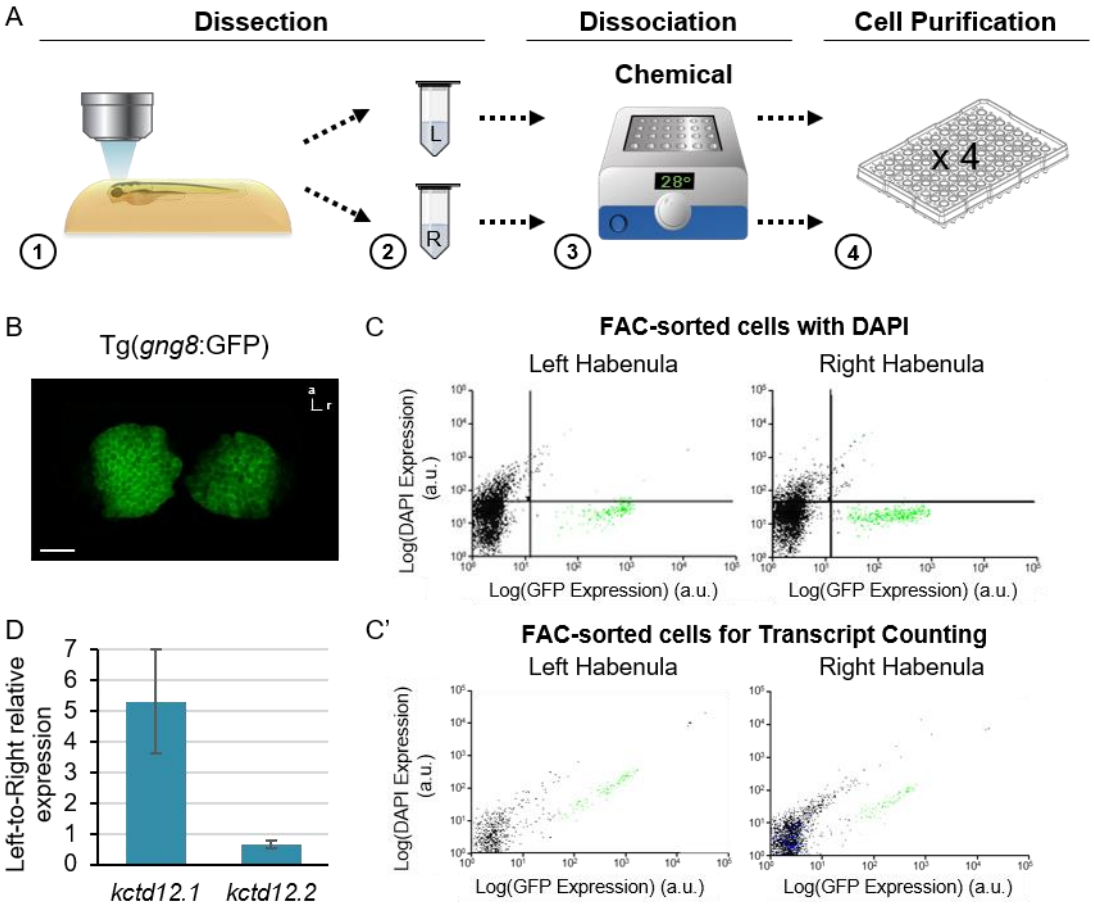

Figure 3.1. Dissociated habenular cells show > 95% viability and retain their dorsal habenular character. **(A)** Scheme of the protocol for obtaining and preparing dHb single cells for DeTcT scRNA-seq. (1) 4 dpf Tg(*gng8:GFP*) habenulae were dissected with a tungsten needle under a fluorescent microscope. (2) Left and right dissected habenulae were collected in two separate 1.5 mL Eppendorf tubes. (3) Habenular cells were chemically dissociated with trypsin for 20 minutes at 28^{o}C, with gentle tapping in 5-minute intervals. (4) GFP-positive dissociated cells from each side of the brain were FAC-sorted to four 96-well plates. **(B)** Dorsal view of the epithalamus of a 4 dpf Tg(*gng8*:GFP), immuno-stained for GFP (green). Scale bar: 10 µm. Legend: a, anterior; r, right. **(C)** FAC-sorting graphs of dissociated cells incubated in the viability dye DAPI. Green dots represent GFP positive cells as classified in a previous gate. Horizontal bar represents threshold of DAPI positive (above) and negative (below) cells. Vertical bar has no biological meaning in this analysis. **(C')** FAC-sorting graphs of dissociated cells collected in 96-well plates for cDNA library synthesis and RNA-seq. Green dots represent GFP positive cells. Legend: a.u., arbitrary units. **(D)** Relative expression of kctd12.1 and

kctd12.2 between the pools of habenular cells from the left versus right nuclei. Expression was calculated by qPCR and normalized to the expression of *actin*, a house-keeping gene with little variation between left and right pools of cells. Equal expression between left and right sides equals 1, higher expression in the left is higher than 1 and higher expression in the right is lower than 1. Error bars represent standard error of the mean calculated from the average expression of three independent experiments.

3.2.2. DeTCT failed to sequence habenular cells

In the DeTCT approach, the 384 cells are pooled together and sequenced in one Illumina Sequencer lane. This is possible because the cDNA library synthesis is performed in individual wells, and a different cell barcode sequence is attributed to each well (Collins *et al.*, 2015). Therefore, 384 GFP-positive cells from the left and right dHb of 4 dpf Tg(*gng8*:GFP) were distributed to four 96-well plates, previously filled with a lysis buffer that disrupts the cell membrane while also stabilising the RNA (Figures 3.1.A and 3.1.C'). From these cells, we were able to build a cDNA library from the extracted RNA (Supplementary Figure 3.2). However, analysis of the resulting Illumina reads revealed two major problems with the cDNA library. First, the de-tagging pipeline failed to remove the UMI sequences from most reads. This meant that the program failed to recognise which part of the sequence was UMI and which part corresponded to the gene. Since UMIs confer a unique identity to each sequence, this made it impossible to distinguish which sequences that mapped to the same gene resulted from a PCR amplification (technical duplicate) or from transcription of that gene (biological duplicate). Furthermore, an unknown problem during either the RNA preparation or the cDNA library synthesis led to poor quality reads which failed to map to the zebrafish genome, even in sequences that were properly de-tagged. For this reason, a different approach was tried.

3.2.3. A new protocol increases GFP-positive cell yield by 8.5x

With the advent of 10x Genomics, a new technique for large scale single-cell cDNA library synthesis, the number of cells that could be sequenced in a single experiment increased to 10,000 cells (Baran-Gale, Chandra and Kirschner, 2018). However, the protocol previously described would give an average of 1,000 cells from each dHb nucleus (data not shown). The main limitation of this protocol was the habenular dissection step, which was time consuming and thus limited the number of habenular nuclei we could retrieve to 6 per experiment. Being precise in isolating habenula cells was important for the DeTCT approach, given this technique only allows for the analysis of 384 cells per experiment. However, by using a 10x Genomics approach, we were not limited by the number of cells that could be sequenced. In light of this, we speculated

that the best strategy would be to sacrifice the purity of the initial pool of habenular cells for the sake of increasing the total number of GFP-positive cells, by dissecting and dissociating whole heads of 4 dpf Tg(*gng8:GFP*) larvae (Figure 3.2.A).

To isolate cells from the severed heads of 4 dpf larvae, the previous protocol was complemented with the dissociation of 50 heads with a 30 G syringe, and the filtration of the resulting cell suspension through a 40 µm mesh (Figure 3.2.A and Methods). This way, the final yield of GFP positive cells increased to 4,500 cells. Furthermore, by collating samples from four different experimental batches, we were able to FAC-sort approximately 17,000 GFP-positive cells (an increase of 8.5x in comparison with the first protocol).

The addition of these new steps could also increase the stress cells were exposed to. To test if this was the case, dissociated cells were incubated in Hoechst33258 to assess for viability (Kasibhatla *et al.*, 2006). This dye labels senescent cells, and thus our aim was to exclude those cells that co-express Hoechst33258 with GFP by FAC-sorting. Despite the percentage of GFP-positive cells still being 0.4% of the total population, 17% of GFP-positive cells also co-stained for Hoechst33258. Although this value is higher than the previous protocol, this methodology would still allow us to retrieve a great number of cells and it is similar to recently published work (Pandey *et al.*, 2018). Therefore, we decided to use this approach to collect cells for scRNA-seq through the 10x Genomics approach.

To collect the final samples, it had to be taken in to account that the 10x Genomics microfluidic system is only able to uptake a cell suspension with 34 µL. However, under the conditions in which the cells were sorted, collecting 17,000 cells would lead to a final volume of 51 µL (approximately 3.5 ρL per cell). Therefore, to concentrate the FAC-sorted cell suspension in a smaller volume, we centrifuged the cells, and the excess supernatant was removed (Figure 3.2.A and Methods). To understand if this extra step affected cell viability, the final number of cells was estimated by manually counting the cells remaining in the re-suspended pellet after centrifugation. This was achieved by loading a haemocytometer with pelleted-cells previously stained with trypan blue, which only permeates dead cells (Strober, 2001). The estimated cell loss was about 20%, while the remaining 80% were GFP-positive and excluded trypan blue. This suggests that the majority of dead cells found during FAC-sorting were removed with the supernatant.

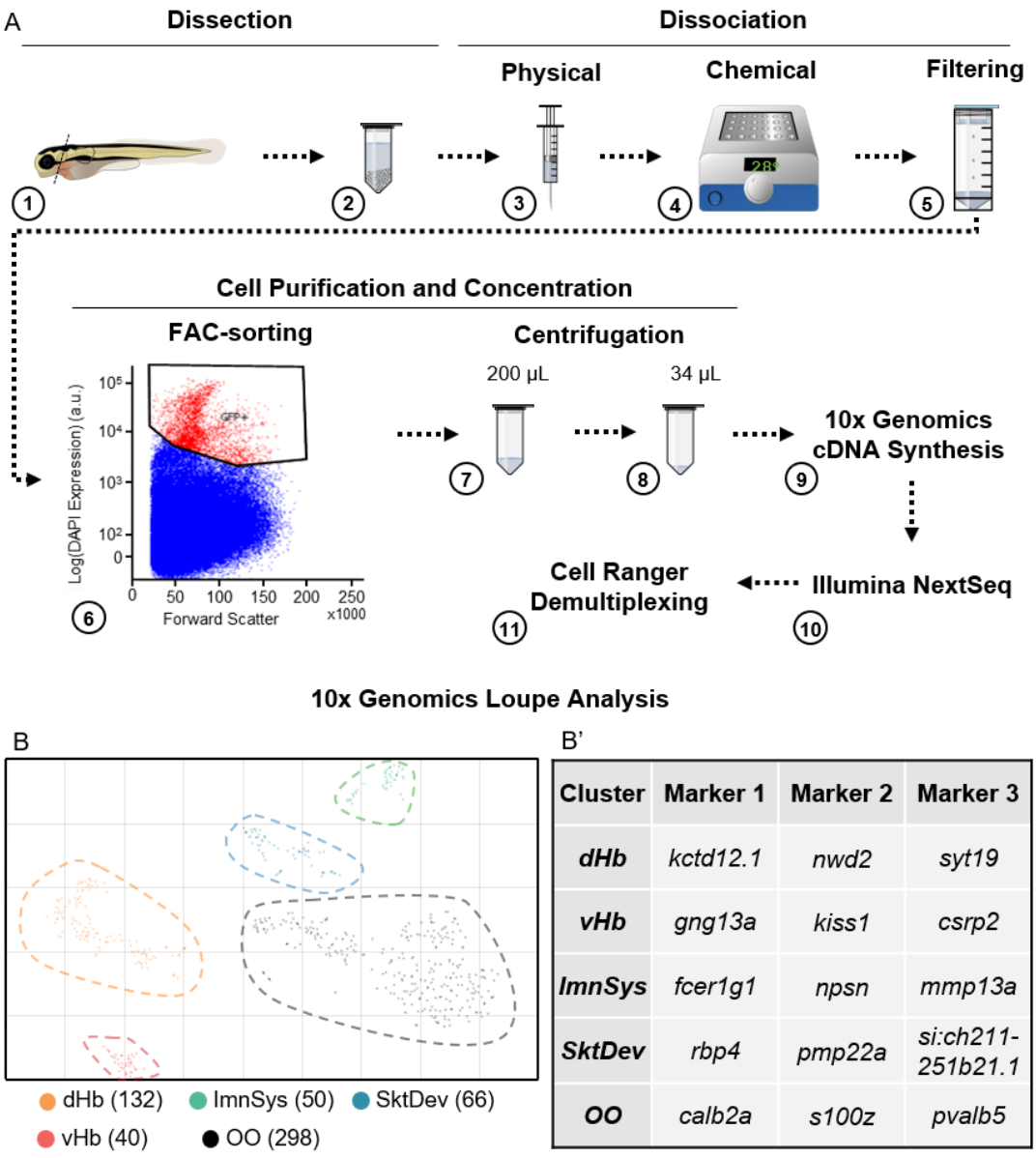

Cluster	Marker 1	Marker 2	Marker 3
dHb	*kctd12.1*	*nwd2*	*syt19*
vHb	*gng13a*	*kiss1*	*csrp2*
lmnSys	*fcer1g1*	*npsn*	*mmp13a*
SktDev	*rbp4*	*pmp22a*	*si:ch211-251b21.1*
OO	*calb2a*	*s100z*	*pvalb5*

Figure 3.2. 10x Genomics Experiment Distinguishes the dHb and vHb populations. **(A)** Scheme of the protocol for obtaining and preparing dHb single cells for scRNA-seq. (1) 4 dpf Tg(*gng8:*GFP)allele? heads were dissected with a scalpel. (2) Severed heads were collected in a 1.5 mL tube with ice-cold PBS. (3) Head tissue was mechanically dissociated with a syringe (7x). (4) Head tissue cells were further dissociated with trypsin incubation for 20 minutes at 28°C. (5) Dissociated cells were filtered in a 40 µm mesh to remove clumps and non-dissociated tissue. (6 and 7) GFP-positive dissociated cells were FAC-sorted to a 1.5 mL Eppendorf tube with Foetal Bovine Serum (FBS) in PBS. GFP-positive cells are represented in red in the FAC-sorting plot. (8) Collected cells were centrifuged at *300 g* for 5 minutes to concentrate the cells in a final 34 µL solution. (9) Concentrated cells were run in the 10x Genomics machine to synthetize the cDNA library. (10) cDNA was sequenced. (11) Reads were analysed in the Cell Ranger Software. **(B)** t-SNE plot of five clusters predicted by the k-means model. Doted lines

delineate the plot-area where most cells of each cluster are positioned. Names of the clusters were attributed based on the list of genes that significantly distinguish a cluster from the remainder cells of the sample. **(B')** Table of the three most significant genes that are differentially expressed in the indicated cluster in relation to the remainder cells of the sample. Legend: dHb, dorsal Habenula; ImmSys, Immune System; OO, Olfactory Organ; SktDev, Skeletal Development; vHb, ventral Habenula.

3.2.4. Sequenced *gng8*-positive cells define dHb, vHb and olfactory organ clusters and two previously uncharacterised clusters

The 10x Genomics microfluidics system has a 50% loss ratio (10x Genomics, 2019). Therefore, since we collected about 14,500 cells, and with a cell loss of 20% after the centrifugation step, we predicted that our experimental conditions would result in the sequencing of about 5,800 cells. However, after performing the experiment, the 10x Genomics Software under default setup analysis, predicted a total of only 586 cells. To understand if this was caused by the software ignoring cells with low amount of total RNA, which is the case in zebrafish neurons, we attempted to detect sequenced data worth of 5,800 cells through the same software (Pandey *et al.*, 2018). However, all resulting cell clusters were based on the expression of mitochondrial genes, which are markers of cell stress (data not shown) (Zhao *et al.*, 2002; Ilicic *et al.*, 2016). Therefore, we proceeded with an analysis of the captured 586 cells.

To detect possible dHb cell clusters identified by the 10x Genomics Loupe Cell Browser, we made a careful analysis of the characterised 586 cells (Supplementary Figure 3.2; Figure 3.2.B and Methods). Out of this analysis, five different populations were shown to be significantly different (Figures 3.2.B and 3.2.B'). The biggest population consisted of 298 cells (50.9%) and most of the top 10 significantly expressed genes (such as calbindin 2a (*calb2a)*, *s100 calcium binding protein z* (*s100z)* and *parvalbumin 5* (*pvalb5)*) are markers of the olfactory organ (OO cluster) (Table 3.1; Figures 3.2.B and 3.2.B') (Rauch *et al.*, 2003; Thisse and Thisse, 2004; Kraemer, Saraiva and Korsching, 2008; Hortopan, Dinday and Baraban, 2010). Therefore, the biggest cluster of *gng8*-expressing cells isolated in our experimental setup, consisted of cells from the olfactory organ.

Two other cell populations were significantly enriched for genes that were not related with the habenula. The gene ontology analysis of the expressed genes that differentiated these clusters from the remainder cells revealed that one of the populations was related to the Immune System (ImnSys, 8.5%), while the other was related to the Skeletal Development (SktDev, 9.4%; Supplementary Tables 3.2 and 3.3; Figures 3.2.B and

3.2.B'). For instance, in the ImnSys Cluster the most abundant transcript is the mast cell marker *Fc receptor, IgE, high affinity I, gamma polypeptide like* (*fcer1gl)* and the second is the granulocyte marker *nephrosin* (*npsn)* (Da'as *et al.*, 2011; Murayama *et al.*, 2015). As for the SktDev Cluster, the most significantly enriched gene is the ectoderm gene *retinol binding protein 4* (*rbp4)* and the second most is the *peripheral myelin protein* 22a (*pmp22a*) (Boczonadi *et al.*, 2014). Some of the remainder genes that were enriched in the SktDev cluster encode for the Collagen, Osteonectin and Keratin family of proteins (Supplementary Table 3.3). Both clusters express very low levels of *gng8* transcripts in comparison with the remainder clusters, which goes in line with the lack of reports of *gng8* being expressed in either skeletal- or immune-related cells (Supplementary Figure 3.3.A).

Finally, the two remaining cell populations identified in this study show high transcript counts for genes related with the dHb (22.5%) or the vHb (6.8%; Supplementary Tables 3.4 and 3.5; Figures 3.2.B and 3.2.B'). The most significantly expressed gene in the dHb population was *kctd12.1* and most of the top ten enriched genes in this cluster are known markers of the dHb (Table 3.4). There is no published information about the expression patterns of the second or third most-enriched genes in this cluster, *NACHT and WD repeat domain containing 2* (*nwd2)* and *synaptotagmin XIX* (*syt19)*, opening the possibility that these are novel dHb markers. As for the vHb cluster, the second most representative gene is *kiss1*. Moreover, two other known vHb markers are expressed in the top-10 list: *protein phosphatase 1, regulatory (inhibitor) subunit 14Ab (ppp1r14ab)* and *amine oxidase, copper containing 1 (aoc1)* (Amo *et al.*, 2010, 2014). This allowed us to conclude that the 10x Genomics software was able to distinguish the dHb and the vHb.

As a proof of principle, we tested if the expression of dHb, vHb and olfactory organ markers was limited to its respective clusters. First, *epithelial cell adhesion molecule* (*epcam)*, a marker of the OO was restricted to the OO population (Supplementary Figure 3.3.B) (Lu *et al.*, 2013; Pandey *et al.*, 2018). Next, the left dHb markers, *kctd12.1 and nrp1a*, and the right dHb markers, *kctd12.2* and *kctd8*, were mostly represented in the dHb cluster, although a few cells of the vHb also expressed a few of these markers (Supplementary Figures 3.2.E to 3.2.H). Complementary to this, the vHb markers *kiss1* and *aoc1* were mostly expressed in the vHb cluster (Supplementary Figures 3.2.G and 3.1.H).

None of the captured cells expressed the habenula progenitor marker *dbx1b* (Supplementary Figure 3.4.A), whose expression is known to be excluded from differentiated dHb neurons (Roberson and Halpern, 2017a). However, a few cells, mostly

in the dHb and vHb clusters, expressed the recently published marker of dHb immature cells *tubb5b* (Supplementary Figure 3.4.B) (Pandey *et al.*, 2018).

The *chemokine (C-X-C motif), receptor 4b* (*cxcr4b)* gene, which is expressed in cells transitioning from habenular progenitors to differentiated dHb neurons was not expressed in any of the identified habenular cell clusters but was highly expressed in the ImnSys cluster (Supplementary Figure 3.4.C) (Roberson and Halpern, 2017a). Moreover, the *chemokine (C-X-C motif), ligand 12b (cxcl12b)*, which is cxcr4b ligand, and important for the axonal projection from the dHb to the IPN, was expressed in a few cells of the SktDev cluster (Supplementary Figure 3.4.D) (Roberson and Halpern, 2017a).

Finally, we investigated the expression of neuronal and neurotransmitter markers known to be expressed in the dHb (Supplementary Figure 3.5). First, the neuronal marker *elav like neuron-specific RNA binding protein 3 (elavl3)* is present in both habenular clusters and in the OO cluster, which suggests that *gng8* expression in the OO is limited to its sensory neurons (Supplementary Figure 3.5.A) (Kim *et al.*, 1996). Expression of the *solute carrier family 17 member 6a* (*slc17a6a)* is only within the dHb cluster, as previously shown (deCarvalho *et al.*, 2013). Moreover, *slc18a3b* (former *vachtb)* which is expressed in the dHb cholinergic neurons, is restricted to the habenular clusters (Supplementary Figure 3.5.B and 3.4.C) (Hong *et al.*, 2013). As for *sst1.1 (*expressed in dHb somatostatinergic cells*)* and *tac3a (*a neurotransmitter of the family of substance P which is expressed in the right dHb), these are only expressed in the dHb cluster (Supplementary Figure 3.5.D and 3.4.E) (Biran *et al.*, 2012; deCarvalho *et al.*, 2014). Moreover, *tac3a* seems to be mutually exclusive with the *nrp1a* population (Supplementary Figure 3.3.D and 3.4.E). Lastly, a very small number of cells in the dHb cluster express *solute carrier family 32 member 1a (slc32a1),* which is expressed in GABAergic neurons. Also, most of these co-express *gad2 and glutamate decarboxylase 1b* (*gad1b)* genes which are known to express in a rare population of dHb GABAergic neurons (Supplementary Figure 3.5.F and data not shown) (Juárez-Morales *et al.*, 2016; Pandey *et al.*, 2018).

Together, these results show that the 10x Genomics is a good approach to identify neuronal cell populations within the zebrafish brain. However, the protocol presented in this work still needs to be improved in order to categorise the full range of dHb subpopulations at 4dpf.

3.3. DISCUSSION

3.3.1. Development of a protocol for dHb single cell purification.

Many attempts have been made towards describing the neuronal subpopulations that constitute the zebrafish dHb, which has opened new doors to the study of its function (Gamse *et al.*, 2005; deCarvalho *et al.*, 2014; Pandey *et al.*, 2018). However, not much is known about the range of sub-populations of neurons that are thought to make the dHb of 4 dpf zebrafish, which is the stage at which most brain asymmetry development studies are assessed. In fact, at 4 dpf, zebrafish larvae still express the habenula progenitor marker *dbx1b* in the most ventral-medial portion of the dHb (Roberson and Halpern, 2017a). There is a population of cells expressing *dbx1b* at least until 30 dpf and there is a sharp increase in the number of habenular neurons from 4 to 10 dpf (from about 450 to about 1500 cells), although dHb asymmetries are very well defined by 4 dpf (Pandey et al., 2018; data not shown). This suggests that habenular development, fuelled by a population of *dbx1b*-positive progenitors, is far from completed by 4dpf (Satija *et al.*, 2015; Roberson and Halpern, 2017a). Therefore, it is not fully understood if the identity of the characterised habenular subpopulations at 10 dpf is already present at 4 dpf, or if such subpopulations are only elaborated and refined later in development. In an effort to fill in this gap, the present work aimed to characterise the transcriptome of single neurons of the zebrafish dHb at 4 dpf.

The advent of Next Generation Sequencing methods, adapted to sequence the full transcriptome of single cells (scRNA-seq), has allowed the molecular dissection of whole tissues to discern their constituent cell types (Wang, Gerstein and Snyder, 2009; Picelli *et al.*, 2014; Satija *et al.*, 2015; Pandey *et al.*, 2018). Currently, there are several approaches to perform scRNA-seq, and choosing the best one depends on various issues including experimental questions/design and costs. A parallel requirement is the successful development of a tissue dissociation protocol, which needs to be adapted to the sequencing approach.

The SMART-Seq2 technique (Switching Mechanism at 5' End of RNA Template Sequencing 2) significantly contributed to the popularisation of scRNA-seq (Picelli *et al.*, 2013, 2014; Baran-Gale, Chandra and Kirschner, 2018). One feature of SMART-Seq2 is to find which alleles of a gene or isoforms of a transcript are being expressed in cells from a tissue. However, to obtain this data, SMART-Seq2 requires the sequencing of full transcripts, sacrificing the power to accurately quantify levels of gene expression and any information about rare transcripts (Baran-Gale, Chandra and Kirschner, 2018; Pandey *et al.*, 2018). This makes SMART-Seq2 a great technique for further

characterising an already established sub-population of a tissue, but not for finding new markers of sub-populations that constitute an uncharacterised structure.

To overcome this problem, Transcript Counting techniques were developed from the SMART-Seq2 approach. An example is the DeTCT. In this approach, the mRNA is fragmented prior to the cDNA library synthesis, which reduces the amount of total cDNA that is sequenced (Collins *et al.*, 2015). Therefore, despite sacrificing the allelic and isoform information, this technique sequences a wider range of transcripts. In parallel, by adding an UMI to all transcripts before the amplification steps, all PCR products can be traced back to the mRNA of origin (Kivioja *et al.*, 2012; Islam *et al.*, 2014; Sena *et al.*, 2018). This is possible because each original transcript is marked with a unique ID that will be shared by all PCR products of one given transcript but will be different between all original transcripts. This renders DeTCT an absolute, rather than relative-quantification approach, with high accuracy at differentiating single cell gene expression (Collins *et al.*, 2015).

Given the advantages of using a DeTCT approach, our first aim was to develop a single cell dissociation protocol that would be compatible with this technique. The requirements were to obtain a minimum of 384 viable cells still retaining their habenular characteristics by the end of the protocol. We achieved this by combining manual dissection of the dHb of embryos in a transgenic line expressing GFP in the dHb, with FAC-sorting these cells into 96-well plates prefilled with lysis buffer. Upon dissection of the dHb nuclei, which were kept separate to account for the asymmetric number of cells in the left and right dHb, we had to choose a dissociation method that generated single cells without affecting their viability and transcriptome profile. The choice of using trypsin as the dissociating agent was based on a previously published protocol, where this proteolytic enzyme was used to dissociate zebrafish neuronal cells at 28.5^{o}C (Knight and Eagle, no date; Chen *et al.*, 2013). The fact that trypsin worked under sub-optimal temperatures (trypsin's optimal temperature is 37°C) rendered this a favourable option. Moreover, our results show that with this approach, dHb cells still expressed the habenular markers *kctd12.1* and *kctd12.2*. However, other studies using Papain (another, less specific, proteolytic enzyme) have been shown to promote less changes to the transcriptome of FAC-sorted zebrafish spinal cord neurons (Worthington Biochemical Corporation, no date; Cerda, Hargrave and Lewis, 2009). Moreover, Pandey et al., who successfully employed this approach to 10 dpf zebrafish dHb, also took the Papain dissociation approach (Pandey *et al.*, 2018). Therefore, and given that this protocol needs now to be adapted to the 10x Genomics approach, changing this step may contribute to increasing of the yield of viable dHb cells.

3.3.2. Why did the DeTCT fail?

When attempting to analyse the reads that resulted from sequencing 384 single cells from each dHb nuclei, two main problems negatively affected the whole experiment. First, the de-tagging pipeline failed to resolve most of the new tags and separate them from the transcript-derived sequence. The DeTCT approach was a relatively new technique when this experiment was taking place, and new modifications were attempted to make it less convoluted and more robust (Kivioja *et al.*, 2012; Collins *et al.*, 2015). In our approach, UMIs of 11 bp were added instead of the usual 8 bp. This was done to increase the number of different UMIs that can be used, since this number is limited by the chance of random mutations resulting in a different UMI sequence during reverse transcription, PCR amplification or sequencing. However, the de-tagging software could not recognise the new tag sequences, which is required for analysing the sequences that originate from the transcripts.

Second, only less than 10% of the sequences that were correctly de-tagged by the software were mapped to a genome. Although the reason why this happened remains unknown to us, it is likely that the RNA or cDNA samples were compromised prior to sequencing. When this happens due to a contamination of RNases, the RNA is fragmented to a point that the resulting cDNA is a unique small band. However, the gel electrophoresis results show a smear, which reflects the many sized bands that result from the protocoled fragmentation of the RNA and its subsequent reverse transcription (Supplementary Figure 3.1). These conflicting results suggest that the problem may have been during the library synthesis process.

3.3.3. Adapting the cell preparation protocol to the 10x Genomics approach.

In both SMART-Seq2 and DeTCT, the library preparation is manually done in 384-well plates. Since after cDNA synthesis, all library products are pooled together and sequenced in the same Illumina sequencer lane, all transcripts of a well need to carry another identifying sequence that is different from any other well (Picelli *et al.*, 2013; Collins *et al.*, 2015). This implies that, even when there is access to a robotic arm, all solutions need to be pipetted in sequence, which increases the error associated to the experiment (Baran-Gale, Chandra and Kirschner, 2018). This renders the technique time consuming and expensive for only obtaining information from less than 384 cells (Goetz and Trimarchi, 2012; Picelli *et al.*, 2013, 2014).

To overcome this problem, several droplet-based fluidic systems were developed, such as the 10x Genomics (AlJanahi, Danielsen and Dunbar, 2018). In this system, a single-cell suspension flows in a microchip to isolate each cell with a single bead and RT enzymes inside an oil-encapsulated droplet (AlJanahi, Danielsen and Dunbar, 2018).

The function of the beads is to hold the DNA oligos composed of a poly(T) tail, and two barcode sequences: the cell barcode which is unique for each bead, and the unique molecular identifier (UMI), a sequence with high variability between oligos of the same bead (Klein *et al.*, 2015; Hanson *et al.*, 2016). The microfluidics system, reduces the number of pipetting steps to one, reducing the associated error. Single-cells are pooled together, and one by one, forced through the system. Given this, the cell capacity of the 10x Genomics is increased to 10,000, the number of total beads in the system (Baran-Gale, Chandra and Kirschner, 2018). Therefore, the generation of a single cell dHb suspension protocol had to be improved in order to increase the final number of cells to be processed in the 10x Genomics pipeline.

The major limiting factor of the initial single cell dHb suspension protocol was the manual dissection of the dHb nuclei in live larvae. Pooling all the cells of 6 habenulae would only yield 2,000 cells, under optimal conditions, which is far from the desired numbers. Moreover, considering that the dissection step takes an average of 20 minutes, and that the 10x Genomics system has a cell loss rate of 50%, it was not feasible to increase the number of habenular dissections. Therefore, the alternative was dissecting the heads of 4 dpf larvae, which is significantly less time consuming and yields a much higher number of embryos (15 minutes for 50 heads). The initial problem with this approach was the fact that the Tg(*gng8:GFP*) expresses GFP in other cell types besides the dHb, namely in the olfactory organ. However, given the high number of cells that the 10x Genomics captures, the analysis pipeline should be able to cluster this population separately from the habenular cells (Pandey *et al.*, 2018; Zeisel *et al.*, 2018). In fact, our results showed that this was true, and that the data was sufficient to further subdivide the habenular cluster in the dorsal and ventral components (Figure 3.2.B). These findings suggest that if we increase the number of analysed cells, we will be able to further tease apart the 4 dpf dHb cluster into its neuronal constituents.

The approach taken by the authors of another published work for obtaining dHb cell populations for 10x Genomics Sequencing differs from that of our study in several points. In their study, the authors successfully obtained a much higher ratio of dHb to Olfactory Organ (OO) cells (Pandey *et al.*, 2018). There is no reason to suspect that individually each one of the modest differences between the Pandey *et al* protocol and ours would affect habenular neuron survival. However, it is plausible that the combination of all differences between the two protocols contributed to the detriment of habenular cells without, for an unknown reason, affecting the olfactory cells as much. The three main differences between both protocols are: (1) the medium in which the heads were dissected; (2) the proteolytic enzyme used for the dissociation step; and (3) the final FAC-sorting volume.

Pandey and colleagues performed head dissection in Neurobasal supplemented with B-27, which has been shown to promote viability of human, rat and mouse primary neuron cell culture (Thermo Fisher Scientific, no date). However, our protocol uses PBS, which in the long-term may not be sufficient to maintain neuronal survival until cell lysis in the 10x Genomics Microfluidics system. As for the dissociation process, this was performed in Papain, rather than Trypsin which, as discussed above, may be less stressing for neurons (Cerda, Hargrave and Lewis, 2009).

Lastly, both approaches purify the populations through FAC-sorting, which was shown to have minimal effect on gene expression of leukocytes or morphology of cultured neurons (Beliakova-Bethell *et al.*, 2014; Richardson, Lannigan and Macara, 2015; Sassen *et al.*, 2017). However, this step increases the time between cell dissociation and library synthesis, which may alter the transcriptome profile (Richardson, Lannigan and Macara, 2015; Llufrio *et al.*, 2018). As mentioned earlier, both protocols differ in the final volume of cell suspension after FAC-sorting. The 10x Genomics system only takes 33.8 µL of cell suspension, and Pandey *et al.* aimed towards collecting less cells in the maximum volume possible (6000-8000 cells in a final concentration of 300 cells/µL). Our protocol, on the other hand, opted for collecting all available GFP-positive cells and subsequently concentrating this cell suspension by centrifugation (achieving approximately 425 cells/µL). This was done to accommodate the 50% cell loss rate of the 10x Genomics System, since it was previously shown that a short centrifugation step would not significantly change cell stress levels (Dahlin *et al.*, 2018; Nguyen *et al.*, 2018; Pandey *et al.*, 2018). Moreover, all pelleted cells were viable, which suggested that cell debris was washed out with the supernatant (data not shown). The addition of this step to our protocol, however, did increase the time lag between cell FAC-sorting and cDNA library synthesis which, in hindsight, might have contributed to loss of dHb neurons. In fact, all changes might have compounded to increase stress levels of dHb cells (more than of olfactory organ cells), while also increasing the time cells were kept in sub-optimal conditions. It is plausible that dissecting heads in a medium that promotes neuronal survival, dissociating cells using Papain, and restricting FAC-sorted cell suspension to the volume limit imposed by 10x Genomics approach may increase the final yield of viable 4dpf dHb cells.

The last step of the protocol is sequencing the pooled cDNA of all cells. We did so by resorting to an Illumina HiSeq platform. However, the sequencing quality control Q30 was only of 56%, which means that only this proportion of sequences have an error ratio lower than 1 in 1000 bases. This value reflects the over-confluency of the reads in the Illumina flow cells and the lack of variability between sequences (Illumina Inc., 2016). This can happen when library concentrations are under estimated, thus resulting in

loading a much higher amount than that suggested by the manufacturer. To circumvent this, and since cDNA fragments are very small, a more sensitive method of quantification, such as Qubit™, needs to be employed (Simbolo *et al.*, 2013). On the other hand, the Illumina sequencing system works on a cluster basis (one molecule is replicated in place, until the signal of each added base can be detected by the sensor) and this affects the resolution of the sequencing (Illumina Inc., 2016). Since the cDNA obtained in this study resulted from a small number of very similar cells, it is highly likely that it would result in a library with low diversity given the high similarity of transcriptome signatures between *gng8*-positive neurons. Lack of sequence diversity creates clusters of reads that are very similar to each other, decreasing the power of resolution, and thus Q30 values. A solution to this problem would be to increase the variability of the starting material by using a high concentration spike-in with the commercially available PhiX v3 Control Library (Illumina) – a mix of highly variable known sequences commonly used for this purpose.

3.3.4. Understanding the clusters found by the 10x Software.

Despite not being able to delineate the several habenula neuronal subpopulations identified in the study by Pandey and colleagues, the 10x Clustering method was able to distinguish clusters from the dHb and the vHb domains. Cells that clustered in the dHb group expressed genes including *kctd12.1, kctd12.2, kctd8* and *nrp1a*, which are known markers of the dorsal habenula (Gamse *et al.*, 2005; Kuan *et al.*, 2007). The fact that these markers are expressed asymmetrically was observable by the fact that the majority, but not all, cells of the dHb cluster expressed the markers. In fact, *nrp1a* is known to solely express in the left nucleus, and was the most restricted marker, out of these four (Supplementary Figure 3.3). On the other hand, ventral habenular markers such as *kiss1* and *aoc1* were more restricted to the vHb cluster (Hong *et al.*, 2013; Lupton *et al.*, 2017). The most significantly expressed gene in this cluster is the *guanine nucleotide binding protein (G protein), gamma 13a (gng13a*, former *gng14*, Figure 3.2.B’), another G protein gamma subunit like *gng8*. To the best of our knowledge, this was never before found to be a marker of the ventral habenula, but its similarity to a protein already known to be expressed in the habenula makes it feasible that it is a valid result.

The expression of the neuronal marker *elavl3a* showed that the two habenular clusters and the OO cluster consisted of neurons expressing *gng8*. However, it leaves unanswered the identity of the remaining two cell populations that express low levels of *gng8*. A detailed analysis of these clusters revealed that cxcr4b was expressed in the ImnSys cluster while its ligand, cxcl12b, was expressed in the SktDev. This allowed us to hypothesize that the ImnSys could actually represent the cells transitioning from habenular progenitors to dHb cells, since these cells express cxcr4b (Dean *et al.*, 2014;

Roberson and Halpern, 2017a). Also, cxcl12b is expressed in cells surrounding the habenula and is involved in directing the habenula axons to the IPN, which suggested that these cells too could be related with the habenular clusters (Roberson and Halpern, 2017a). However, the ontogeny analysis revealed that the genes that were significantly expressed in these populations were part of important mechanisms for the Immune System (ImnSys Cluster) or of bone development (SktDev). Moreover, cxcl12b is also expressed in the branchial arches, which is in line with its ontogeny (Thisse and Thisse, 2014). Since we have no evidence of *gng8* being expressed in the skeleton or in cells of the immune system, we cannot be sure of the identity of these clusters. Therefore, to identify them, we will have to perform a double WISH for *gng8* and *cxcr4b* or *cxcl12b* at 4 dpf to find which cells express both markers.

In an attempt to understand the role of asymmetry for habenular function, a zebrafish habenular neurotransmitter map was built (deCarvalho *et al.*, 2014). In 4 dpf larvae, virtually all neurons of the dHb are glutamatergic, as seen by the colocalization of *gng8* and *slc17a6a* (deCarvalho *et al.*, 2014). This is strongly supported by our sequencing data (Supplementary Figure 3.5.A). Moreover, several dHb cells are cholinergic (*slc18a3b*) and somatostatinergic (*sst1.1*), and express the substance P-family neurotransmitter marker *tac3a* (Supplementary Figure 3.5.D). Lastly, a rare population of dHb cluster cells also express GABBA markers, as shown to be the case in 10 dpf zebrafish (Pandey *et al.*, 2018).

The 10 dpf larva has 15 habenular clusters, and a few of these already are represented at 4 dpf (Pandey *et al.*, 2018). The two right dHb enriched clusters (*cavin4b/murcb* in 5 cells and *adrb2a* in 8), the four left-enriched clusters (*adcyap1a* in 7 cells, *ppp1r1c* in 7, *pcdh7b* in 8, and *wnt7aa* in 19), and the vHb cluster (*kiss1* in the vHb cluster). Four other clusters were also represented (*cbln2b* in 16 cells, *lrrtm1* in 14, *c1ql4b* in 1 and *gad2* in 5) and two were not represented (*sox1a* and *htr1aa*). However, the most relevant of all is the high expression of the marker of immature habenular neurons at 4 dpf (*tubb5b* in 60 cells, Supplementary Figure 3.4.B). At 10 dpf, this population only represents about 5% of the dataset, despite all clusters having a fraction of cells that express this gene in very low levels (Pandey *et al.*, 2018). This suggests that at 4 dpf there are more immature neurons than at 10 dpf. On the other hand, this result must be taken with caution, since it could be the result of a confounding factor. If the mature cells are more sensitive to the current protocol and died along the process, then these will naturally be less represented, leaving the non-fully-committed neurons (Sassen *et al.*, 2017).

3.3.5. Concluding Remarks

Despite room for improvement, the protocol here optimised allowed for the collection of single cells of *gng8*-expressing tissue of 4 dpf larvae. By further optimising the protocol as suggested above, this methodology can be used to answer many more developmental questions. For instance, by isolating and transcriptionally profiling habenular progenitors, we may be able to characterise the signals that are important during earlier stages of development for the correct assignment of the left and right character of dHb cells. Also, by applying this technique directly to study several of the recently isolated habenular mutants at 4 dpf, we will be able to fully characterise the populations that are missing in each line, and correlate that with the molecular pathway that is affected.

3.4. SUPPLEMENTARY FIGURES

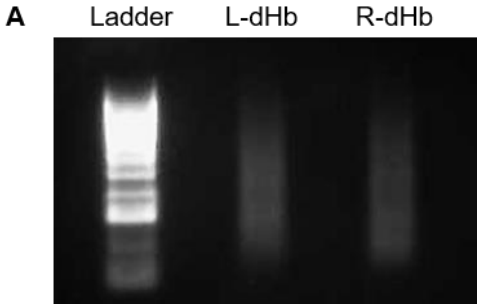

Supplementary Figure 3.1. cDNA library of left and right dHb cells. Gel Electrophoresis of the synthetized cDNA from the 384 left and right GFP-positive cells collected in Figure 3.1.C'. The cDNA smear is expected due to fragmentation of the RNA at the beginning of the protocol.

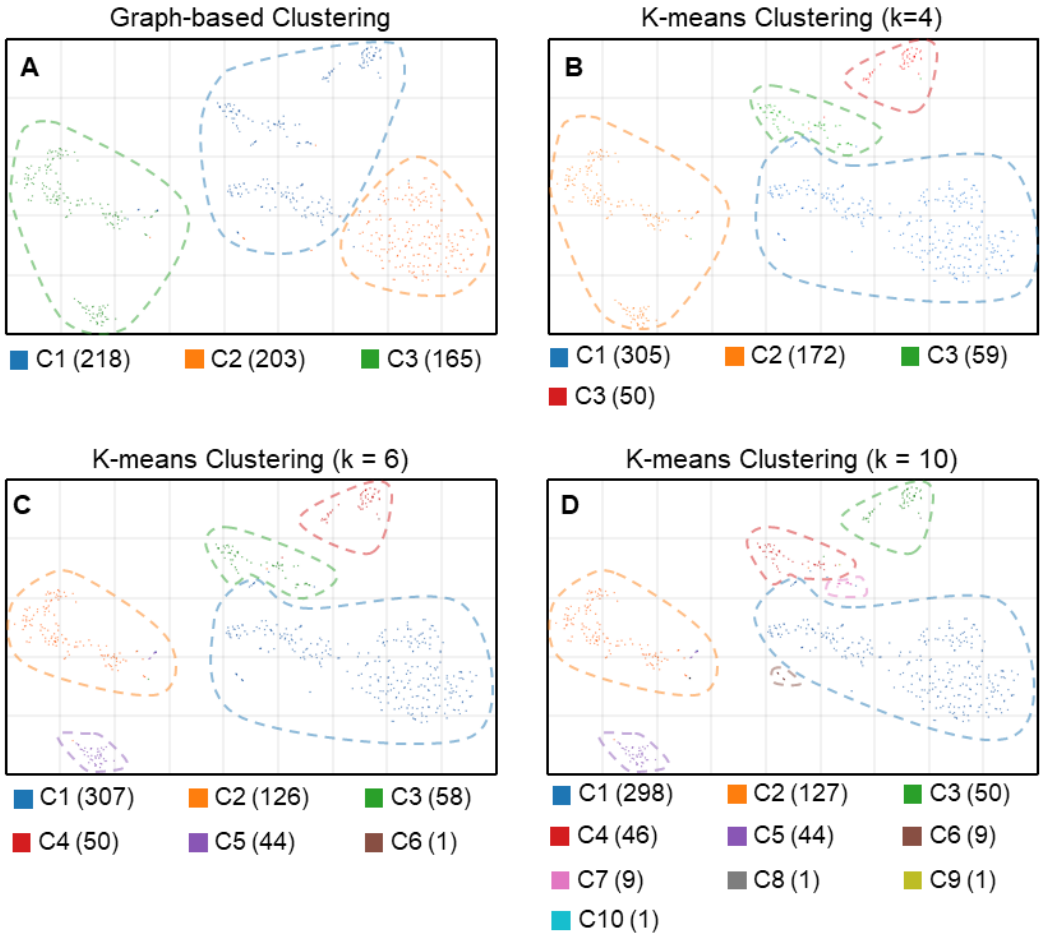

Supplementary Figure 3.2. t-SNE plots of Graph Based and K-Mean analysis of scRNA-seq data. (A) Graph Based analysis predicts three significantly different clusters. **(B-D)** K-Mean analysis predicts up to 10 significantly different clusters. Note that (K = 6) analysis is sufficient to distinguish the five main populations and (K=10) detects two more populations with nine cells, each, but none in the habenular clusters (C6 and C7).

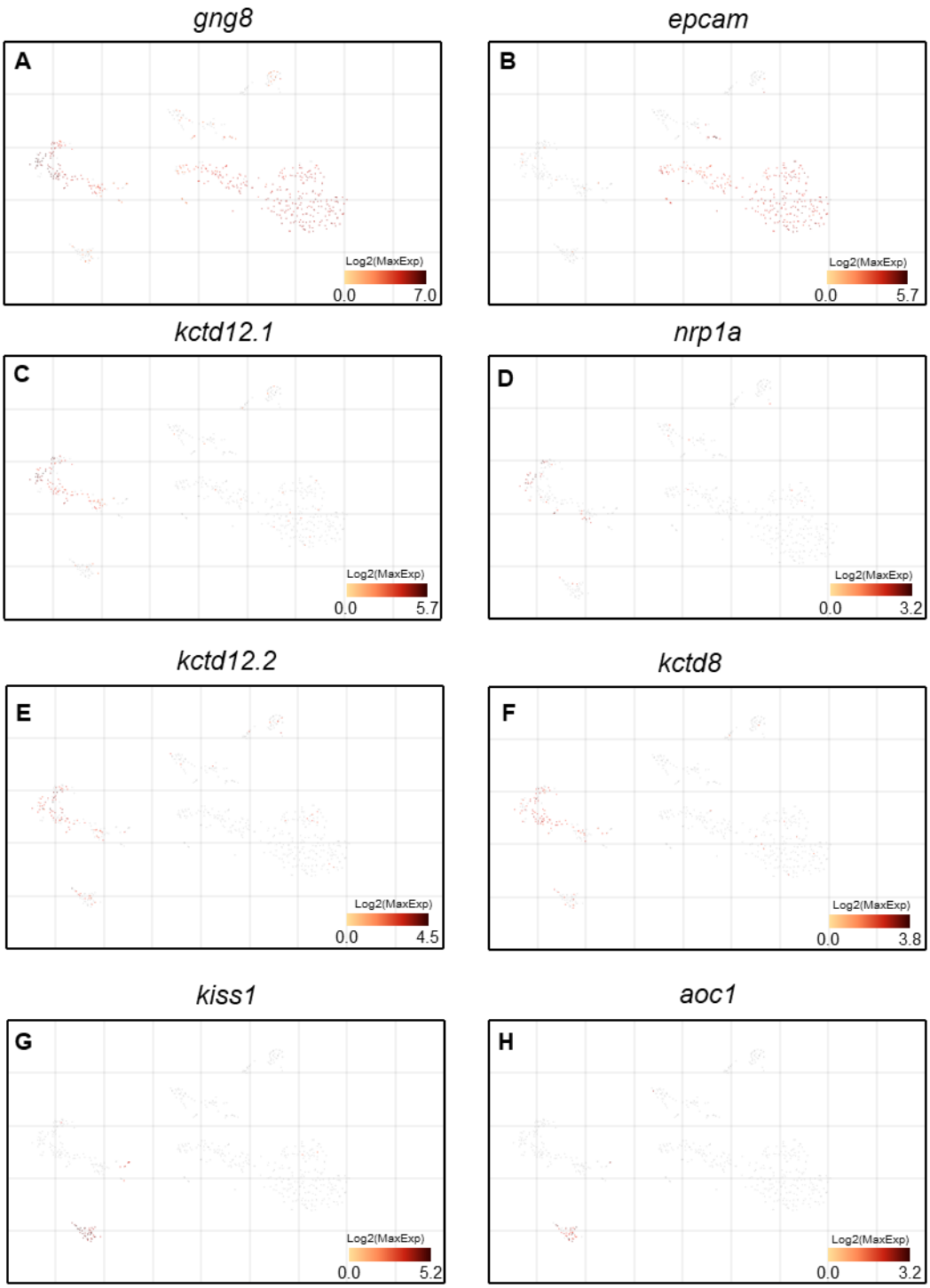

Supplementary Figure 3.3. Gene heatmap of known markers of Hb and OE. (A-J) Heatmap of the maximum expression of a known dHb marker (A); OO marker (B); two left dHb markers (C and D); two right dHb markers (E and F); and two vHb markers (G and H). Log_2(MaxExp) is the logarithm of the maximum expression of a gene in each cell as calculated by the 10x Genomics Loupe Cell Browser.

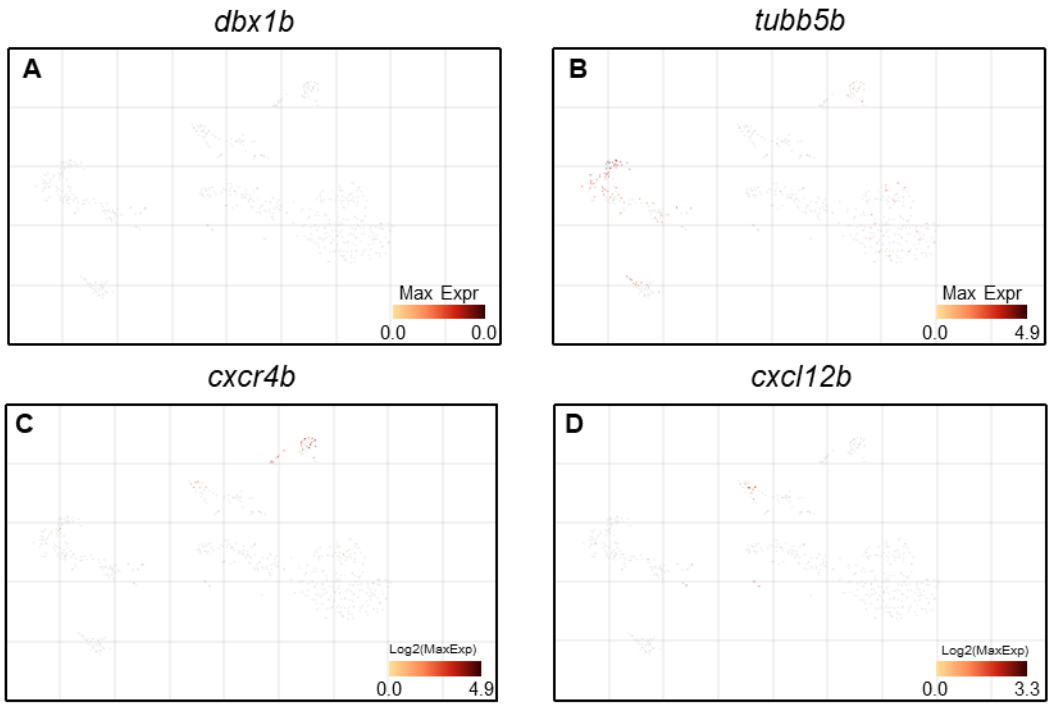

Supplementary Figure 3.4. Gene heatmap of known markers of pHb. (A-D) Heatmap of the maximum expression of a known pHb marker (A); a pHb marker showed to be expressed in 10 dpf gng8-positive cells (B); a pHb to dHb transition marker (C); and its ligand (D). Log_2(MaxExp) is the logarithm of the maximum expression of a gene in each cell as calculated by the 10x Genomics Loupe Cell Browser.

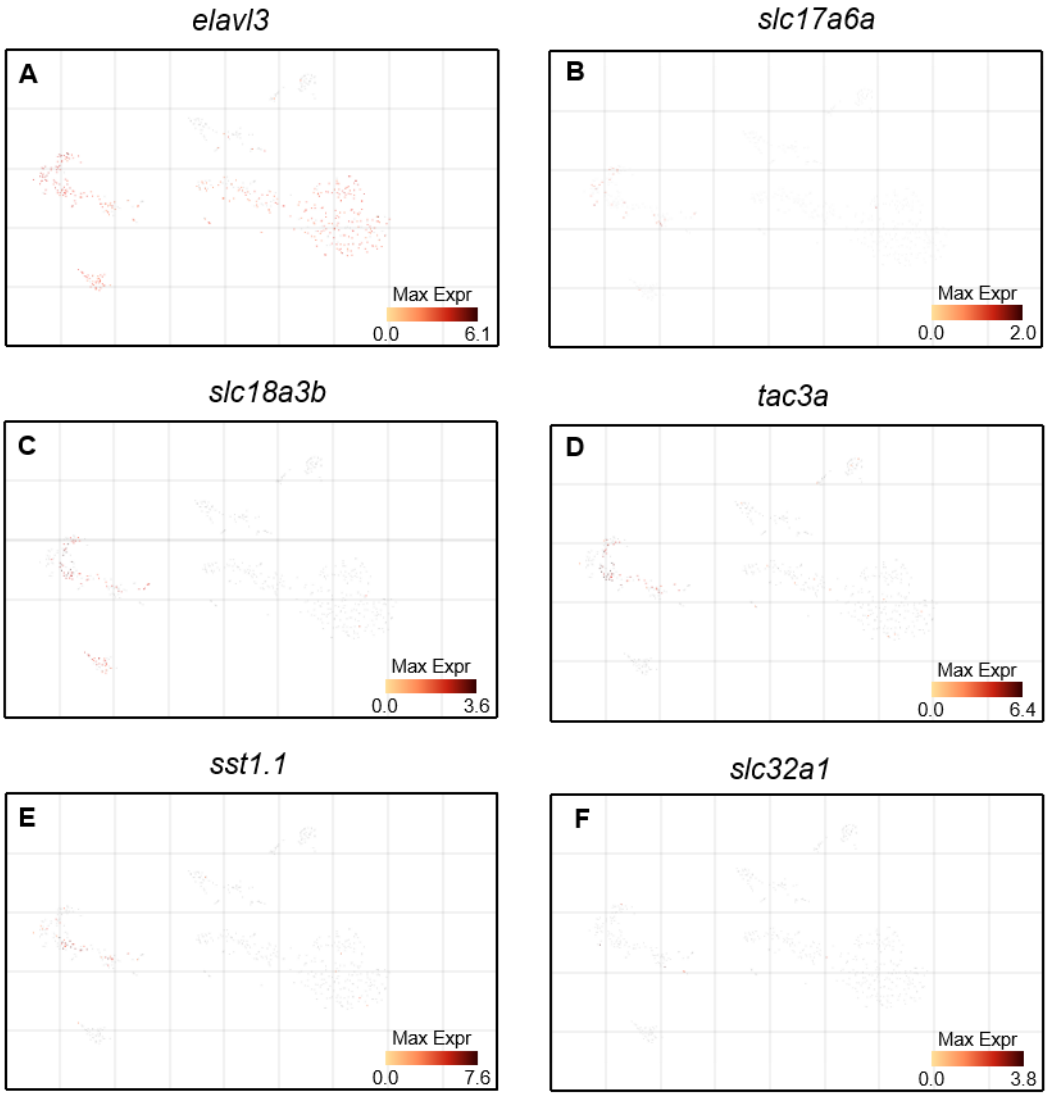

Supplementary Figure 3.5. Gene heatmap of neuron markers and neurotransmitters known to be expressed in the dHb. (A-D) Heatmap of the maximum expression of markers of a known neuronal marker (A) and of the following neurotransmitters: glutamate (B), acetylcholine (C), substance P (D), somatostatin (E), and GABA (F). Log_2(MaxExp) is the logarithm of the maximum expression of a gene in each cell as calculated by the 10x Genomics Loupe Cell Browser.

Table 3.1. Top ten significantly up-regulated genes in the Olfactory Organ cluster. List of the top 10 up-regulated genes in the Olfactory Organ Cluster as calculated by the 10x Genomics Loupe Software. Gene Name categories were collected by manual search using the ZFIN online database. Gene Symbol, ENSEMBL ID, Log_2 Fold Change and p-value categories were exported from the Loupe Software. Log_2 Fold Change values were calculated between the cluster and all remaining sample cells. p-values were adjusted using the Benjamini-Hochberg correction for multiple tests.

Gene Symbol	Gene Name	ENSEMBL ID	Log_2 Fold Change	p-value
calb2a	calbindin 2a	ENSDARG00000041062	7.14	1.42E-41
s100z	S100 calcium binding protein Z	ENSDARG00000038729	6.75	1.41E-37
pvalb5	parvalbumin 5	ENSDARG00000032836	6.57	9.75E-37
prr15la	proline rich 15-like a	ENSDARG00000025615	6.77	1.03E-36
zgc:173593	ferritin, heavy polypeptide-like 30	ENSDARG00000077360	6.1	1.03E-33
selenow2b	selenoprotein W, 2b	ENSDARG00000089936	6.55	1.07E-33
abhd2b	Ab hydrolase domain containing 2b	ENSDARG00000045804	6.93	1.20E-32
si_ch211-153b23.5	N/A	ENSDARG00000058206	5.77	1.20E-32
gsnb	gelsolin b	ENSDARG00000045262	6.64	5.60E-32
thrap3a	thyroid hormone receptor associated protein 3a	ENSDARG00000101989	7.61	1.22E-31

Table 3.2. Top ten significantly up-regulated genes in the ImnSys cluster. List of the top 10 up-regulated genes in the Immune System cluster as calculated by the 10x Genomics Loupe Software. Gene Name categories were collected by manual search using the ZFIN online database. Gene Symbol, ENSEMBL ID, Log_2 Fold Change and p-value categories were exported from the Loupe Software. Log_2 Fold Change values were calculated between the cluster and all remaining sample cells. p-values were adjusted using the Benjamini-Hochberg correction for multiple tests.

Gene Symbol	Gene Name	ENSEMBL ID	Log2 Fold Change	p-value
fcer1gl	Fc receptor, IgE, high affinity I, gamma polypeptide like	ENSDARG00000104077	9.29	1.51E-45
npsn	nephrosin	ENSDARG00000010423	9.40	1.06E-44
mmp13a	matrix metallopeptidase 13a	ENSDARG00000012395	9.28	3.05E-44
arpc1b	actin related protein 2/3 complex, subunit 1B	ENSDARG00000027063	9.04	2.52E-42
si:ch211-9d9.1	N/A	ENSDARG00000099839	10.63	1.78E-40
mmp9	matrix metallopeptidase 9	ENSDARG00000042816	8.52	1.00E-39
pfn1	profilin 1	ENSDARG00000088091	7.35	4.62E-37
coro1a	coronin, actin binding protein, 1A	ENSDARG00000054610	8.09	5.75E-35
il1b	interleukin 1, beta	ENSDARG00000006029	7.45	1.81E-34
lta4h	leukotriene A4 hydrolase	ENSDARG00000098700	8.72	2.00E-34

Table 3.3. Top ten significantly up-regulated genes in the SktDev cluster. List of the top 10 up-regulated genes in the Skeletal Development cluster as calculated by the 10x Genomics Loupe Software. Gene Name categories were collected by manual search using the ZFIN online database. Gene Symbol, ENSEMBL ID, Log_2 Fold Change and p-value categories were exported from the Loupe Software. Log_2 Fold Change values were calculated between the cluster and all remaining sample cells. p-values were adjusted using the Benjamini-Hochberg correction for multiple tests.

Gene Symbol	Gene Name	ENSEMBL ID	Log2 Fold Change	p-value
rbp4	retinol binding protein 4, plasma	ENSDARG00000101199	9.53	3.88E-28
pmp22a	peripheral myelin protein 22a	ENSDARG00000105223	8.25	6.12E-20
si:ch211-251b21.1	N/A	ENSDARG00000007275	8.33	1.01E-18
sparc	secreted protein, acidic, cysteine-rich (osteonectin)	ENSDARG00000019353	6.72	1.69E-18
zgc:77517	keratin 18b	ENSDARG00000028618	7.44	8.02E-18
col1a1a	collagen, type I, alpha 1a	ENSDARG00000012405	8.76	1.91E-16
krt18	keratin 18a, tandem duplicate 1 (?)	ENSDARG00000058358	5.46	3.48E-15
krt8	keratin 8	ENSDARG00000058358	5.46	3.48E-15
cebpd	CCAAT enhancer binding protein delta	ENSDARG00000087303	5.18	1.89E-14
cyr61	cellular communication network factor 1, like 2	ENSDARG00000023062	7.43	9.28E-14

Table 3.4. Top ten significantly up-regulated genes in the dHb cluster. List of the top 10 up-regulated genes in the Dorsal Habenula cluster as calculated by the 10x Genomics Loupe Software. Gene Name categories were collected by manual search using the ZFIN online database. Gene Symbol, ENSEMBL ID, Log_2 Fold Change and p-value categories were exported from the Loupe Software. Log_2 Fold Change values were calculated between the cluster and all remaining sample cells. p-values were adjusted using the Benjamini-Hochberg correction for multiple tests.

Gene Symbol	Gene Name	ENSEMBL ID	Log_2 Fold Change	p-value
kctd12.1	potassium channel tetramerisation domain containing 12.1	ENSDARG00000069843	6.97	6.34E-33
nwd2	NACHT and WD repeat domain containing 2	ENSDARG00000077162	6.26	8.24E-33
syt9b	synaptotagmin Ixb	ENSDARG00000029239	7.90	4.56E-32
kctd4	potassium channel tetramerization domain containing 4	ENSDARG00000068691	8.04	3.44E-31
zgc:162707	n.a.	ENSDARG00000061664	7.74	1.90E-30
tac3a	tachykinin 3a	ENSDARG00000093089	7.91	4.94E-30
pcp4a	Purkinje cell protein 4a	ENSDARG00000053130	5.50	1.06E-26
cadps2	Ca++-dependent secretion activator 2	ENSDARG00000013312	6.18	1.30E-26
tmem178	transmembrane protein 178	ENSDARG00000020758	7.71	2.95E-26
cckb	cholecystokinin b	ENSDARG00000100052	8.52	9.62E-26

Table 3.5. Top ten significantly up-regulated genes in the VHb cluster. List of the top 10 up-regulated genes in the Ventral Habenula cluster as calculated by the 10x Genomics Loupe Software. Gene Name categories were collected by manual search using the ZFIN online database. Gene Symbol, ENSEMBL ID, Log_2 Fold Change and p-value categories were exported from the Loupe Software. Log_2 Fold Change values were calculated between the cluster and all remaining sample cells. p-values were adjusted using the Benjamini-Hochberg correction for multiple tests.

Gene Symbol	Gene Name	ENSEMBL ID	Log2 Fold Change	p-value
gng14	guanine nucleotide binding protein (G protein), gamma 13a	ENSDARG00000062537	9.43	8.17E-38
kiss1	KiSS-1 metastasis suppressor	ENSDARG00000075829	7.87	6.96E-29
csrp2	cysteine and glycine-rich protein 2	ENSDARG00000011961	8.02	5.84E-28
fo704871.1	N/A	ENSDARG00000078272	7.78	1.93E-22
ak5	adenylate kinase 5	ENSDARG00000012555	6.68	1.70E-20
lmo3	LIM domain only 3	ENSDARG00000008720	6.11	3.56E-19
prkcq	protein kinase C, theta	ENSDARG00000034173	7.69	3.81E-18
necab1	N-terminal EF-hand calcium binding protein 1	ENSDARG00000056566	6.49	2.06E-17
ppp1r14ab	protein phosphatase 1, regulatory (inhibitor) subunit 14Ab	ENSDARG00000017710	6.03	6.47E-16
zfhx4	zinc finger homeobox 4	ENSDARG00000075542	5.89	8.86E-16
aoc1	amine oxidase, copper containing 1	ENSDARG00000061355	7.69	1.19E-15

CHAPTER 4.

ASSESSING IF THERE IS A ROLE FOR HABENULAR ASYMMETRY IN ACQUIRING AND MODULATING HEAT-STIMULI RESPONSES.

4.1. INTRODUCTION

The habenula has been shown to play a role in the modulation of circadian timekeeping, stress, fear, depression and the reward system (Matsumoto and Hikosaka, 2007; Agetsuma *et al.*, 2010; Baño-Otálora and Piggins, 2017). Although it is not well understood how the habenula plays a role in these diverse behavioural pathways, the accumulated evidence suggests that this structure signals the negative value of an experience (Hikosaka, 2010). This means that the habenula is activated by aversive stimuli, the lack of reward or in response to cues associated to these negative-valued experiences.

In humans, primates and rodents, the lateral habenula is activated in response to the negative value of a stimulus (such as a punishment or the lack of reward) and to the cues of such stimuli (Matsumoto and Hikosaka, 2007, 2009a; Agetsuma *et al.*, 2010; Stephenson-Jones *et al.*, 2016; Liu *et al.*, 2017). This activation is modulated by a subdomain of the Globus Pallidus that is also activated by negative stimuli (Hong and Hikosaka, 2008, 2013; Stephenson-Jones *et al.*, 2016).

The vHb of zebrafish was previously shown to have increased activity as expectation of punishment grows, and have reduced activity as avoidance learning consolidates (Amo *et al.*, 2014). Like in mammals, the vHb receives input from the fish homolog of the Globus Pallidus: the ventral entopeduncular nucleus (vENT) (Amo *et al.*, 2014; Turner *et al.*, 2016). However, the vENT also projects to the dHb, rendering the whole habenula a candidate for signalling the negative value of a stimulus (Turner *et al.*, 2016). In line with this, the habenula of both mammals and fish projects to the IPN and Raphe, providing a route to influence dopaminergic and serotonergic pathways (Aizawa *et al.*, 2005; McCallum *et al.*, 2012). Both these neurotransmitter pathways play a role in reward prediction, which puts the habenula in a unique position to signal negative stimuli to the pathway (Matsumoto and Hikosaka, 2009b; Cohen, Amoroso and Uchida, 2015; Matias *et al.*, 2017; Elston, Kalhan and Bilkey, 2018).

In zebrafish, dHb functional studies have focused on its asymmetric character. The left dHb mostly responds to visual stimuli, while the right dHb mostly responds to odour (Dreosti *et al.*, 2014). This is likely due to the asymmetric input from sensory centres: the olfactory bulbs project to the right nucleus, while the *Eminentia Thalami* (EmT) projects to the left (Hendricks and Jesuthasan, 2007; deCarvalho *et al.*, 2013; Turner *et al.*, 2016). On the other hand, both habenular nuclei respond to heat stimuli, despite the right habenula being more activated than the left (Haesemeyer *et al.*, 2018). This is because the right habenula consists of more neurons that respond to the start of the heat stimulus, while the left habenula has more neurons that respond at its termination (Haesemeyer

et al., 2018). Likewise, the activation of the habenula by carbon dioxide is also seen first in the right then in the left habenula and IPN (Koide, Yabuki and Yoshihara, 2018). This suggests that the asymmetry of larval zebrafish habenula may be important for its lateralised function whilst signalling the negative value of a response. However, no study has specifically shown this to be the case.

Therefore, to understand if the habenular asymmetry is important for signalling negative-valued stimuli, I aimed to test habenular asymmetry mutants in an operant learning paradigm: the Relief Of Aversive Stimulus by Turn (ROAST) assay. In this assay, we test the capacity of zebrafish to terminate an aversive heat stimulus by reversing their directional preference during the response to that stimulus (Li, 2012). The first response of larval zebrafish to heat is a high-angle amplitude flick of the tail, which is directionally biased in each individual fish (Li, 2012; Haesemeyer *et al.*, 2015, 2018). By terminating the heat stimulus only when the direction of the first response opposes the naïve preference, this assay promotes the reversal of the directional preference. If the habenular asymmetry is needed to signal the negative-valued stimuli (i.e. the heat), then learning this task should be dependent on the correct formation of this structure.

In this work, wild-type larvae and two habenula asymmetry mutants which develop with symmetric dHb with left-habenula character, were tested in the ROAST assay. By comparing the performance of groups of fish, the ROAST assay detected a possible phenotype in a GFP expressing transgenic line, but not in any of the habenula asymmetry mutants. However, these experiments allowed the optimisation of the assay and through retrospective data analysis, to increase throughput. This way, if the ROAST assay is able to detect differences in mutants with symmetric dHb with right-habenula character, the assay may be included in a pipeline of habenular asymmetry mutant studies.

4.2. RESULTS

4.2.1. The ROAST assay as an operant learning paradigm applied to larval zebrafish.

To understand if habenular asymmetry is needed for establishing association between the response to a stimulus with a negative value and its outcome, we established a version of the ROAST assay in our laboratory (Li, 2012). In this assay, 6-8 dpf tail-free tethered larvae are exposed to an infrared laser and tail responses are recorded (Figure 4.1.A). The laser, pointing to the head, generates increasing heat which promotes an escape response. The stereotypical first response of zebrafish to aversive heat is a high-angle unilateral flick of the tail, which shows a directional bias (Haesemeyer *et al.*, 2015). Thus, if a fish is exposed to heat stimulus and its first tail flick is towards the left, it is very likely that in following trials its first response to the stimulus will also be to the left. The ROAST assay explores the capacity of zebrafish to reverse this bias, by rewarding the direction that opposes the fish preference.

To achieve this, the ROAST assay is split in two blocks. In the first one, the directional preference is assessed for each individual fish in the first 3 trials. Each of these trials start with the laser switching ON and the tail response is monitored by a camera above the mounted fish (Figure 4.1.A). Once the fish responds with a long-angle tail response the laser is switched OFF. This is done independently of the side of the turn, to allow us to assess the preferred direction of the first response.

Having established a fish directional preference, the ROAST assay attempts to reverse this bias during the second block, the Contingency Block, which consists of 30 trials (Figure 4.1.B). This is achieved by switching the laser OFF when the tail response is towards the side that opposes the larva preference (Figure 4.1.B). For example, if during the first 3 trials a fish responds to the heat stimulus by turning to the left, during the contingency block it has to turn to the right for the laser to be switched OFF. Otherwise, the laser is kept ON until the larva responds in the correct direction.

To assess the fish performance during the ROAST assay, we extracted three parameters. The first parameter represented if the direction of the first response to the laser during each trial was towards the preferred side (Correctness = 0) or to the opposite side (Correctness = 1; Figure 4.1.D). Since what is intrinsic to heat-response behaviour is the direction of the first turn, this was the behaviour that we aimed to reverse. Therefore, being able to turn the laser OFF on the first try is classified as a correct trial, otherwise it is classified as a wrong trial.

Second, we extracted the time between the laser being switched ON and the first response of the larva (Latency of First Turn, LFT), and the time between the laser being switched ON and the correct response (Latency to Laser Off, LLO) (Figures 4.1.D and 4.1.E). Since the population of neurons that are activated by the beginning of heat stimuli are mostly localised in the right dHb, and the neurons activated by the end of heat stimuli in the left dHb, the loss of one of the nuclei in a habenula asymmetry mutant could alter the ability to respond to the beginning or the end of the stimulus (Haesemeyer *et al.*, 2018). Thus, loss of asymmetry could affect the capacity to detect the beginning of the stimulus and this would be detected by changes in LFT. Alternatively, it could affect the capacity to associate reversal of the direction with rewarding outcome (i.e. end of the stimulus), and this would be detected by no changes in LLO since fish would not attempt a reversal earlier than in previous successful trials.

To test if the assay was performing as reported, 5 to 9 dpf wild-type larvae were tested for one contingency block of the ROAST assay (Figure 4.1.C). In the first trial, only 25% of the larvae responded to the laser towards the opposite side of their bias (Figure 4.1.C). However, during the first ten trials, the response significantly increased to about 75%, and remained above 50% for the remainder of the experiment (one-way ANOVA, p-value < 0.05). This suggests that during the first ten trials, the larvae were able to modulate their behaviour in order to terminate the aversive stimulus at the first try. In fact, the LFT decreased from 6 to 4 seconds in the first two trials, showing that on top of reversing their bias, wild-type larvae started responding faster to the stimulus (Figure 4.1.D). Moreover, this latency remained stable throughout the experiment, suggesting that the heat stimulus was not harmful and that the ROAST assay did not drive helplessness behaviour. The LLO values also illustrated the gradual learning process, decreasing from 17 to 5 seconds in the first 10 trials, concurrent with the increased fraction of larvae that started responding correctly.

Altogether, these results suggest that wild-type larvae zebrafish are able to establish a correlation between the side of the tail flick and its outcome. Moreover, the ROAST assay allows us to study this behaviour at the population level, which is important for habenular asymmetry mutant studies.

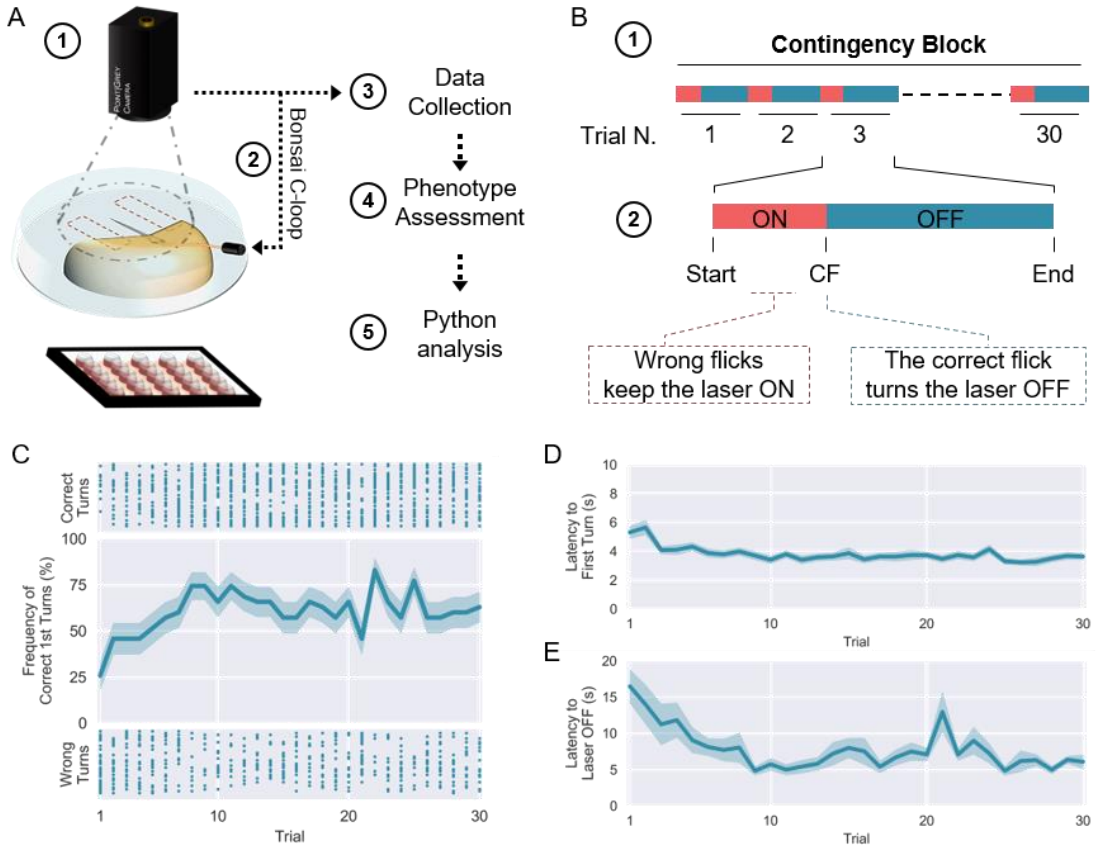

Figure 4.1. Wild-type zebrafish improve performance in ROAST assay. (A) Schematic of ROAST assay setup. (1) Larvae zebrafish were embedded in 2% low-melting point agarose on a 10 cm petri dish filled with fish water. To allow free tail movements, the agarose was removed caudal to the swim bladder. A laser is positioned directly in front of the fish and targets the head. Infrared light-source under the rig allow for homogeneous recording image by the camera above the rig. (2) A Bonsai Closed-loop program controls the laser activity based on the tail response. Two regions of interest (ROI) are digitally placed on each side of the tail. Their activation depends on the level of pixel change (see Methods and panel B). (3) Data is stored for offline analysis (5), after assessment of the larvae phenotype or genotype (6). **(B)** The ROAST assay consists of a Contingency Block where the laser only turns OFF in response to a turn against the fish bias (analysed before the first trial, in a best-of-three-trials basis). (1) The block consists of 30 uninterrupted trials, with random duration, calculated between one and two minutes. (2) Each trial starts with the laser ON. If the zebrafish flicks to the biased side during this phase, the trial is marked as Wrong Turn. In this case, the laser remains ON and the system is unresponsive for 200 ms. Then, the laser will only turn OFF once the larvae flicks to the opposite side of its bias. If this is the first response to the laser, the trial is marker as Correct Turn. In either case, the laser stays OFF until the end of the calculated duration, after which a trial begins. **(C)** Frequency of wild-type larvae that turned to the opposite side of their internal bias as a first response to the laser (n = 35). Shaded colour represents the standard error of the mean. Dots plotted above

and below represent the correct or incorrect first response of individual fish, respectively. **(D)** Average latency of the first response to the laser in each trial. Shaded colour represents the standard error of the mean. **(E)** Average latency of the correct turn in response to the laser. Shaded colour represents the standard error of the mean.

4.2.2. *tcf7l2*^{u754},Tg(*gata2a:eGFP*)^{pku588} mutants and siblings fail to respond to heat-stimuli.

The first block of 30 trials of the ROAST assay, the contingency block, tests the acquisition of a response to heat stimuli. However, it does not test the flexibility of an animal to switch that response for a better outcome. Learning implies that the increase in performance during the contingency block is not definitive, but rather reversible when a fish is faced with a reversal of the contingency. For instance, after a successful contingency block, a larval zebrafish should be able to switch back to its preferred direction if the laser is kept ON after turns in the opposite direction. Therefore, in the ROAST assay, the contingency block is followed by a contingency reversal block, where the preferred direction is favoured (Figure 4.2.A).

The increase in performance of wild-type larvae during the contingency block was very similar to during the contingency block reversal (two-way ANOVA, p-value > 0.05; Supplementary Figure 4.1.A). Like in the previous results, the first trial of both blocks started at 25% and gradually increased to above 50%. Since the larvae had no cue signalling the start of the new block, the decrease in performance in the first trial of the contingency reversal block shows that most larvae still responded as if in the contingency block (i.e. opposing the bias). Moreover, both LFT and LLO increased in the first trials of the contingency reversal block (Supplementary Figures 4.1.C and 4.1.D). Again, only when the performance increased did latencies decrease back to stable levels. These results show that wild-type larvae were able to acquire and modulate their response to the heat stimulus during two consecutive blocks of the ROAST assay.

To understand if habenular asymmetry had a role in learning, we tested a mutant of dHb asymmetry in the ROAST assay (Figure 4.2.B). *tcf7l2*^{u754} homozygous mutants develop a left isomerized dHb, while siblings do not show any molecular or anatomical phenotype (Hüsken *et al.*, 2014). Therefore, we compared the performance of *tcf7l2*^{u754} phenotypic mutants and siblings in the ROAST assay (Figure 4.2.B). We used the Tg(gata2a:eGFP)^{pku588} transgene to determine habenular phenotype and infer genotype. As was shown in Chapter 2, this transgene expresses more GFP in the left dHb (Figure 2.2.A and 4.2.C). However, homozygous mutants for *tcf7l2* express GFP in both dHb

nuclei (Figure 4.2.C). This way, after the ROAST assay, larvae were assessed for their GFP expression so that the data from siblings and mutants could be analysed separately.

Despite using *tcf7l2*^{u754},Tg(*gata2a:eGFP*)^{pku588} siblings as controls for the performance of mutants, both groups showed a phenotype (Figure 4B). Although the frequency of correct responses of siblings increased from 25% in the first ten trials of both blocks, it oscillated above and below 50% for the rest of the block (p-value > 0.05; Figure 4.2.B, blue). The *tcf7l2*^{u754},Tg(*gata2a:eGFP*)^{pku588} mutants did not show an increase in performance in any of the blocks (p-value > 0.05; Figure 4.2.B, red). Nevertheless, both groups showed very high levels of FTL and LLO, much higher than those observed for wild-type (Figures 4.2.D and 4.2.E). This showed that both mutant and siblings took longer to respond to the laser than what had been previously observed in wild-types.

Since both groups showed a phenotype, we performed a careful analysis to understand what was causing the phenotype. This revealed that 4 out of 8 siblings and 8 out of 11 mutants did not respond to the laser in the majority of the trials. When re-analysing the remaining larvae, the performance of mutants and siblings improved, becoming similar to wild-type results (Supplementary Figures 4.4.A, 4.5.A and 4.6.A). However, the variability of responses was very high, possibly due to the low number of analysed larvae. Moreover, despite both latency values decreasing significantly, FTL values still reached an average of 20 seconds in several trials and LLO levels were still very high for siblings in most of the trials (Supplementary Figures 4.4.C to 4.4.D', 4.5.C to 4.5.D' and 4.6.C to 4.6.D'). Therefore, even the larvae that responded to most of the trials did not perform as expected by the analysis of wild-type behaviour data.

In summary, despite wild-type fish showing the capacity to acquire and modulate their response to the heat stimulus during the ROAST assay, *tcf7l2*^{u754},Tg(*gata2a:eGFP*)^{pku588} mutants fail to do so. However, sibling Tg(*gata2a:eGFP*)^{pku588} wild-type or heterozygous for the *tcf7l2* mutation also show a behavioural phenotype, suggesting that the eGFP expression may affect behaviour during the ROAST assay.

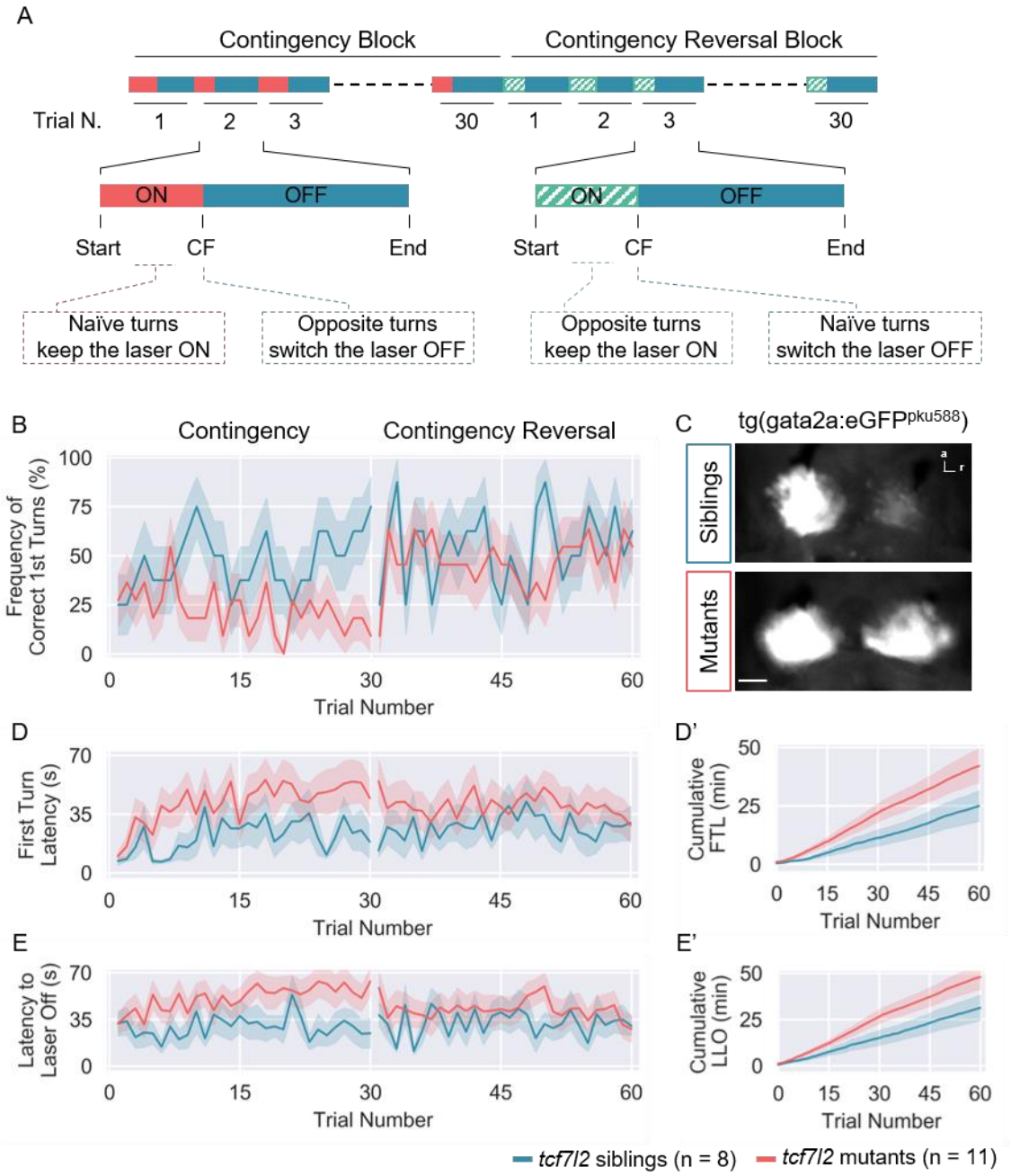

Figure 4.2. The tcf7l2^{u754},Tg(gata2a:eGFP)^{pku588} mutants have longer FTL and LLO than siblings. **(A)** Schematic of ROAST assay setup with a Contingency Block and Reversal Contingency Block. In this version of the assay, after the first 30 blocks, the naïve side is rewarded. This block resembles the first one (explained in Figure 4.1.B) with the exception that the laser is only switched OFF in response to a turn to the biased side, forcing a reversal of the first contingency. **(B)** Frequency of *tcf7l2*^{u754},Tg(*gata2a:eGFP*)^{pku588} siblings (blue, n= 8) and mutants (red n = 11) larvae that turned to the opposite side of their internal bias in the Contingency Block or to their naïve preference in the Reversal Contingency Block, as a first response to the laser. Shaded colour represents the standard error of the mean. **(C)** Dorsal view of the epithalamus of *tcf7l2*^{u754},Tg(*gata2a:eGFP*)^{pku588} siblings and mutants, *in vivo.* Legend: a, anterior; r, right.

Scale bar: **35** um. **(D)** Average latency of the first response to the laser in each trial. Shaded colour represents the standard error of the mean. **(D')** Cumulative latency of the first response to the laser. Shaded colour represents the standard error of the mean. **(E)** Average latency of the correct turn in response to the laser. Shaded colour represents the standard error of the mean. **(E')** Cumulative latency of the correct turn in response to the laser. Shaded colour represents the standard error of the mean.

4.2.3. *rorschach*^{u761} mutants behave like siblings in the ROAST assay.

Given the results with the *tcf7l2*^{u754},Tg(*gata2a:eGFP*)^{pku588} mutants, another habenula asymmetry mutant was tested in the ROAST assay: the *rorschach*^{u761} (*rch*^{u761}) mutant. When in homozygosity, the *rch*^{u761} mutation drives the formation of a left-isomerized dHb (similar to the *tcf7l2*^{u754},Tg(*gata2a:eGFP*)^{pku588} mutant), while no abnormal phenotype is seen in sibling heterozygotes (personal communication). Since these mutants do not show any other overt nervous system or other phenotypes, these mutants are well-suited to study the role of dHb asymmetry to acquire and/or modulate a behavioural response to heat stimuli (Faro, A., Powell, G., Wilson, S.W., unpublished data). Therefore, *rch*^{u761} mutants and siblings were tested in the ROAST assay and genotyped afterwards such that the analysis of wild-type, heterozygotes and mutants could be performed separately (Figure 4.3).

Since the increase of performance in the ROAST assay occurs in the first ten trials, the *rch*^{u761} mutants were tested in blocks of 20 trials rather than 30 trials, as in the previous experiments (Figure 4.3.A). This was done to decrease the duration of the assay, aiming for an increase of the throughput of future habenular mutant experiments. Like in the previous assays, all fish groups showed a low frequency of fish flicking to the correct side in the first trials of both blocks, followed by a progressive increase to above 50%. However, unlike in the experiment with *tcf7l2*^{u754},Tg(*gata2a:eGFP*)^{pku588} fish, these values tended to stabilize above 50% for the duration of both blocks. Moreover, the LTF and LLO of all groups were below 10 and 30 seconds, respectively, which are comparable to what was observed in the previous assays with wild-types (Figures 4.3.C to 4.3.D'). These results show that the response to the laser happens before 10 seconds, and that in trials when the first response was towards the unrewarded side, larvae took up to 30 seconds to reverse their bias.

Altogether, the ROAST assay showed that *rch*^{u761} mutants have the capacity to acquire and modulate their response to the heat stimuli, in a comparable way to wild-type fish. Also, their capacity to respond to the heat stimuli is not affected. Therefore, the habenular

asymmetry defect of *rch*^{u761} mutants does not affect the acquisition or modulation of learning nor the nociceptive perception.

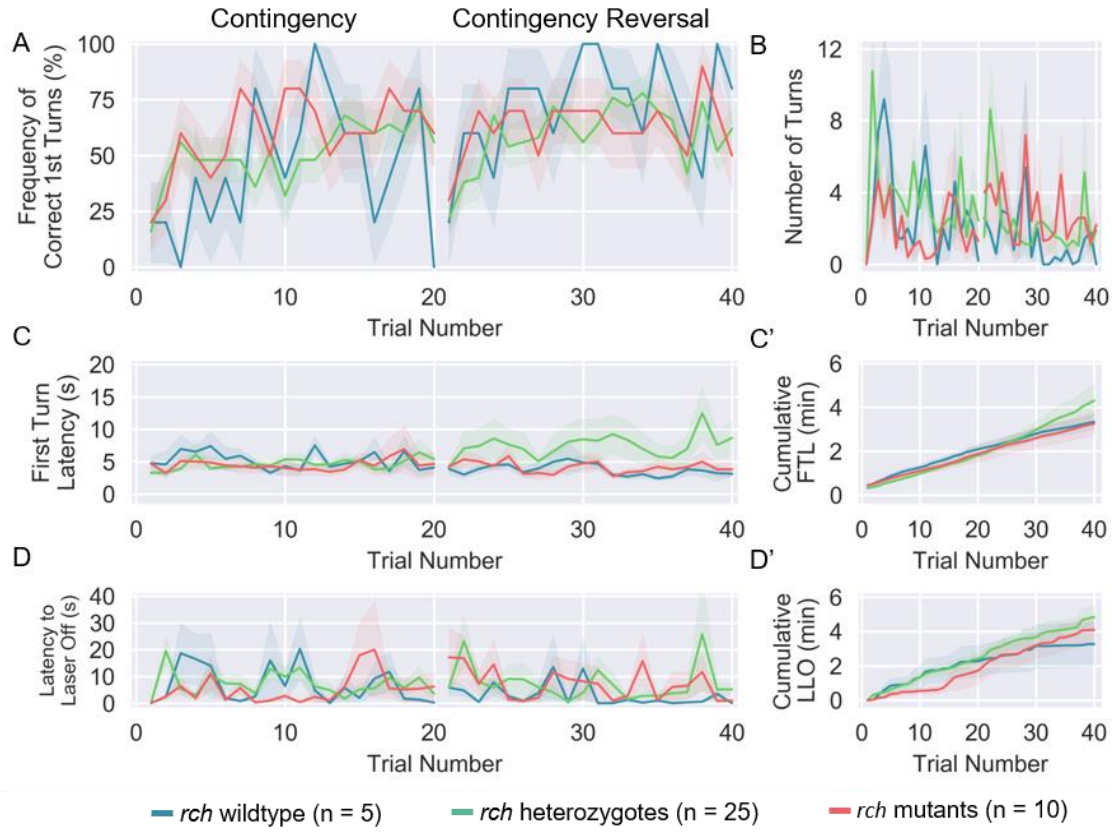

Figure 4.3. The rch^{u761} mutants have shorter FTL and LLO than wild-type. (A) Frequency of *rch*^{u761} mutants (red, n = 10), heterozygotes (green, n = 25) and wild-type siblings (blue, n = 5) that turned to the opposite side of their internal bias in the Contingency Block or to their naïve preference in the Contingency Reversal Block, as a first response to the laser. Shaded colour represents the standard error of the mean. **(B)** Average Number of tail flicks per trial before the laser is turned OFF. **(C)** Average latency of the first response to the laser in each trial. Shaded colour represents the standard error of the mean. **(C')** Cumulative latency of the first response to the laser. Shaded colour represents the standard error of the mean. **(D)** Average latency of the correct turn in response to the laser. Shaded colour represents the standard error of the mean. **(D')** Cumulative latency of the correct turn in response to the laser. Shaded colour represents the standard error of the mean.

4.3. DISCUSSION

4.3.1. Reversal learning in zebrafish larvae.

In this work, an operant learning assay was used to study the role of habenular asymmetry in the acquisition and modulation of a response to aversive-heat stimuli. Zebrafish larvae have previously been shown to perform well in learning paradigms. Larvae at 6 to 8 dpf already associate a visual cue (stimulus) with a touch on the side of the body, in a classical Pavlovian paradigm (Aizenberg and Schuman, 2011). Likewise, startle responses prompted by acoustic stimulus can be inhibited by weaker pre-pulses of the stimulus, which shows the capacity of association (Burgess and Granato, 2007). The capacity of associating an action (swimming to a dark compartment of an arena in response to a light) and its outcome (avoiding a shock) was shown to be present in adult zebrafish (Xu *et al.*, 2007). However, before the ROAST assay, this had not been tested in larval stages.

During the ROAST assay, wild-type zebrafish larvae responded to the stimulus with a high amplitude unilateral flick of the tail (Haesemeyer *et al.*, 2015, 2018). The frequency of larvae that switched the laser OFF in the first try increased during the initial trials (Figure 4.2.1). This showed that a response to the aversive heat is initially biased. However, it also shows that zebrafish larvae are able to associate the termination of the heat-stimulus with a turn that opposes the preferred direction. Moreover, this is not simply due to the learning of a timed sequence of movements because the duration of the trials is randomized and, therefore, the beginning of a trial cannot be predicted (Kawai *et al.*, 2015).

When the contingency was reversed, the frequency of correct responses sharply decreased. This showed that the majority of larvae were now biased towards opposing the naïve response (Supplementary Figure 4.1.1). Moreover, after the first trial of the reversal block, the frequency of correct turns increased back to levels higher than 50%, showing the capacity of extinction of a learned behaviour to optimise the outcome. This was shown before in adult zebrafish in a reversal learning paradigm, but seems to never have been tested in zebrafish larvae before the ROAST assay (Colwill *et al.*, 2005; Parker *et al.*, 2012; Ruhl *et al.*, 2015).

Reversal learning is an important characterise cognitive deficits in several human conditions, such as Obsessive-Compulsive Disorder or Schizophrenia (Valerius *et al.*, 2008; Reddy *et al.*, 2016). Although this is not in the scope of our research, the implementation of this assay may be of interest for the study of mutations known to have an impact in such disorders. On the other hand, despite not showing signs of structural defects, the habenula of schizophrenic patients lacks appropriate activity modulation in

response to negative feedback (Shepard, Holcomb and Gold, 2006). Therefore, there may be a link between some schizophrenia-associated behavioural symptoms and habenular malfunction.

4.3.2. ROAST assay controls and adjustments.

4.3.2.1. Minimising an association between wrong turns and good outcomes.

During the first trials of the ROAST assay, the zebrafish larva has to establish a correlation between the direction of its response to the stimulus and the outcome of that response. The zebrafish response to an aversive heat-stimulus consists of a fast (50 ms), large-amplitude turn followed by a quiescence state (Haesemeyer *et al.*, 2018). This means that any responses that closely follow the first response may be due to muscle compensatory movements, rather than a new reaction to heat. If this happens during a wrong response and the refractory movement of the response terminates the stimulus, then it is very likely that an association between response and outcome is not established. To account for this, there is a 120 ms refractory period after each wrong response, to minimise the chances that an unintentional flick to the correct side switches the laser off.

4.3.2.2. Using infrared laser as a source of heat.

The source of heat stimulus for the ROAST assay had to have a rapid onset, but more importantly, a rapid decrease to be sensed by the zebrafish. Without this, the association between the turn and the termination of the stimulus would not be established due to the lack of association between response and outcome. This is the main reason why the ROAST assay uses a laser that targets the head of zebrafish (Li, 2012; Haesemeyer *et al.*, 2015). However, this could be a confounding variable, since the dHb is activated by light stimuli, through the EmT (Hendricks and Jesuthasan, 2007; Dreosti *et al.*, 2014). Nevertheless, there are no reports of infrared opsins in fish. Thus, using an infrared laser as the heat stimulus and a source of infrared light for the rig illumination, there should be no effect on habenular activity driven by visual cues (Nawrocki *et al.*, 1985; Morris and Fadool, 2005). Therefore, the infrared sources of light should not be detected by the habenula during the ROAST assay.

4.3.2.3. Helpless behaviour.

During the ROAST assay, it was important to not drive a helpless-like behaviour, since the habenula is also implicated in modulating this behaviour (Lee *et al.*, 2010; Duboué *et al.*, 2017). Helpless behaviour can be promoted in behavioural experiments by creating an open, instead of a closed loop. In this case, an aversive stimulus is uncoupled to the larvae's response, and animals stop responding to the stimulus as their response

has no perceived effect upon outcome (Portugues and Engert, 2011). Although the ROAST assay is a closed loop, it was possible that short trials would also drive this behaviour because a late response could quickly be followed by the beginning of a new trial (i.e. Laser ON). However, the 1 to 2 minute trials seemed to be long enough to avoid helpless behaviour, since most larvae responded to all trials, and only 25% of *rch*^{u761} siblings, heterozygotes and mutants failed to respond to more than one trial (two wild-types, two mutants and five heterozygote fish), as reported before (Haesemeyer *et al.*, 2018).

4.3.2.4. Latency, lack of response.

In most experiments, the latency of response to the laser was stably under 10 seconds throughout most of the experiments. However, 4 out of 8 t*cf7l2*^{u754},Tg(*gata2a:eGFP*)^{pku588} siblings and 8 out of 11 mutants did not respond to the heat shock stimulus (Supplementary Figures 4.4 to 4.6). It is improbable that this could be due to heterozygotes also showing a phenotype since no molecular or anatomical defects are observed in heterozygotes for the mutation (Hüsken *et al.*, 2014). If heterozygotes did show a phenotype, this could mean that the behaviour assay is more sensitive at detecting a phenotype than the anatomical analyses. However, a small fraction of the mutants showed a wild-type-like phenotype, which makes it unlikely that the delay in responding to the stimulus is linked to the mutation. What we could ascertain, however, was that these results are not due to a technical failure, since wild-types from a separate line were tested in parallel and none showed this behavioural phenotype (Supplementary Figure 4.1). Although we have no proof to support this, it is possible that this could either be caused by an additional mutation(s) present in the background of the *tcf7l2*^{u754},Tg(*gata2a:eGFP*)^{pku588} line, or that the expression of GFP affected the correct brain function during the ROAST assay.

4.3.3. Is the left dHb sufficient for reversal of learning?

When testing the *rch*^{u761} mutants and siblings in the ROAST assay, we observed that all fish, independently of the habenular phenotype, performed like wild-types (Figure 4.3). This could be because the left dHb, rather than the right, is sufficient for learning the task in the ROAST assay. If this is the case, then right-isomerized habenula larvae would show decreased frequency of correct responses. It would also go in line with the asymmetric distribution of dHb neurons that signal the beginning and end of aversive heat stimuli (Haesemeyer *et al.*, 2018). It is possible that signalling the end of the stimulus by the left habenula is more important for reversal learning than signalling its beginning, since that is the point when the correct response triggers the end of the aversive stimulus. However, this does not explain why the latency of response did not increase in *rch*^{u761}

mutants, as would be expected if the right dHb neurons are important for signalling the beginning of the stimulus (Haesemeyer *et al.*, 2018). Possibly by revisiting the studies with the *tcf7l2*^{u7548} mutants in a non-transgenic background we would be able to understand if the same happens in all left-isomerised mutants. However, we must take into consideration that these mutants also lack the vHb, which could influence the ROAST assay given its role in learning (Hüsken *et al.*, 2014; Lupton *et al.*, 2017).

The results with the *rch*^{u761} mutants and siblings could also be explained by the habenula not being needed for the assay. If this is the cases then larvae with ablated or inactive dHb would be able to perform in the ROAST assay (Lupton *et al.*, 2017). Although we considered the *rerea*^{u757} mutant for this assay, the lack of swim bladder rendered it unsuitable for 6 to 8 dpf behavioural studies. Therefore, the best approach would be to generate transgenic lines that allow us to ablate or silence dHb cells. This can be achieved by expressing Killer Red in the dHb, which generates reactive oxygen species upon intense green light illumination, killing the cells that express it (Teh *et al.*, 2010). Neuron inactivation can be achieved by expressing botulinum toxin light chain B in the dorsal habenula, which binds to nerve terminals and blocks neurotransmitter release (Auer *et al.*, 2015).

4.4. SUPPLEMENTARY FIGURES

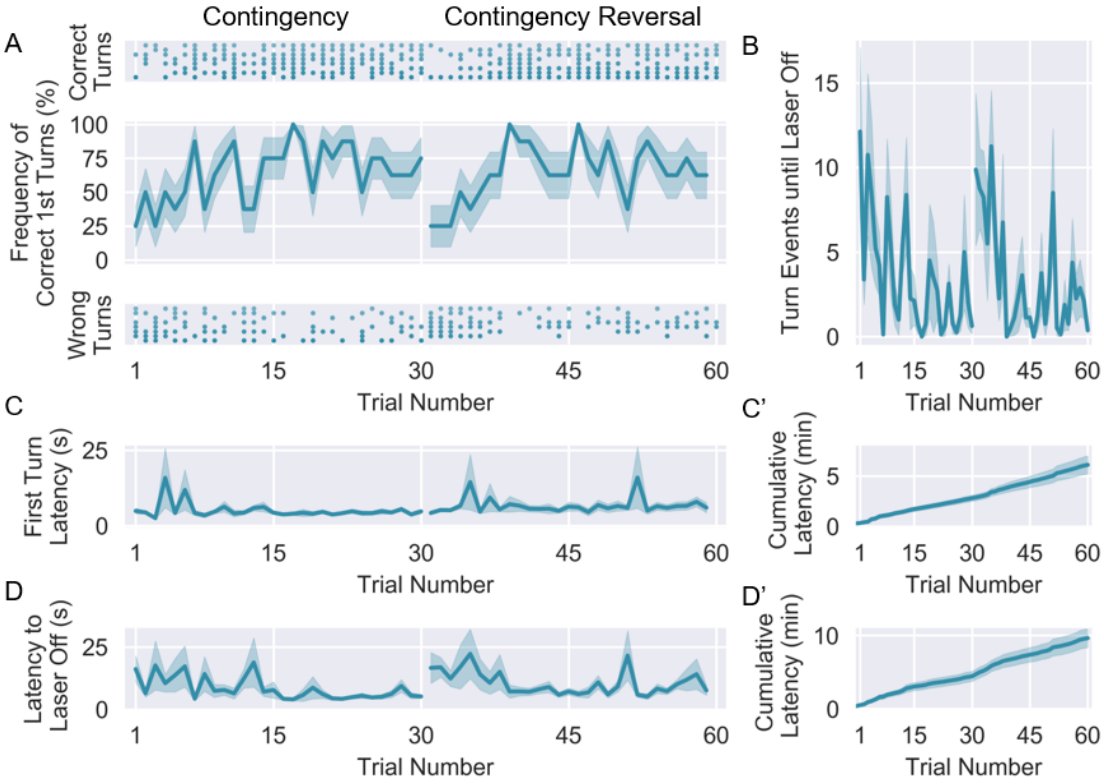

Supplementary Figure 4.1. Wild-type zebrafish improve performance in both blocks of the ROAST assay. **(A)** Frequency of wild-type larvae (blue, n = 8) that turned to the opposite side of their internal bias in the Contingency Block or to their naïve preference in the Contingency Reversal Block, as a first response to the laser. Shaded colour represents the standard error of the mean. Dots plotted above and below represent the correct or incorrect first response of individual fish, respectively. **(B)** Average Number of tail flicks per trial before the laser is turned OFF. **(C)** Average latency of the first response to the laser in each trial. Shaded colour represents the standard error of the mean. **(C')** Cumulative latency of the first response to the laser. Shaded colour represents the standard error of the mean. **(D)** Average latency of the correct turn in response to the laser. Shaded colour represents the standard error of the mean. **(D')** Cumulative latency of the correct turn in response to the laser. Shaded colour represents the standard error of the mean.

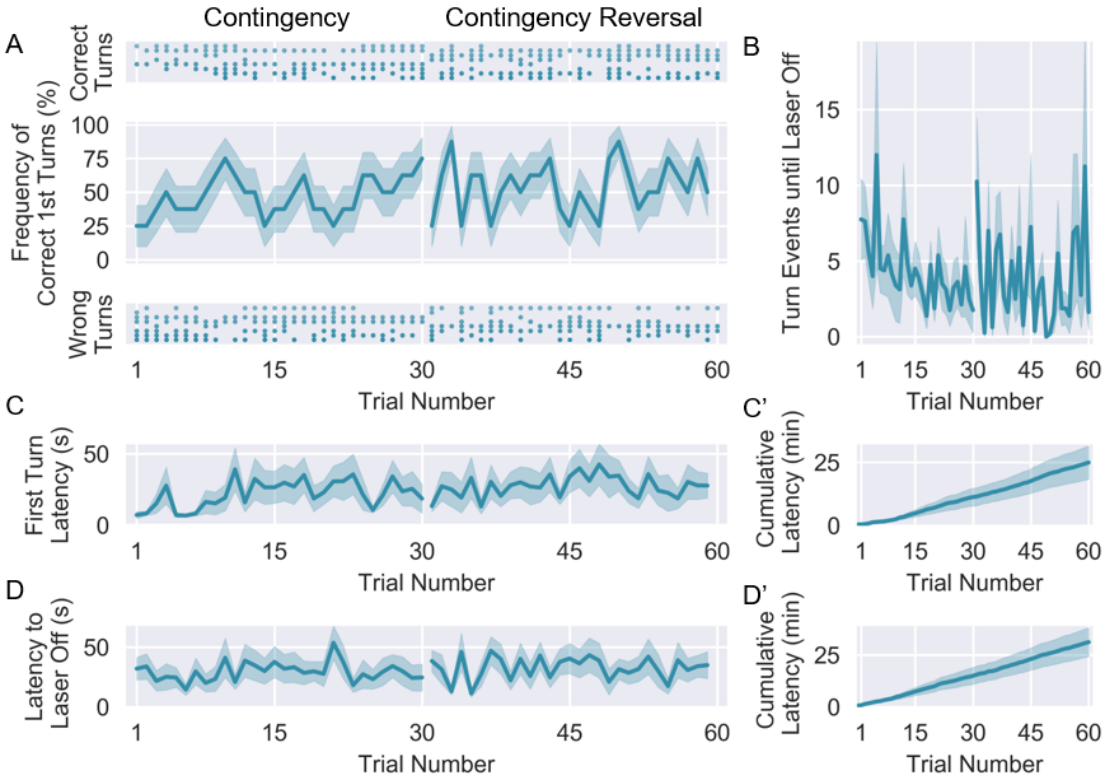

Supplementary Figure 4.2. ROAST assay of tcf7l2^{u754},Tg(gata2a:eGFP)^{pku588} siblings. **(A)** Frequency of *tcf7l2*^{u754},Tg(*gata2a:eGFP*)^{pku588} siblings larvae (n = 8) that turned to the opposite side of their internal bias in the Contingency Block or to their naïve preference in the Contingency Reversal Block, as a first response to the laser. Shaded colour represents the standard error of the mean. Dots plotted above and below represent the correct or incorrect first response of individual fish, respectively. **(B)** Average Number of tail flicks per trial before the laser is turned OFF. **(C)** Average latency of the first response to the laser in each trial. Shaded colour represents the standard error of the mean. **(C')** Cumulative latency of the first response to the laser. Shaded colour represents the standard error of the mean. **(D)** Average latency of the correct turn in response to the laser. Shaded colour represents the standard error of the mean. **(D')** Cumulative latency of the correct turn in response to the laser. Shaded colour represents the standard error of the mean.

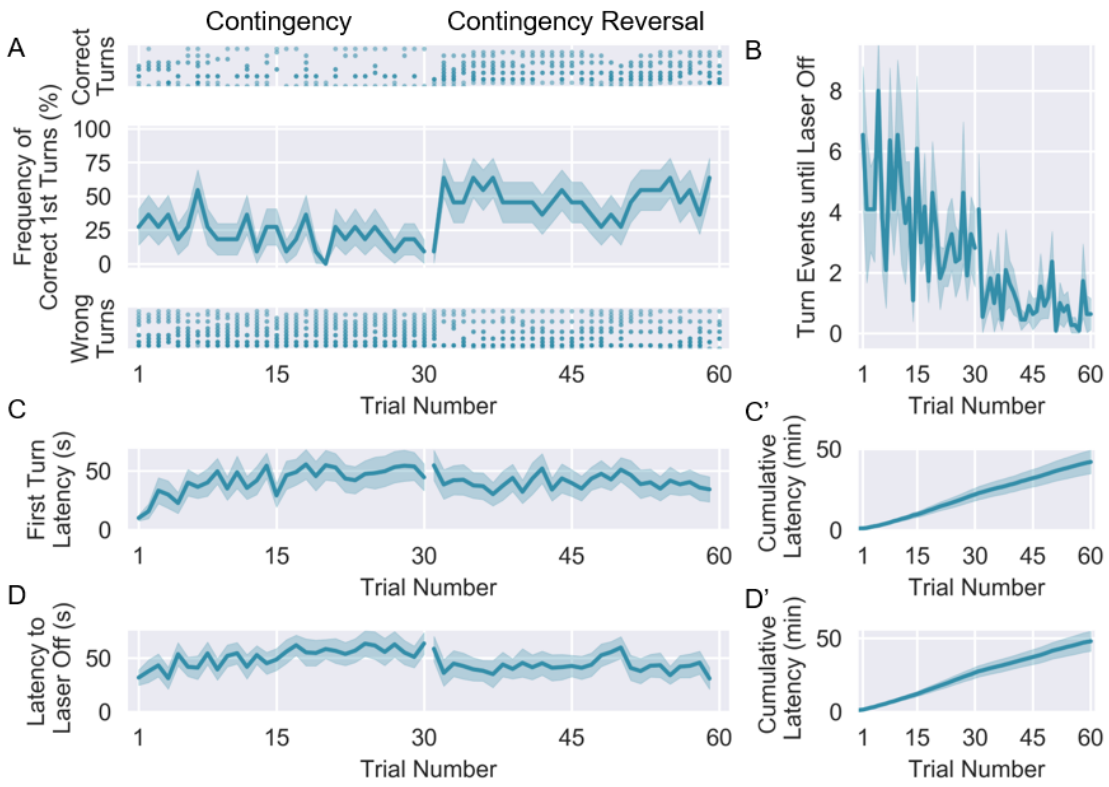

Supplementary Figure 4.3. ROAST assay of tcf7l2^{u754},Tg(gata2a:eGFP)^{pku588} mutants. **(A)** Frequency of mutant larvae (n = 11) that turned to the opposite side of their internal bias in the Contingency Block or to their naïve preference in the Contingency Reversal Block, as a first response to the laser. Shaded colour represents the standard error of the mean. Dots plotted above and below represent the correct or incorrect first response of individual fish, respectively. **(B)** Average Number of tail flicks per trial before the laser is turned OFF. **(C)** Average latency of the first response to the laser in each trial. Shaded colour represents the standard error of the mean. **(C')** Cumulative latency of the first response to the laser. Shaded colour represents the standard error of the mean. **(D)** Average latency of the correct turn in response to the laser. Shaded colour represents the standard error of the mean. **(D')** Cumulative latency of the correct turn in response to the laser. Shaded colour represents the standard error of the mean.

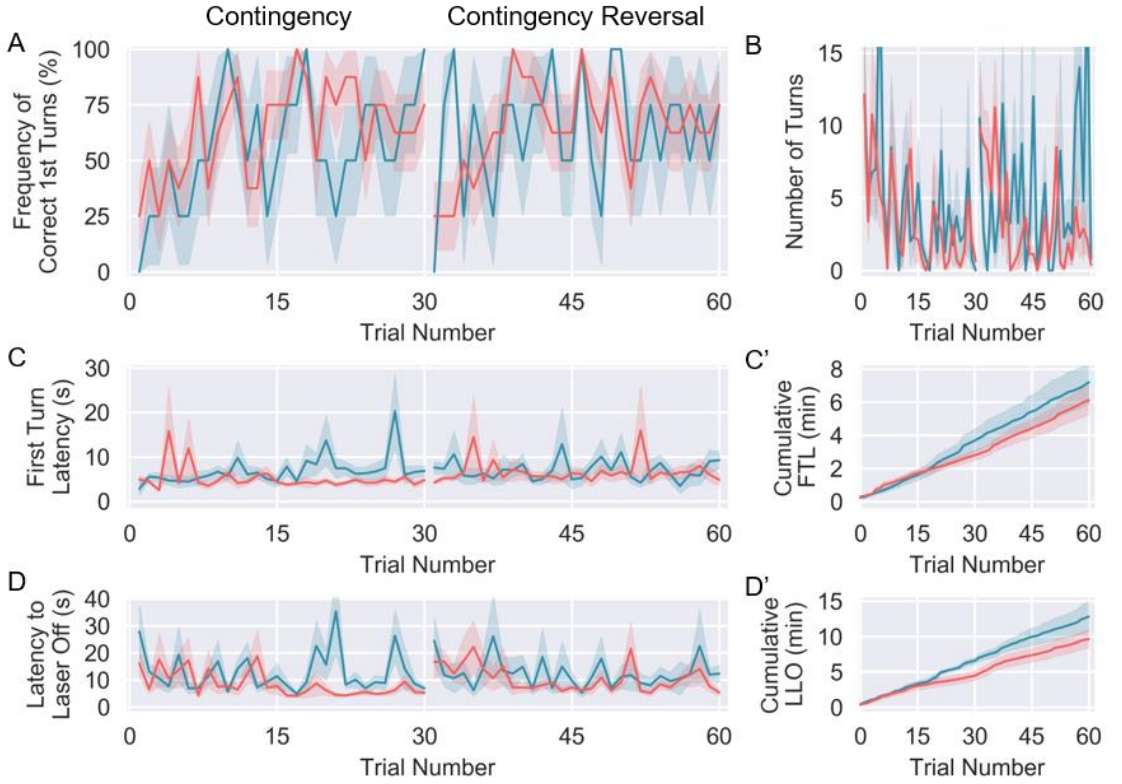

Supplementary Figure 4.4. ROAST assay of tcf7l2^{u754},Tg(gata2a:eGFP)^{pku588} siblings and mutants which responded to, at least, 59 trials. **(A)** Frequency of *tcf7l2*^{u754},Tg(*gata2a:eGFP*)^{pku588} mutants (red, n = 3) and siblings (blue, n = 4) that turned to the opposite side of their internal bias in the Contingency Block or to their naïve preference in the Contingency Reversal Block, as a first response to the laser. Shaded colour represents the standard error of the mean. **(B)** Average Number of tail flicks per trial before the laser is turned OFF. **(C)** Average latency of the first response to the laser in each trial. Shaded colour represents the standard error of the mean. **(C')** Cumulative latency of the first response to the laser. Shaded colour represents the standard error of the mean. **(D)** Average latency of the correct turn in response to the laser. Shaded colour represents the standard error of the mean. **(D')** Cumulative latency of the correct turn in response to the laser. Shaded colour represents the standard error of the mean.

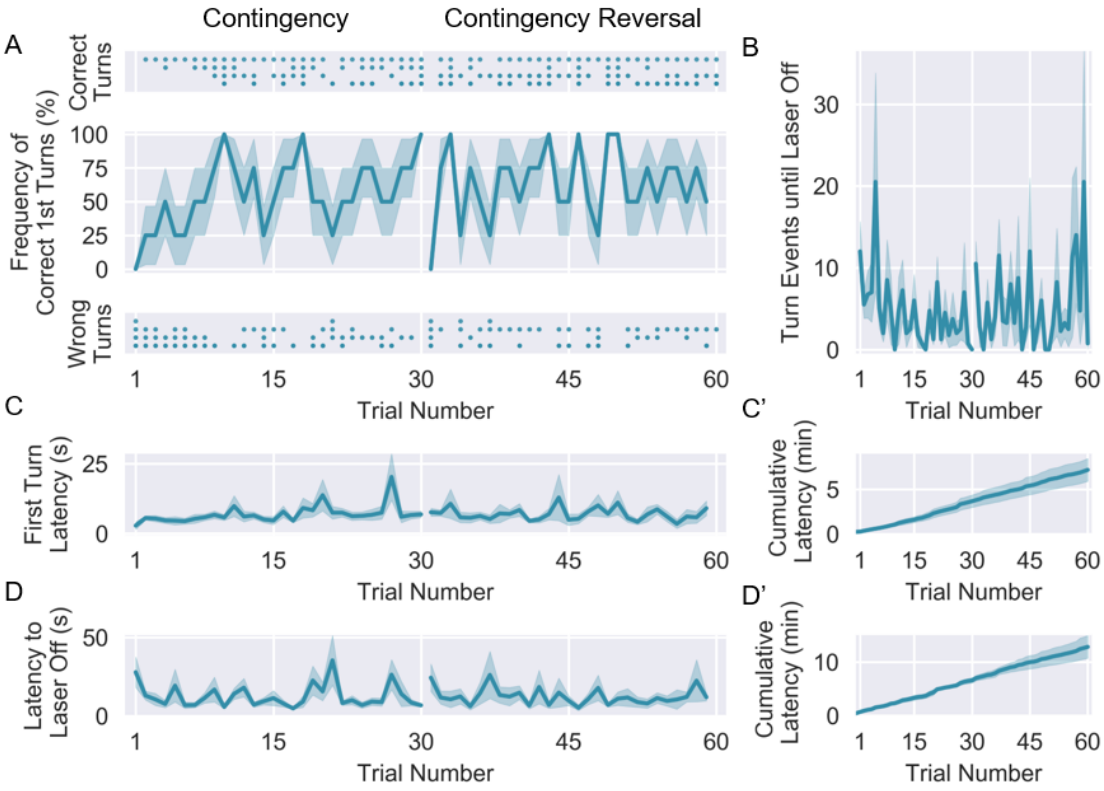

Supplementary Figure 4.5. ROAST assay of tcf7l2^{u754},Tg(gata2a:eGFP)^{pku588} siblings that responded to, at least, 59 trials. **(A)** Frequency of *tcf7l2*^{u754},Tg(*gata2a:eGFP*)^{pku588} siblings (n = 4) that turned to the opposite side of their internal bias in the Contingency Block or to their naïve preference in the Contingency Reversal Block, as a first response to the laser. Shaded colour represents the standard error of the mean. Dots plotted above and below represent the correct or incorrect first response of individual fish, respectively. **(B)** Average Number of tail flicks per trial before the laser is turned OFF. **(C)** Average latency of the first response to the laser in each trial. Shaded colour represents the standard error of the mean. **(C')** Cumulative latency of the first response to the laser. Shaded colour represents the standard error of the mean. **(D)** Average latency of the correct turn in response to the laser. Shaded colour represents the standard error of the mean. **(D')** Cumulative latency of the correct turn in response to the laser. Shaded colour represents the standard error of the mean.

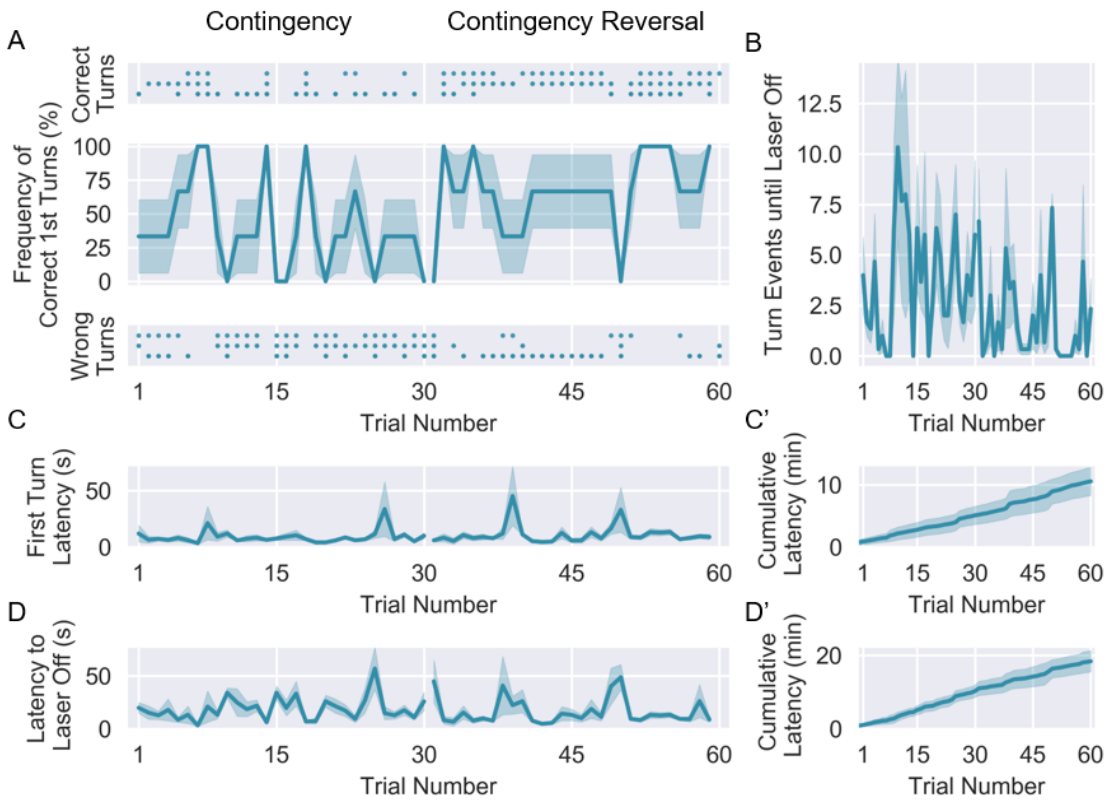

Supplementary Figure 4.6. ROAST assay of tcf7l2^{u754},Tg(gata2a:eGFP)^{pku588} mutants that responded to, at least, 59 trials. **(A)** Frequency of *tcf7l2*^{u754},Tg(*gata2a:eGFP*)^{pku588} mutants (n = 3) that turned to the opposite side of their internal bias in the Contingency Block or to their naïve preference in the Contingency Reversal Block, as a first response to the laser. Shaded colour represents the standard error of the mean. Dots plotted above and below represent the correct or incorrect first response of individual fish, respectively. **(B)** Average Number of tail flicks per trial before the laser is turned OFF. **(C)** Average latency of the first response to the laser in each trial. Shaded colour represents the standard error of the mean. **(C')** Cumulative latency of the first response to the laser. Shaded colour represents the standard error of the mean. **(D)** Average latency of the correct turn in response to the laser. Shaded colour represents the standard error of the mean. **(D')** Cumulative latency of the correct turn in response to the laser. Shaded colour represents the standard error of the mean.

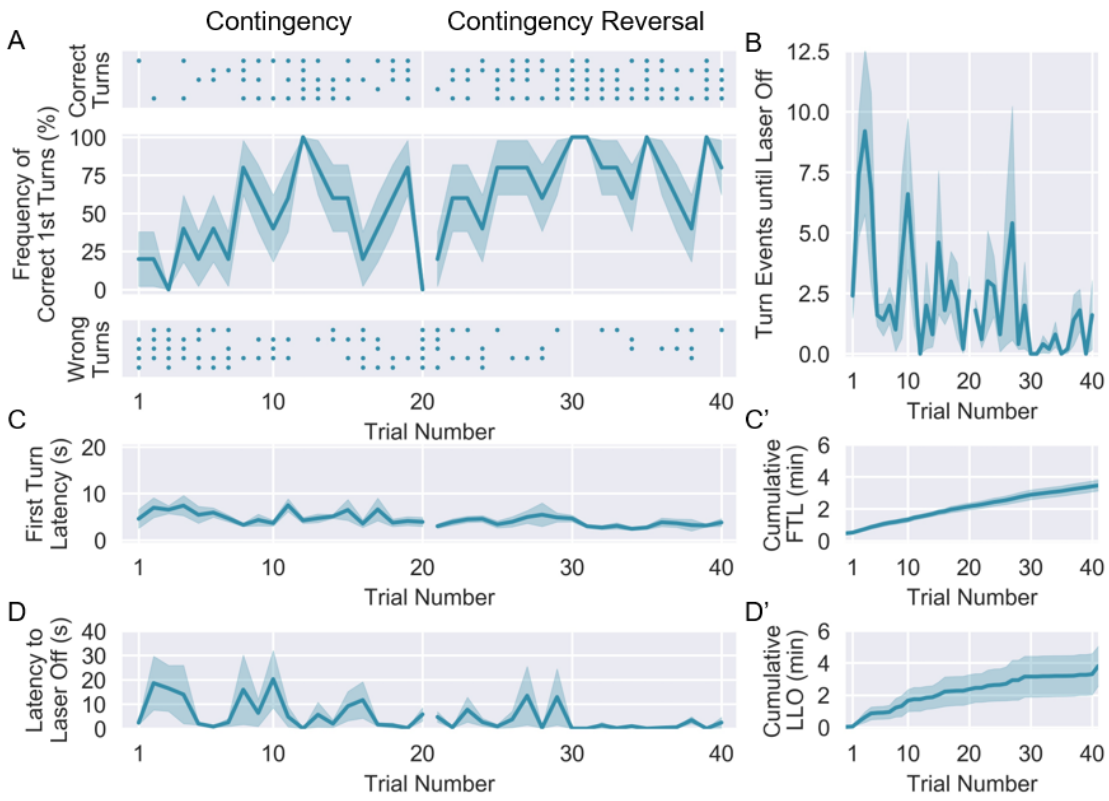

Supplementary Figure 4.7. ROAST assay of wild-type siblings of rch^{u761}. **(A)** Frequency of r*ch*^{u761} wild-type siblings (n = 5) that turned to the opposite side of their internal bias in the Contingency Block or to their naïve preference in the Contingency Reversal Block, as a first response to the laser. Shaded colour represents the standard error of the mean. Dots plotted above and below represent the correct or incorrect first response of individual fish, respectively. **(B)** Average Number of tail flicks per trial before the laser is turned OFF. **(C)** Average latency of the first response to the laser in each trial. Shaded colour represents the standard error of the mean. **(C')** Cumulative latency of the first response to the laser. Shaded colour represents the standard error of the mean. **(D)** Average latency of the correct turn in response to the laser. Shaded colour represents the standard error of the mean. **(D')** Cumulative latency of the correct turn in response to the laser. Shaded colour represents the standard error of the mean.

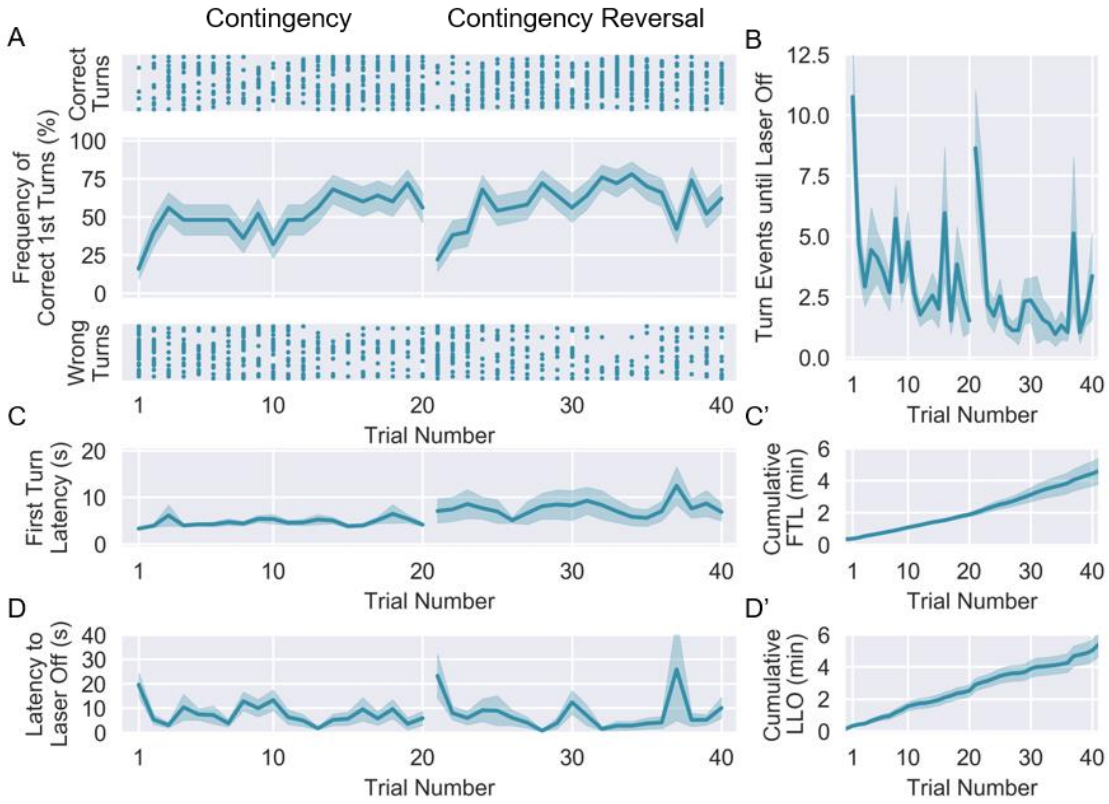

Supplementary Figure 4.8. ROAST assay of heterozygote siblings of rch^{u761}. **(A)** Frequency of *rch* ^{u761} heterozygote siblings (n = 25) that turned to the opposite side of their internal bias in the Contingency Block or to their naïve preference in the Contingency Reversal Block, as a first response to the laser. Shaded colour represents the standard error of the mean. Dots plotted above and below represent the correct or incorrect first response of individual fish, respectively. **(B)** Average Number of tail flicks per trial before the laser is turned OFF. **(C)** Average latency of the first response to the laser in each trial. Shaded colour represents the standard error of the mean. **(C')** Cumulative latency of the first response to the laser. Shaded colour represents the standard error of the mean. **(D)** Average latency of the correct turn in response to the laser. Shaded colour represents the standard error of the mean. **(D')** Cumulative latency of the correct turn in response to the laser. Shaded colour represents the standard error of the mean.

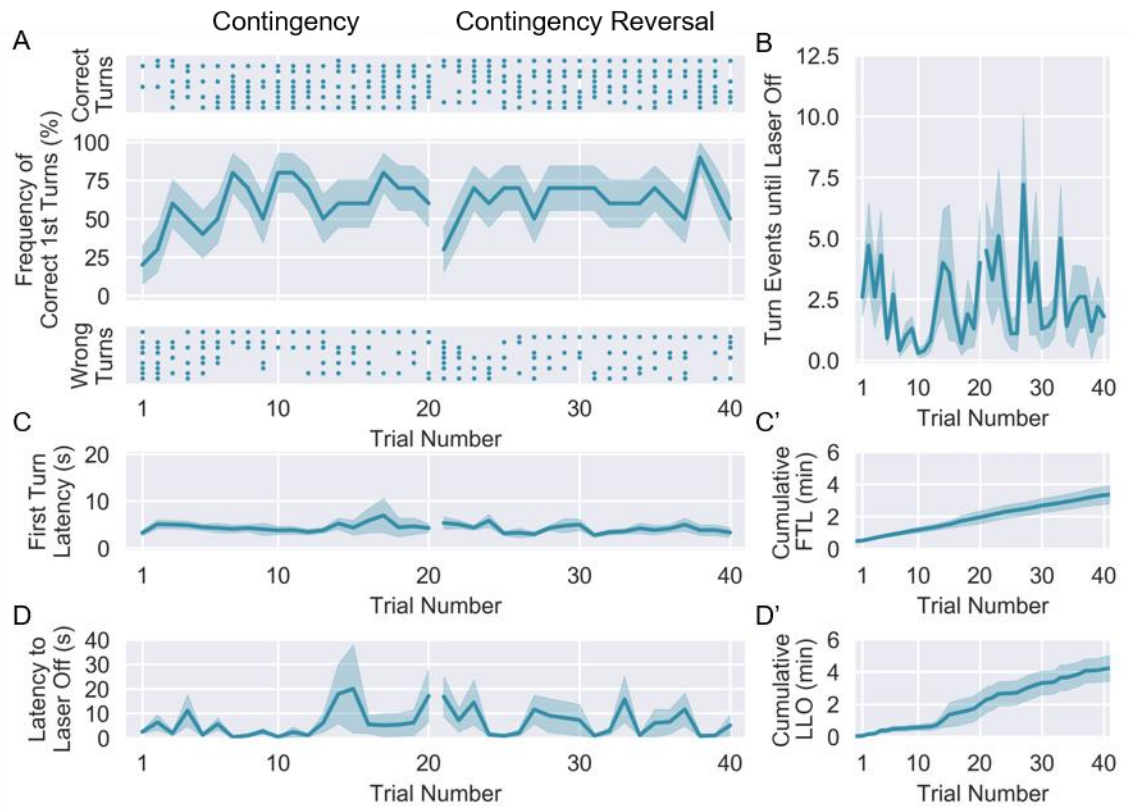

Supplementary Figure 4.9. ROAST assay of mutants for rch^{u761}. **(A)** Frequency of *rch*^{u761} mutants (n = 10) that turned to the opposite side of their internal bias in the Contingency Block or to their naïve preference in the Contingency Reversal Block, as a first response to the laser. Shaded colour represents the standard error of the mean. Dots plotted above and below represent the correct or incorrect first response of individual fish, respectively. **(B)** Average Number of tail flicks per trial before the laser is turned OFF. **(C)** Average latency of the first response to the laser in each trial. Shaded colour represents the standard error of the mean. **(C')** Cumulative latency of the first response to the laser. Shaded colour represents the standard error of the mean. **(D)** Average latency of the correct turn in response to the laser. Shaded colour represents the standard error of the mean. **(D')** Cumulative latency of the correct turn in response to the laser. Shaded colour represents the standard error of the mean.

CHAPTER 5.

GENERAL DISCUSSION

5.1. Habenular progenitors and asymmetry development

The habenula of zebrafish is a great model to study the development of the nervous system asymmetries. The transparency of the zebrafish embryo, combined with its amenability for genetic manipulation, facilitates the study of the molecular mechanisms regulating the development of brain laterality. As seen in **Chapter 2** and in many other works, the generation and characterisation of lines with mutations that cause habenular asymmetry defects have elucidated the pathways that affect the establishment of brain asymmetries (eg. Regan *et al.*, 2009; Roussigné *et al.*, 2009; Hüsken *et al.*, 2014). This approach has allowed us to identify mutations affecting the formation of habenular progenitors, their neurogenesis into dHb neurons, or the elaboration of the habenular cytoarchitecture, thus allowing us to expand our understanding on the molecular players orchestrating epithalamic asymmetries in vertebrates.

One of the steps of habenular formation that is still largely not understood, is how habenular progenitors are formed and what types of cells constitute this population. What is currently known is that the specification of this population is delayed in *fgf8, med12 and wls* mutants (Dean *et al.*, 2014; Wu *et al.*, 2014; Kuan *et al.*, 2015). However, it has not been assessed whether these signalling pathways interact with each other or work independently to specify habenular progenitor cells. It is possible that these pathways interact since *med12* mutants show inhibition of the FGF pathway in the pineal, and Wnt and FGF signalling pathways often interact as for instance was shown for the formation of somites and maintenance of the nucleus isthmus identity (Canning *et al.*, 2007; Stulberg *et al.*, 2012). Nevertheless, during the specification of the anteroposterior axis of the neural ectoderm, both Wnt and FGF signals suppress expression of anteriorizing genes in the posterior ectoderm, even when one of the pathways is inactivated (Kudoh, Wilson and Dawid, 2002). This shows that these pathways can also work independently despite being expressed in the same domains.

In **Chapter 2** we characterised the novel *rerea*^{u757} mutant, which develops a small dorsal habenula likely due to a delay in habenular progenitor formation. The *rerea* gene encodes a nuclear receptor coregulator, which means that it is directly linked to transcription regulation (Asai *et al.*, 2006; Plaster *et al.*, 2007; Vilhais-Neto *et al.*, 2010). Furthermore, its genetic interaction with the FGF pathway, both in this *rerea* mutant and in other previously published mutants for the same gene, suggests that it may be regulating the expression of *fgf8* during critical steps of habenular progenitor formation (Plaster *et al.*, 2007). In line with this, in *rerea*^{u757} mutants the development of the parapineal is affected, a phenotype also observed in *fgf8* mutants (Regan *et al.*, 2009). This suggests that the habenular defects observed in *rerea*^{u757} mutants could be partially due to the FGF pathway being suppressed during the critical steps of habenular

progenitor formation. Consequently, this would lead to a delay in expression of habenular progenitor markers and to the development of reduced habenular nuclei. A delay in habenular progenitor specification probably results in a reduced number of cells that would be competent to start neuronal differentiation during the first wave of habenular neurogenesis. Since most dHbL are formed in the first wave, this domain is reduced in the 4 dpf habenula of *rerea*^{u757} mutants. On the other hand, more progenitors enter neurogenesis in the second wave, forming a larger dHbM in both sides of the epithalamus. Altogether, this chapter showed that the *rerea*^{u757} mutation may affect FGF signalling in the presumptive habenula domain, thus leading to the delayed specification of habenular progenitors and, ultimately, to the development of a smaller and symmetric dorsal habenula.

We still do not know the cellular composition of the habenular progenitor population affected by the *rerea*^{u757} mutation, or how FGF and Wnt control its formation. Both transcript and protein expression studies showed that these cells express *dbx1b* but there is no evidence as of yet that this gene is needed for the formation of habenular progenitors (Dean *et al.*, 2014; Roberson and Halpern, 2017a). These *dbx1b*-expressing cells are proliferative until neurogenesis starts, when *dbx1b* transcription is downregulated (Dean *et al.*, 2014). However, in fully differentiated habenular cells there is no expression of *dbx1b* as seen by WISH studies, and in **Chapter 3** and other single cell RNAseq experiments (Dean *et al.*, 2014; Pandey *et al.*, 2018). Therefore, the same way that it is now possible to sequence single neurons of the functionally mature habenula to understand the cellular composition of this structure, it would be interesting to do the same for habenular progenitors. This would be possible by using the transgenic lines for the *dbx1b* gene (Roberson and Halpern, 2017a). Moreover, in our lab, we found other genes that are expressed in the habenular progenitor population and at least one of these may be expressed before *dbx1b* (Faro, A.; Powell, G., Wilson, S.W.; unpublished data). Since we have transgenic lines that express GFP controlled by the promotor of these genes, we could also sequence the transcriptome of these cells and gain a better understanding of the formation of habenular progenitors and habenular neurogenesis.

Current evidence shows that the habenular progenitors are formed symmetrically (Dean *et al.*, 2014; Roberson and Halpern, 2017a). This is important, since it implies that these are the cells that will receive the signals that initiate asymmetric development of the dHb. Therefore, understanding the characteristics of these cells will help us understand how the brain breaks symmetry of a specific subdomain without affecting the development of the whole structure. To do this, we still need to identify the receptors that

make the habenular progenitors responsive to the epithalamic molecular environment and that distinguish them from the surrounding structures.

5.2. Identifying early-stage habenular neuronal populations

The characterisation of habenular asymmetry mutants has relied upon studying the expression of genes that are broadly, but asymmetrically expressed in the habenular nuclei. This has proved to be useful to understand how Nodal, FGF and Wnt pathways affect the general formation of each habenular nucleus (Concha *et al.*, 2000; Regan *et al.*, 2009; Hüsken *et al.*, 2014). However, we still have no understanding of how these signals affect the formation of the smaller subpopulations that are found in 10 dpf larvae (Pandey *et al.*, 2018). In fact, we have no information of whether these populations are already present at 4 dpf, the stage when most asymmetry mutant studies are performed.

In **Chapter 3** we aimed to fill this gap by identifying the neuron populations that constitute the 4 dpf zebrafish habenula by sequencing the transcriptome of the dorsal habenula cells. To achieve this, we optimised a protocol to dissociate and isolate dorsal habenula neurons, using an enhancer trap line that expresses GFP in cells of the habenula and olfactory organ. Despite our best efforts, we were only able to successfully sequence 586 GFP-positive cells from this line. However, we believe to have pinpointed the problems of our protocol and that in the future we will be able to sequence the required number of habenular cells to perform a more thorough analysis (published results have achieved this with at least 4000 cells) (Pandey *et al.*, 2018). Moreover, the data we obtained was sufficient to identify clusters that corresponded to the olfactory organ, dorsal and ventral habenula, which suggest that our protocol will be effective at distinguishing discrete cell populations of the dorsal habenula once we obtain the optimal number of cells.

Once we gather information on the neuronal populations that constitute the dorsal habenula, we envisage building a map of the markers that define each cluster of neurons at 4 dpf. This will allow us to study the effect of known and new mutations that affect habenular asymmetry and understand how each individual neuronal subpopulation is affected in these different backgrounds. For instance, we know that in *tcf7l2*^{u754} and *rch*^{u761} mutants, the dHbM is reduced on the right side in comparison to wildtypes (Hüsken *et al.*, 2014; Faro A., Powell, G., Wilson, S.W., unpublished). However, understanding which specific neuronal subpopulations are affected would provide us better information to comprehend behavioural changes driven by habenular dysfunction.

Understanding the habenular neuron subpopulations may also help us studying human diseases with symptoms linked to this structure. Habenular activity has been implicated

in several conditions such as depression, schizophrenia and nicotine addiction (Shepard, Holcomb and Gold, 2006; Velasquez, Molfese and Salas, 2014; Liu *et al.*, 2017). Genetically, these are very complex conditions where no single gene is associated with their manifestation. However, there are directed mutational approaches in zebrafish, such as CRISPR, which can be multiplexed, allowing the targeting of several genes in one experiment (Varshney *et al.*, 2015). Being able to affect several genes at once could help understand how their combinatorial effects lead to habenular malformation and behavioural phenotypes. Therefore, by studying genes that are shown to be common between patients with an habenular phenotype, we might be able to identify the habenular subpopulations affected. This could also provide directions for new targets for specific drug treatments of several of the symptoms linked to the habenula, as has been done in other studies using rat models of depression (Cui *et al.*, 2018).

5.3. Characterising habenular function

The laterotopic connectivity of the habenula to the IPN is fairly well explained by the ratio of dHbL and dHbM neurons present in each side of the epithalamus: dHbL are more abundant in the left epithalamus and these neurons innervate the dIPN, therefore the left dorsal habenula nuclei mostly innervates the dIPN; conversely, dHbM are more abundant in the right epithalamus and these neurons innervate the vIPN, thus the right dorsal habenula nuclei mostly innervates the vIPN (Aizawa *et al.*, 2005; Bianco *et al.*, 2008). However, at 10 dpf, the dHb consists of 14 different types of neuronal subpopulation and 6 of these are asymmetrically represented (Pandey *et al.*, 2018). This raises the possibility that these subpopulations project to different parts of the IPN and, therefore, propagate different types of signals. Understanding how the different populations contribute to the habenular function would allow us to understand the link between the habenular asymmetry and its function. However, two problems hinder this approach: (1) the lack of transgenic lines that mark discrete functional sub-types of habenular neurons and (2) the lack of experimental setups to easily study habenula-dependent behaviours in larvae zebrafish.

The first problem is at the brink of a solution, as markers of the habenular subpopulations are found. There are well established techniques for the development of transgenic lines in zebrafish (Burket *et al.*, 2008; Charpentier *et al.*, 2018). Therefore, by knowing the genes that are only expressed in one or few habenular subpopulations, we can build transgenic lines driven by the promoters of these genes. Once these transgenic lines are established, it is possible to ablate specific habenular neurons or modulate their activity, to understand their importance for behavioural expression (see section 5.4.3).

The second problem is currently being tackled in our lab, where efforts are being made to expand the repertoire of behavioural set ups that will help us understand the functional role of habenular asymmetry in vertebrates. Nevertheless, to study the behaviours for which habenular neuronal subpopulations are important, we need to increase the throughput of the experimental assays. Several works performed by us and others have shown that habenular neurons of larval zebrafish respond to light, odour, heat and carbon dioxide stimuli. In these studies the primary aim was to characterise habenular responses through imaging neuronal activity of wild type fish (Dreosti *et al.*, 2014; Haesemeyer *et al.*, 2018; Koide, Yabuki and Yoshihara, 2018). Although this is an important endeavour, it is quite time consuming and thus would not be a suitable platform in which to do a high throughput characterisation of habenular asymmetry mutants. Therefore, in the Wilson lab we have been increasing the number of behavioural experimental setups that are able to assay habenular phenotypes in a faster and, yet, reliable way.

In **Chapter 4** we established a version of the ROAST assay that allowed us to assay for differences between wildtype and habenular mutant fish in an operant learning paradigm. In this chapter, we showed that in ten trials of 1-2 minutes, the zebrafish larvae were able to modulate their behaviour in order to terminate an aversive heat stimulus. However, this ability was present in larvae with normal but also in those with left-isomerized habenulae, where we predicted an increase in latency of response to the heat stimuli (Haesemeyer *et al.*, 2018). This generated two hypotheses: (1) right habenula-specific neurons are not necessary for the habenular function in this operant learning paradigm; (2) habenular asymmetry is not necessary for the operant learning paradigm, and therefore mutations affecting asymmetry do not change behaviour in the ROAST assay. Therefore, there is still an uncertainty as to whether this experimental assay will be included in a pipeline for the characterisation of habenular mutants. Nevertheless, we need to repeat the experiments with right-isomerised habenula mutants to understand if habenular asymmetry and left-specific neurons are important for the performance of larvae during this operant learning assay.

5.4. Future directions

In each results chapter of this thesis I have outlined the main findings of each experiment and the future directions that will help us complete the work. In the following sections I will make a summary of these future experiments.

5.4.1. How does *rerea*^{u757} affect habenular development?

The *rerea*^{u757} mutants developed a small symmetric dHb, with a larger dHbM domain in both nuclei, due to a delay in the formation of the habenular progenitors. Our evidence suggests that this delay restricted the number of habenular progenitors available to enter the first wave of neurogenesis, when most dHbL neurons are specified. Therefore, a larger number of habenular progenitors would be available to start neurogenesis during the second wave, when most dHbM neurons are formed. To check that this is the case, we will perform BrdU pulse-chase labelling experiments to understand when dHb neurons are born in *rerea*^{u757} mutants (Aizawa *et al.*, 2007). To complement these experiments, we will characterise the development of habenular differentiated neurons by analysing the expression of the neuronal marker Elavl3 in the presumptive habenula of *rerea*^{u757} mutants between 24 and 52 hpf (Colombo *et al.*, 2013).

At 24 hpf, when habenular progenitors should be present, the *fgf8* expression pattern is expanded in the diencephalon of *rerea*^{u757} mutants. However, the habenular phenotype of the mutant resembles that of a *fgf8* mutant (Regan *et al.*, 2009). It was previously shown that in *rerea*^{ru622} mutants both *fgf8* and the FGF antagonists *il17rd* and *spry4,* are overexpressed, which in turn led to the inhibition of the FGF pathway thorough a negative feedback loop. To test if this is the case in the *rerea*^{u757} mutants we will: (1) assess changes in levels and patterns of expression of *fgf8* and FGF antagonists by qPCR and WISH, respectively, between 24 hpf and 36 hpf in *rerea*^{u757} mutants and siblings; (2) monitor the activity of the FGF pathway in the diencephalon of *rerea*^{u757} mutants and siblings between 24 and 36 hpf with the FGF reporter Tg(*dusp6:d2EGFP*)^{pt6}; and (3) inhibit the transcription of FGF antagonists in *rerea*^{u757} mutants to assess if this rescues the wildtype habenular phenotype (Asai *et al.*, 2006; Molina, Watkins and Tsang, 2007).

To validate the studies of habenular efferent projections to the IPN, we will repeat the axon tracing experiment with the DiI and DiD lipophilic dyes. The main problem of this approach is the reduced habenular size in mutants, which makes it hard to target and specifically label this structure with the lipophilic dyes. One way we attempted to increase accuracy of habenular targeting was by using transgenic lines that express GFP in the habenula. However, the habenular labelling is done in fixed larvae and the PFA fixation method quenched the fluorescence. Therefore, we may have to attempt fixation methods other than PFA to guarantee the correct targeting of the small habenula of *rerea*^{u757} mutants.

Understanding how Retinoic Acid affects the habenular development of wildtype and *rerea*^{u757} mutants may help us dissect the mechanism through which the *rerea*^{u757}

mutation delays the formation of habenular progenitor cells. To do this we will study whether the habenular development in *rerea*^{u757} mutants is sensitive to drug-induced changes in the retinoic acid signalling (Hyatt *et al.*, 1992; Le, Dowling and Cameron, 2012).

To formally prove that *rerea*^{u757} mutation is causative of the observed phenotype in A66 mutants, a complementation test using *rerea*^{u757} and *rerea*^{sa1112} mutant alleles will be performed. The latter mutation results in a premature stop in *rerea* exon 16, which leads to the formation of a truncated protein with a reduction of the Atrophin domain. A genetic complementation test is done using two strains with different homozygous recessive mutations. If the two mutations affect the same gene, then the trans-heterozygous organisms should display the same phenotype as the homozygous mutants for any of the two recessive mutations (Kettleborough *et al.*, 2013). In this case, if the mapped lesion in the *rerea* locus of *A66* were indeed causative of the observed habenular phenotype, then we would expect that embryos *rerea*$^{u757/sa1112}$ should display a smaller dHb.

Finally, to better understand if the reduced Atrophin domain of the Rerea^{u757} protein is causative to the habenular phenotype, we would carefully study and compare *rerea*^{sa1112} homozygous mutants, *rerea*^{u757} homozygous mutants and *rerea*$^{u757/sa1112}$ embryos. Although the mutant Rerea^{sa1112} protein is smaller than the Rerea^{u757} mutant variant, it may inform if it is this domain of the protein that is important for the timely formation of habenular progenitors.

5.4.2. Which subpopulations compose the 4 dpf zebrafish habenula?

The protocol developed and presented in **Chapter 3** allowed us to sequence the RNA of single cells of the habenula at 4dpf. However, we did not obtain data on enough cells to distinguish different subpopulations of the dHb. The quality indicators of the sequencing experiment suggest that an error might have occurred in the quantitation of the cDNA library. Accurately estimating the amount of DNA we load onto an Illumina flow cell is an important part of any Next Generation sequencing pipeline. Loading too much DNA results in sequencing clusters that are too close together, which creates problems in obtaining good quality sequencing readings. Therefore, we will first reassess the quality and quantity of the cDNA library that was synthetized with the 10x Genomics Microfluidics System, using Qubit/Bioanalyser. If this analysis reveals that we grossly overestimated the cDNA amount, we will adjust the concentration we input onto the flow cell and re-sequence the data. However, if this still reveals that we do not have enough information to discern the habenular subpopulations, we will repeat the experiment by implementing changes in the steps that may have affected the recovery of single cells.

First, we will dissect the zebrafish brains and dissociate their cells in Neurobasal supplemented with B-27, which should promote the survival of neuronal cells. Then, we will dissociate cells with the Papain kit, which was shown to have less side effects in dissociated cells. Lastly, we will FAC-sort enough cells to fit the final volume required for the 10x Genomics Microfluidics System. Having obtained data from enough habenular cells (a predicted minimum of 4000), we will analyse them to detect highly variable genes to identify markers that define habenular subpopulations. This will be achieved by using the same computational approach that was developed and tested by Pandey et al. (Pandey *et al.*, 2018). Having identified such genes, we will be able to synthetize RNA probes for the genes that define habenular subpopulations and characterise their expression pattern in 4 dpf larvae. Furthermore, and to have a more comprehensive understanding of the development of habenular subpopulations, we will characterise the expression of these markers in previously described and novel habenular mutants.

Ideally, we will also be able to create several transgenic lines regulated by the genes that define each of these populations. This would allow the precise characterisation of the habenular afferent and efferent projections to the IPN. Moreover, we would be able to perform behaviour studies in larvae expressing optogenetic actuators, to modulate neuronal activity, or KillRed, to specifically ablate discrete habenular neuron populations (Teh *et al.*, 2010; Pama, Colzato and Hommel, 2013).

5.4.3. Is habenular asymmetry important for signalling negative stimuli?

In **Chapter 4** we established the ROAST assay to study the importance of habenular asymmetry in the performance in an operant learning assay. Based on reports of the asymmetric activation of neurons in the habenula in response to light, odour, heat or carbon dioxide, we hypothesised that habenular asymmetry mutants would perform differently under this assay (Dreosti *et al.*, 2014; Haesemeyer *et al.*, 2018; Koide, Yabuki and Yoshihara, 2018). However, *rorschach*^{u761} mutants, that display left-side habenular isomerism, did not show any performance differences in the ROAST assay, compared to genotyped wild-type siblings. One possible explanation for this result is that only neurons present in the left habenula are important for the execution of this behaviour. To test this hypothesis, we will repeat the ROAST assay experiment in asymmetry mutants where the habenula displays right-side isomerism. If only dHb neurons found in the left nuclei are important for this behavioural output, we would then expect that double right mutants would fail to show any learning or avoidance upon exposure to a heat stimulus. If this is, in fact, what we observe, then we could confidently include the ROAST assay in a pipeline for the identification and/or characterisation of habenular mutants.

Furthermore, combining the ROAST assay with the molecular characterisation of neuronal dHb subpopulations may allow us to further dissect how maintaining the asymmetry of specific dHb neuronal subtypes is important in the avoidance response to heat stimuli and/or in establishing the association between the stimulus and the direction of the response. Despite not being in our near future plans, these experiments may be part of a long-term project.

5.4. CONCLUSION

In this work we were able to tackle the study of habenular asymmetry in three different ways:

1. Through a forward-genetics approach we contributed towards understanding how the delay in the formation of habenular progenitors may drive the formation of symmetric habenulae;

2. By developing a protocol to obtain single cells of the habenula we started work towards characterising its subpopulations. In the near future we will be aim to provide information of which neuronal subtypes exist in the dHb of zebrafish at 4 dpf and which ones are asymmetrically represented in each nucleus;

3. By establishing a behavioural assay, we tested the importance of habenular functional asymmetry during an operant learning paradigm. This work showed us that the right habenula is not essential to perform in the ROAST operant conditioning task.

Completing these works will provide us new information about the development and function of habenular asymmetries.

CHAPTER 6.

METHODS

6.1. Embryos and fish lines

Zebrafish embryos were obtained from natural spawning, raised at 28.5°C and staged according to hours or days post-fertilisation (hpf, dpf). 0.003% 1-phenyl-2-thiourea (PTU) was added to the water at 24-26 hpf to prevent pigmentation of imaged fish. Previously established fish lines used in this study were as follows: A66^{u757}; Tg(*foxD3:GFP*;*flh:eGFP*); from incross of Tg(*foxD3:GFP*)^{zf104} and Tg(*flh:eGFP*)^{U711}, Et(*gata2a:eGFP*)^{pku588}, Tg(*lhx2a:GFP*)^{zf176Tg}, *tcf7l2*^{u754},Tg(*gata2a:eGFP*)^{pku588}, *rch*^{u761}, TL(wild-type) (Gilmour, Maischein and Nüsslein-Volhard, 2002; Concha *et al.*, 2003; Wen *et al.*, 2008; Miyasaka *et al.*, 2009; Hüsken *et al.*, 2014).

6.2. Axon tracing by lipophilic dye labelling

Tracing of habenula efferent projections was carried out by labelling with membrane-bound lipophilic dyes DiI (DiIC18(3), Molecular Probes, Cat# D3911) and DiD (DiIC18(5), Molecular Probes, Cat# D7757) in 4 dpf embryos. 4 dpf embryos were fixed by overnight incubation at 4°C in 4% PFA (w/v) in PBS. Fixed embryos were transferred to PBS, immobilised by pinning down with needles to dissect the brains and then repositioned for dorsal view by placing the body between two needles. Crystals of DiI (left dHb) and DiD (right dHb) were manually applied to dorsal habenulae with tungsten needles under 7x magnification, distinguishing the 4 dpf habenulae of an unstained brain by using the distinct forebrain-midbrain boundary as a landmark. The dyes were prepared as follows: after dissolving the solid dye in 96 % ethanol, the solution was spread on a glass slide to acquire small crystals, which were then collected with the tungsten needle by carefully scraping the slide. Tungsten needles were sharpened by electrolysis in concentrated NaCl solution prior to use. Each habenula was labelled with 2-3 gentle piercings leaving a visible small crystal dot. Brains were incubated in PBS overnight at 4°C, mounted (ventral up) in 1.5 % low melting point agarose (Sigma) in PBS the next day and imaged by confocal laser scanning microscopy (see below).

6.3. Whole-mount RNA *in situ* hybridization (WISH)

Plasmids for synthesising RNA antisense probes for *kctd12.1*, *kctd12.2, gng8*, *kiss1, prss1, lfabp* and *dbx1b* were previously generated in the Wilson lab (Biemar *et al.*, 2001b; Gamse, 2003; Her *et al.*, 2003; Gamse *et al.*, 2005; Ogawa *et al.*, 2012; Dean *et al.*, 2014; deCarvalho *et al.*, 2014). Plasmids were linearized with Promega restriction enzymes EcoRI (lfabp, prss1, *kctd12.1*), EcoRV (*kctd12.2, gng8, kiss1*). *In vitro* transcription was carried at 37°C over-night, using digoxigenin (DIG) or fluorescein (FLUO) labelled nucleotide mix (Roche, Cat# 112777073910 and 11685619910) and T7

or SP6 RNA polymerase (Promega, Cat# P2017 and P1085) according to manufacturer's instructions. The probes were purified using Qiagen RNeasy Mini Kit, eluted in 30 µL of nuclease free water and tested on 1% RNase-free agarose gel in Tris-acetate-EDTA (TAE) buffer (40 mM Tris, 20 mM acetic acid, 1 mM EDTA).

Embryos were fixed in 4% PFA (w/v) in PBS at 4°C overnight, dehydrated through a graded series (25, 50, 75 and 100%) of methanol/PBST (PBS with 0.5% Tween-20, Sigma, Cat# P1379) and kept at -20°C overnight. Samples were rehydrated through 100, 75, 50 and 25% methanol, washed 3x 5 minutes in PBST and treated with 0.02 mg/ml proteinase K (PK, Sigma, Cat# 03115887001) for 10 minutes (24 hpf embryos), 20 minutes (36 hpf embryos), 30 minutes (48 hpf embryos) or 40 minutes (4 dpf embryos). Embryos were post-fixed in 4% PFA (w/v) in PBS for 20 minutes, washed in PBST 4x 5 minutes, incubated for one hour at 70°C in standard hybridisation solution containing 50% formamide and overnight at 70°C in probe solution (2 ng/µL probe in hybridisation solution). The next day, embryos were washed at 70°C through a graded series of hybridisation solution and 2x saline sodium citrate (SSC) (100, 75, 50 and 25%, 15 minutes each), followed by a 15-minute wash in 2x SSC and 2x 30-minute wash in 0.2x SSC. At room temperature, the embryos were further washed through a graded series of 0.2x SSC and PBST (100, 75, 50 and 25%, 10 minutes each) and blocked in maleic acid buffer (150 mM maleic acid, 100 mM NaCl, 2% sheep serum, 2 mg/ml BSA) for 2-3 hours.

DIG and FLUO labelled probes were detected by over-night incubation with anti-Digoxigenin-AP Fab fragments (1:5000) (Roche, Cat# 11093274910) for colorimetric *in situ* hybridization (alkaline phosphatase conjugated antibody), or anti-Fluorescein-POD Fab fragments (1:500) (Roche, Cat# 11426338910) and anti-Digoxigenin-POD Fab fragments (1:500) (Roche) for Tyramide-based double-fluorescent *in situ* hybridisation (horseradish peroxidase conjugated antibody). Embryos were washed over day (minimum 6x 30 minutes) in PBST.

Colorimetric *in situ* hybridisation was detected by standard Nitro Blue Tetrazolium (NBT) and 5-Bromo-4-chloro-3-indolyl phosphate (BCIP) (Roche, Cat# N6876 and 11383221001) protocol. The staining solution contained 1 µL of NBT and 3.5 µL BCIP per 1 ml of freshly prepared 0.1M Tris buffer (pH 9.5) with 50 mM MgCl2, 0.1 M NaCl and 0.01 % Tween-20. Fluorescent *in situ* hybridisation was carried out using Fast Blue BB Salt (Sigma, Cat# D9805) and NAMP (Sigma, Cat# N5000) staining (Schumacher *et al.*, 2014). Fast Blue staining was performed in 0.1M Tris buffer (pH 8.2) containing 50 mM MgCl2, 0.1 M NaCl and 0.01% Tween-20. 0.5 mg/ml Fast Blue and NAMP solutions were prepared in Tris buffer, mixed while stirring and filtered before use. Since Fast Blue is a chromogenic substrate to alkaline phosphatase, they also give a colorimetric

precipitate in addition to fluorescent signal, which allows following of the reaction while the signal develops. Depending on the specific probe, NBT/BCIP and Fast Blue signals developed within 1-5 hours.

For double fluorescent *in situ* labelling, Tyramide Signal Amplification (TSA) Plus Fluorescein (PerkinElmer, Inc., Cat# NEL741E001KT) and TSA plus Cyanine 3 (Cy3) (PerkinElmer, Inc., Cat# NEL744001KT) were used according to manufacturer's instructions. FLUO-labelled probe was made for *cxcr4b* and DIG-labelled probe for *dbx1b*. Antibody staining and detection for the FLUO-labelled probe was carried out first, followed by detection of the DIG-labelled probe. The signal was developed for 60 minutes for both probes.

6.4. Whole-mount Immunohistochemistry (IHC)

4 dpf larvae were fixed in 4% PFA (w/v) in PBS at 4°C overnight, dehydrated through a graded series (25, 50, 75 and 100%) of methanol/PBSTr (PBS with 0.5% Triton X-100, Sigma Cat# X100) and incubated in 100% methanol overnight at -20□C. After rehydration through a graded series of methanol/PBSTr (100, 75, 50 and 25%), embryos were permeabilised with 0.02 mg/ml proteinase (PK, Sigma, Cat# 03115887001) for 30 minutes, post-fixed with 4% PFA (w/v) in PBS for 20 minutes, washed 3x 5 minutes in PBSTr and blocked with 10% Heat--- inactivated Normal Goat Serum (Sigma, Cat# G9023) in PBSTr and 1% Dimethylsulfoxide (Sigma, Cat# 276855) for one hour. Primary antibody incubation was carried out overnight at 4°C in block solution using the following antibodies: rabbit anti-GFP (dilution 1:1000, Torrey Pines Biolabs, Cat# TP401), mouse anti-acetylated tubulin (dilution 1:250, IgG2b, α-tubulin, Sigma Cat# T7451) and mouse anti-SV2 (dilution 1:250, IgG1, sv2, DSHB Cat# sv2-c). Embryos were washed over day (minimum 6x 30 minutes) and secondary antibody incubation was carried out over night at 4°C using Alexa Fluor 488-conjugated and 568- conjugated secondary antibodies (1:200, Molecular Probes, Cat# A32731 and A21144). Samples were again washed over day (minimum 6x 30 minutes) and mounted for confocal imaging.

6.5. Image acquisition and analysis

Confocal imaging was carried out using Leica TCS SP8 system with a 25x/0.95 NA PL IRAPO water-immersion objective with coverslip correction (Leica). Whole mount fluorescent *in situ* hybridisation and immunohistochemistry samples were mounted in 1.5 % low melting point agarose (Sigma, Cat# 16520050), using glass rings fitted on a slide by silicone grease and VWR Thickness No.1 coverslips (approximately 130-160 µm).

Imaging was performed by scanning at 600 Hz, with 1024x1024 pixel resolution, line averaging of 3-4 and z-step size of 1 µm. Sequential scanning was used for DiI/DiD labelling and double-fluorescent *in situ*. 3D rendering of IPN terminals and maximum projections for z-stacks were created using Fiji (ImageJ) software. Volumetric and area analysis of fluorescent *in situ* hybridisation signals was performed with Imaris 7.7.1 (Bitplane) software by building a surface around the expression domain (Surface tool).

Microsoft Excel and GraphPad Prism 6 were used for data presentation and statistical analysis. Wilcoxon-Mann-Whitney test was carried out for unpaired comparisons of fluorescent *in situ* hybridisation expression volumes and area.

6.6. Rerea morpholino experiments

Morpholino antisense oligonucleotide covering *rerea* splice acceptor between intron 12 and exon 13 (5'-TCCTTGGAGGCTGTAAACACAAATT-3') was synthesised by Gene Tools, LLC and suspended in DEPC ddH_2O as 1 ng/nL stock. 3 ng of morpholino was pressure-injected into the cell of one-cell stage embryos from crosses of Et(*gata2a:eGFP*^{pku588}) fish. Injected fish were checked daily for viability and screened at 4 dpf for habenular and morphological defects.

6.7. Genomic DNA extraction

Genomic DNA from embryos or fin-clips was extracted by classical HotSHOT (Sodium Hydoxide and Tris) method (Meeker *et al.*, 2007). 50 µL (fin-clips) or 25 µL (embryos) of alkaline lysis solution (25 mM KOH, 0.2 mM EDTA, pH 12) were added and samples were incubated at 95°C for 30 minutes. Reaction was neutralised with 50 or 25 µL of neutralisation solution (40 mM Tris-HCl, pH 5).

6.8. Genotyping KASP assay

Genotyping of rerea^{u757} and rch^{u761} mutants was performed using the KASP assay to detect SNP mutation in the nucleotide 4122, C>T of *rerea* and for the mutation in *rch*. Reaction was performed by preparing a master mix with 4 µL of 2x KASP reaction, 0.11 µL of primer mic, 1 µL of DEPC ddH_2O per sample. The master mix was distributed to each well of a white 96-well plate, and to each well was added 3 µL of the extracted DNA. PCR reaction was performed in a thermocycler (Eppendorff, vapo.protec) with the following program: 94^{o}C for 15 minutes, 1 cycle; 94 ^{o}C for 20 seconds, 1 cycles; touchdown over 65-57 ^{o}C for 60 seconds, 10 cycles dropping 0.8 ^{o}C per cycle; 94 ^{o}C for 20 seconds, 57 ^{o}C for 60 seconds, 26 cycles.

6.9. RNA extraction and cDNA library preparations

Total RNA was extracted from 30-40 zebrafish embryos in 1 ml of Trizol (Invitrogen, Cat# 15596026). Tissue was homogenised with a pestle and by using a 30G needle, after which the samples were incubated at room temperature for 5 minutes. For RNA extraction, 200 µL of chloroform was added, the samples were incubated at room temperature for 3 minutes and centrifuged at 4°C for 15 minutes (12 000 g). The aqueous phase was transferred into a clean tube and RNA was precipitated by a 10-minute incubation at room temperature with 500 µL of ice-cold isopropanol added to the sample. After a 15-minute centrifugation at 4°C (12 000 g), the pellet was washed in 75 % ethanol, dried, resuspended in RNase free water and stored at -80°C. cDNA synthesis was carried out using Invitrogen SuperScript II Reverse Transcriptase (Cat# 18064014). 200 ng of random primers (Invitrogen, Cat# 48190011), 10 mM dNTP mix (Promega, Cat# U1511) and 2.5 ng of total RNA were mixed together in a final volume of 12 µL, incubated at 65°C for 5 minutes and chilled on ice for 5 minutes. 4 µL of 5x First-Strand Buffer (SS II RT Kit), 2 µL of 0.1 M DTT (SS II RT Kit) and 1 µL of RNaseOUT (Invitrogen, Cat# 10777019) were added to the reaction and the samples were incubated at 25°C for 2 minutes. After adding 1 µL of SuperScript II Reverse Transcriptase, cDNA synthesis was carried out in a thermocycler using the following programme: 25°C for 10 minutes, 42°C for 50 minutes, 70°C for 15 minutes, 4°C to end the reaction.

Extracted RNA was sequenced by the Institute of Childs Health Genomics Microarray and High Throughput Sequencing (HiSeq) with a 1x 150 cycle high output NextSeq run. Analysis that mapped the mutation was performed in the Galaxy platform. Briefly, reads were aligned to the zebrafish genome (GRCz10) using Hisat2. SNPs were detected using Freebayes, and the resulting VCF file was analysed using a modified version of the Cloudmap script (Garrison and Marth, 2012; Minevich *et al.*, 2012; Kim, Langmead and Salzberg, 2015). This tool uses local regression to highlight genomic regions which are homozygous in the mutant sample but not in the sibling sample.

6.10. Habenula dissection, dissociation and cell sorting (DeTCT)

All steps of this process were carried out in an RNase free area. 4 dpf Tg(*gng8:GFP*) zebrafish were terminally anaesthetized with tricaine and mounted in 300 µL of 2% agarose in PBS supplemented with tricaine in a dorsal position. A drop of PBS was added to cover the agarose. Left and right habenulae were manually dissected with a tungsten needle and scooped with a tungsten loop. All dissected left and right habenulae, were collected to two separate 10 µL PBS drops in a petri-dish on ice. After dissecting 6

habenulae, these were pipetted to a 90uL solution of trypsin-EDTA (0.27 mM in PBS) supplemented with 10uL of DNase (8 KU) and incubated at 28.5 ºC for 20 minutes. After shaking, 500uL of 4% FBS in PBS were added to the cells and these were kept on ice until FAC-sorting. Sorting of habenulae cells was performed at the Institute of Childs Health by Fluorescence-activated Cell Sorting in a MoFlo XDP. For quantitative PCR, the GFP positive cells were collected to a 500uL solution of trizol in a 1.5 mL Eppendorf tube and fast frozen in dry ice. For single cell sequencing, the GFP positive cells were collected to eight 96-well plates (4 plates per habenula nuclei side) filled with 5 µL of triton x100 (Sigma-Aldrich, X100-500mL; 0.002% in RNase free water). cDNA synthesis was performed at the Sanger Institute, Cambridge, by Steven A. Harvey. Illumina High Throughput Sequencing (HiSeq) with a 1x 150 cycle high output was also performed at the sequencing facility of the Sanger Institute.

6.11. Habenula dissection, dissociation and cell sorting (10x Genomics)

The procedure for the 10x Genomics approach was performed at Tatjana Sauka-Spengler's lab, with Vanessa Chong-Morrison at the MRC Weatherall Institute of Molecular Medicine, Oxford. Two hundred, 4 dpf Tg(gng8:GFP) larvae were terminally anaesthetised and their heads dissected in PBS. Each group of 50 heads were moved to 8 different 1.5 mL Eppendorf tubes and the PBS was substituted for 720uL of Tricaine diluted 1:2 in PBS. Heads were triturated with a 40 G needle and 1 mL syringe and incubated for 20 minutes at 29ºC for further dissociation. During incubation samples were mixed twice by tapping, and one last time at the end of incubation. Then, all samples were filtered in a 40 µm nylon mesh and pooled together. To wash the mesh and stop the Trypsin/EDTA reaction, the mesh was rinsed with 5 mL of a 3.2% solution of FBS in PBS. To reduce the duration of FAC-sorting, as to decrease the time between the collection of the first and last GFP positive cells, the cells were centrifuged at 500 g for 10 minutes at Room Temperature. Approximately 9 mL of the supernatant were dispensed, cells were resuspended in the remaining 2 mL of solution and FAC-sorted. Cells were collected to a 50uL solution of 6% FBS in PBS, aiming for a final solution of 200uL with 20000 cells in 1.5% FBS in PBS. Lastly, collected cells were centrifuged at 500 g for 10 minutes at Room Temperature and 170 µL of the supernatant were removed. Centrifuged cells were resuspended and ran in the 10x Genomics Microfluidics System, for cDNA library synthesis. cDNA was sequenced using the High Throughput Sequencing (HiSeq) with a 1x 150 cycle high output run.

6.12. 10x Genomics data analysis

The raw Illumina sequencing data was converted to expression counts matrices with the *cellranger* software from 10X genomics (©2018 10x Genomics, 2018). Briefly, BCL file from the Illumina HiSeq was demultiplexed into paired-end, gzip-compressed FASTQ files using *cellranger-mkfastq*. FASTQ file was provided as input to *cellranger-count,* which attributed each read to the cell of origin based on the 16 bp cell barcode. Reads were aligned to the GRCz10 zebrafish reference transcriptome. The number of transcript counts were accurately quantified for each annotated gene in every cell by using the 10 bp unique molecular identifier (UMI). The UMI was also used to identify and remove PCR duplicates. This resulted in an expression matrix (genes x cells) of UMI counts for each sample. Apart from when we tested the capacity of the software to detect a higher number of cells than those initially captured, the software was used with its default settings.

The *cloupe* file that results from the *cellranger* analysis was analysed using the Loupe Cell Browser (LCB) software from 10x Genomics, version 2.0.0 (©2018 10x Genomics., 2018). In the LCB software, cell clustering can be performed using the graph-based algorithm or the k-means algorithm. The graph-based clustering is performed in three steps: First, it builds a sparse nearest-neighbour graph, where cells are linked if they belong to the k nearest Euclidian neighbours of one another (i.e. if they have the shortest distance after PCA analysis). Second, it uses the Louvain Modularity Optimization algorithm to find highly-connected clusters formed by the previous step (i.e. clusters with little variability between them). Lastly, it performs a hierarchical clustering to merge pairs of sibling clusters in the PCA space if there are no genes differentially expressed between them. This step is repeated until there are no pairs to merge. This process resulted in the graph in Supplementary Figure 3.2.A which fused the dHb and vHb clusters, due to their nearness (both in the PCA space and gene expression) in comparison to the remaining clusters.

The k-means clustering, only performs the first step of the graph-based algorithm. The default selected K-value wields the best Davies-Bouldin Index, a measure of clustering quality. For the data of the sequenced cells, K-value = 10. However, this formed three clusters with only one cell each (Supplementary Figure 3.2.D). Moreover, it formed two clusters of 9 cells each (C6 and C7), that we were not able to distinguish from the OO cluster (C1) or the SktDev cluster (C4), respectively, by analysing each significantly expressed gene of each cluster. On the other hand, the K = 4 and lower fused the dHb and vHb clusters, not allowing us to analyse them separately (Supplementary Figure 3.2.B). Therefore, we analysed the clusters from the first K-value that distinguished the

dHb and vHb cluster, K-value = 6 (Supplementary Figure 3.2.C). In this k-value there was one cluster formed by one cell which we ignored.

To obtain a list of the significantly variable genes that defined each cluster, the software compares the gene variability of each cluster with all of the cells in the sample that do not belong to the cluster. To obtain the table of these genes we used the function *Significant Genes* > *Globally Distinguishing* of the software. The top 10 genes are represented in the Tables 3.1 to 3.5.

To obtain a graphic representation of the cells that express single genes we used the function *Categories* > *Gene Expression* and manually analysed the expression pattern of several genes of interest in the t-SNE plot built by the software. The results of this analysis are in the Supplementary Figures 3.3 to 3.5.

6.13. ROAST assay

Larval zebrafish between 6-8 dpf were embedded in 2% intermediate melting point agarose, in a 10 cm petri dish. To allow the tail to move freely, the agarose caudal to the swim bladder was cut perpendicularly to the anterior-posterior axis and removed. After overnight incubation, animals were inspected for healthy morphology. Healthy larvae were positioned below an infrared camera (120 frames per second, Point Grey) and illuminated from below with a 950 nm LED array. To monitor motor output, two regions of interest were created at each side of the fish. The distance between the fish tail and the regions of interest was such that only high amplitude tail responses would activate them.

Aversive heat was delivered using a 980 nm laser (Thorlabs), collimated to a beam size that allowed the targeting solely the head of larvae. Real-time thermal stimuli were generated using a high-power laser driver (Thorlabs) controlled by a data acquisition board (Arduino Uno) based on tail movements detected by the Bonsai software (Lopes *et al.*, 2015).

To account for movement events involving multiple deflections (such as turn-and-swim or turn-counterturn), the laser remained active for 100 ms after any wrong response. Only after this refractory period, the laser stimulus can be terminated by a correct turn. Any turn during the refractory period resets the 100 ms counter.

Before the beginning of the ROAST assay, fish were allowed to habituate to the environment, without any stimulus, for 5 minutes. The ROAST assay was performed in blocks of 20-30 trials. Trials had a randomized duration between one to two minutes. At the start of each trial, the aversive heat-stimulus was presented to the fish. Before the

first block, 3-5 trials assessed the preferred direction of turning response to the heat stimulus. During these trials, the laser was terminated in response to the first turn of the fish, regardless of the direction. For the contingency and contingency reversal blocks, he laser was terminated in response to a turn in the rewarded direction. During the contingency block, the rewarded direction opposed the preference of the fish. During the contingency reversal block, the rewarded direction favoured the preference of the fish.

The ROAST experimental pipeline was written in Python (state machine code) and embedded in the Bonsai software using the Python node. The state machine code consisted of 10 states. State 0 was an adaptation period of 5 minutes, where no stimulus was presented. At the end of state 0 the duration of the first trial was randomly calculated between 1 and 2 minutes. In state 1 the laser was switched ON for as long as (a) the fish responded to the stimulus with a high amplitude turn, or (b) the trial ended. If (a) happened first, the direction of the turn was recorded, and State 2 started, where nothing happened until the end of the trial time. If (b) happened first, the direction of the turn was recorded as 0 and the laser was switched OFF for one frame and State 1 restarted. This was repeated for 3-5 times, and a new trial duration was calculated between trials. If by the end of the 3-5 trials no preference was detected due to the lack of response to the laser, the trial would be terminated. Otherwise, State 3 or State 6 started, depending of the fish showing a turn direction preference for the right or left sides, respectively. In States 3/6 each trial started with laser ON for as long as (1) the larva flicks to the left or right sides, respectively, or (2) the trial ended. If (1) happened first, State 4/6 started, respectively, where nothing happened until the end of the trial time. If (2) happened first, the laser was switched OFF for one frame and State 3/6 restarted. If during State 3/6 the fish flicked to the right/left, State 5/8 started, where a refractory period of 100 ms would start. During this period, no tail flick was able to switch the laser OFF, but any flick would restart the refractory period counter. At the end of the refractory period State 3/6 resumed. State 3/6 was repeated for 20-30 trials, depending on the experiment (see results), and a new trial duration was calculated between trials. After 20-30 trials the state favouring the opposite direction would start (i.e. larvae that started with State 3 switched to State 6 and vice-versa). After 20-30 trials in the new State, the State 9 was triggered, which ensured that the laser was turned OFF and that the program stopped recording.

The output of the program was a *csv* file which contained information of state of the laser (ON = 1; OFF = 0), trial number (1 to 63-65), machine state (0 to 9), direction preference (-5 (left) to +5 (right)), refractory period counter (see below), block number (1 or 2), frame number, activity (0 or 1) of the region of interest on the left side of the fish and activity

of the region of interest on the right side of the fish. This information was obtained for each frame of the experiment, recorded at 120 frames per second.

6.14. ROAST assay analysis pipeline

Analysis of the obtained data was performed using Python v3.6.3. Briefly, the program was built to search each frame of the experiment for specific conditions using *if* statements. The frame of the beginning of a trial was found by detecting when the laser was switched ON. The frame and direction of the first response to the laser was found by detecting the first time the left or right regions of interest were activated after the beginning of a trial. The direction was considered as being to the correct (1) or incorrect side (0) by comparing the side of response with the bias of calculated in the first 3-5 trials and the block number to which the trial being analysed belonged to. The time between the beginning of the trial and the first response was named Latency of First Turn (LFT). The frame and direction of the response that switched the laser OFF was found by detecting when the laser was switched OFF. The time between the beginning of the trial and the frame the laser was switched off was named Latency of Laser OFF (LLO). The number of turns until the laser was switched OFF was calculated by counting the number of times any of the regions of interest was activated between the beginning of a trial and the frame the laser was switched OFF. The cumulative latency was calculated by summing the LFT or LLO of all trials before and including the trial the cumulative latency was being calculated for (i.e. to calculate the cumulative LFT at trial 10, LFT values from trial 1 to 10 were summed).

The average and standard error of the mean were calculated for each group of fish using the *numpy* library of python. To calculate the frequency of fish that responded to the correct side, the average and standard error of the mean of correct (1) and incorrect (0) turns was calculated for each trial. The same was done for LFT, LLO and their cumulative values.

Statistical tests were performed using GraphPad Prism 6. To show significant change along one block of any ROAST experiment we performed a one-way ANOVA with adjusted p-value for multiple tests (Greenhouse-Grisser Correction). To show significant difference between two blocks of any ROAST experiment we performed a two-way ANOVA with adjusted p-value for multiple tests (Tukey Correction).

REFERENCES

©2018 10x Genomics. (2018) *What is Loupe Cell Browser? - Software - Single Cell Gene Expression - Official 10x Genomics Support*. Available at: https://support.10xgenomics.com/single-cell-gene-expression/software/visualization/latest/what-is-loupe-cell-browser (Accessed: 30 January 2019).

©2018 10x Genomics (2018) *What is Cell Ranger? - Software - Single Cell Gene Expression - Official 10x Genomics Support*. Available at: https://support.10xgenomics.com/single-cell-gene-expression/software/pipelines/latest/what-is-cell-ranger (Accessed: 28 January 2019).

10x Genomics (2019) *Single-Cell RNA-Seq: An Introductory Overview and Tools for Getting Started*. Available at: https://community.10xgenomics.com/t5/10x-Blog/Single-Cell-RNA-Seq-An-Introductory-Overview-and-Tools-for/ba-p/547.

Agetsuma, M. *et al.* (2010) 'The habenula is crucial for experience-dependent modification of fear responses in zebrafish.', *Nature neuroscience*, 13(11), pp. 1354–6. doi: 10.1038/nn.2654.

Ahumada-Galleguillos, P., Lemus, C. G., D??az, E., *et al.* (2017) 'Directional asymmetry in the volume of the human habenula', *Brain Structure and Function*, 222(2). doi: 10.1007/s00429-016-1231-z.

Ahumada-Galleguillos, P., Lemus, C. G., Díaz, E., *et al.* (2017) 'Directional asymmetry in the volume of the human habenula', *Brain Structure and Function*, 222(2), pp. 1087–1092. doi: 10.1007/s00429-016-1231-z.

Aizawa, H. *et al.* (2005) 'Laterotopic representation of left-right information onto the dorso-ventral axis of a zebrafish midbrain target nucleus.', *Current biology : CB*. Elsevier, 15(3), pp. 238–43. doi: 10.1016/j.cub.2005.01.014.

Aizawa, H. *et al.* (2007) 'Temporally regulated asymmetric neurogenesis causes left-right difference in the zebrafish habenular structures.', *Developmental cell*. Elsevier, 12(1), pp. 87–98. doi: 10.1016/j.devcel.2006.10.004.

Aizawa, H. *et al.* (2012) 'Molecular characterization of the subnuclei in rat habenula', *The Journal of Comparative Neurology*, 520(18), pp. 4051–4066. doi: 10.1002/cne.23167.

Aizawa, H. *et al.* (2013) 'The Synchronous Activity of Lateral Habenular Neurons Is Essential for Regulating Hippocampal Theta Oscillation', *Journal of Neuroscience*, 33(20), pp. 8909–8921. doi: 10.1523/JNEUROSCI.4369-12.2013.

Aizenberg, M. and Schuman, E. M. (2011) 'Cerebellar-Dependent Learning in Larval Zebrafish', *Journal of Neuroscience*. Society for Neuroscience, 31(24), pp. 8708–8712. doi: 10.1523/JNEUROSCI.6565-10.2011.

AlJanahi, A. A., Danielsen, M. and Dunbar, C. E. (2018) 'An Introduction to the Analysis of

Single-Cell RNA-Sequencing Data.', *Molecular therapy. Methods & clinical development*. American Society of Gene & Cell Therapy, 10, pp. 189–196. doi: 10.1016/j.omtm.2018.07.003.

Amo, R. *et al.* (2010) 'Identification of the zebrafish ventral habenula as a homolog of the mammalian lateral habenula.', *The Journal of neuroscience : the official journal of the Society for Neuroscience*, 30(4), pp. 1566–74. doi: 10.1523/JNEUROSCI.3690-09.2010.

Amo, R. *et al.* (2014) 'The Habenulo-Raphe Serotonergic Circuit Encodes an Aversive Expectation Value Essential for Adaptive Active Avoidance of Danger', *Neuron*, 84(5), pp. 1034–1048. doi: 10.1016/j.neuron.2014.10.035.

Andersen, B. *et al.* (1996) 'Corpus callosotomy: Seizure and psychosocial outcome A 39-month follow-up of 20 patients', *Epilepsy Research*. Elsevier, 23(1), pp. 77–85. doi: 10.1016/0920-1211(95)00052-6.

Andres, K. H., von Düring, M. and Veh, R. W. (1999) 'Subnuclear organization of the rat habenular complexes.', *The Journal of comparative neurology*, 407(1), pp. 130–50. Available at: http://www.ncbi.nlm.nih.gov/pubmed/10213193 (Accessed: 8 January 2019).

Asai, Y. *et al.* (2006) 'Mutation of the atrophin2 gene in the zebrafish disrupts signaling by fibroblast growth factor during development of the inner ear', *Proceedings of the National Academy of Sciences*, 103(24), pp. 9069–9074. doi: 10.1073/pnas.0603453103.

Auer, T. O. *et al.* (2015) 'Deletion of a kinesin I motor unmasks a mechanism of homeostatic branching control by neurotrophin-3', *eLife*, 4. doi: 10.7554/eLife.05061.

Baker, K., Holtzman, N. G. and Burdine, R. D. (2008) 'Direct and indirect roles for Nodal signaling in two axis conversions during asymmetric morphogenesis of the zebrafish heart.', *Proceedings of the National Academy of Sciences of the United States of America*. National Academy of Sciences, 105(37), pp. 13924–9. doi: 10.1073/pnas.0802159105.

Baño-Otálora, B. and Piggins, H. D. (2017) 'Contributions of the lateral habenula to circadian timekeeping', *Pharmacology Biochemistry and Behavior*. Elsevier, 162, pp. 46–54. doi: 10.1016/J.PBB.2017.06.007.

Baran-Gale, J., Chandra, T. and Kirschner, K. (2018) 'Experimental design for single-cell RNA sequencing', *Briefings in Functional Genomics*. Oxford University Press, 17(4), pp. 233–239. doi: 10.1093/bfgp/elx035.

Baynes, K. *et al.* (1998) 'Modular organization of cognitive systems masked by interhemispheric integration.', *Science (New York, N.Y.)*, 280(5365), pp. 902–5. Available at: http://www.ncbi.nlm.nih.gov/pubmed/9572734 (Accessed: 20 January 2019).

Bedell, V. M. *et al.* (2012) 'The lineage-specific gene ponzr1 is essential for zebrafish pronephric and pharyngeal arch development', *Development*, 139(4), pp. 793–804. doi: 10.1242/dev.071720.

Beliakova-Bethell, N. *et al.* (2014) 'The effect of cell subset isolation method on gene expression in leukocytes', *Cytometry Part A*, 85(1), pp. 94–104. doi: 10.1002/cyto.a.22352.

Beretta, C. A. *et al.* (2013) 'The ventral habenulae of zebrafish develop in prosomere 2 dependent on Tcf7l2 function.', 8(1), p. 19. doi: 10.1186/1749-8104-8-19.

Bertrand, S. *et al.* (2007) 'Unexpected Novel Relational Links Uncovered by Extensive Developmental Profiling of Nuclear Receptor Expression', *PLoS Genetics*. Public Library of Science, 3(11), p. e188. doi: 10.1371/journal.pgen.0030188.

Bianco, I. H. *et al.* (2008) 'Brain asymmetry is encoded at the level of axon terminal morphology', *Neural Development*. BioMed Central, 3(1), p. 9. doi: 10.1186/1749-8104-3-9.

Bianco, I. H. and Wilson, S. W. (2009) 'The habenular nuclei: a conserved asymmetric relay station in the vertebrate brain.', *Philosophical transactions of the Royal Society of London. Series B, Biological sciences*, 364(1519), pp. 1005–20. doi: 10.1098/rstb.2008.0213.

Biemar, F. *et al.* (2001a) 'Pancreas Development in Zebrafish: Early Dispersed Appearance of Endocrine Hormone Expressing Cells and Their Convergence to Form the Definitive Islet', *Developmental Biology*. Academic Press, 230(2), pp. 189–203. doi: 10.1006/DBIO.2000.0103.

Biemar, F. *et al.* (2001b) 'Pancreas Development in Zebrafish: Early Dispersed Appearance of Endocrine Hormone Expressing Cells and Their Convergence to Form the Definitive Islet', *Developmental Biology*, 230(2), pp. 189–203. doi: 10.1006/dbio.2000.0103.

Binder, J. R. (2015) 'The Wernicke area: Modern evidence and a reinterpretation.', *Neurology*. American Academy of Neurology, 85(24), pp. 2170–5. doi: 10.1212/WNL.0000000000002219.

Biran, J. *et al.* (2012) 'Neurokinin Bs and neurokinin B receptors in zebrafish-potential role in controlling fish reproduction.', *Proceedings of the National Academy of Sciences of the United States of America*. National Academy of Sciences, 109(26), pp. 10269–74. doi: 10.1073/pnas.1119165109.

Boczonadi, V. *et al.* (2014) 'EXOSC8 mutations alter mRNA metabolism and cause hypomyelination with spinal muscular atrophy and cerebellar hypoplasia', *Nature Communications*, 5(1), p. 4287. doi: 10.1038/ncomms5287.

Bowen, N. J. *et al.* (2004) 'Mi-2/NuRD: multiple complexes for many purposes', *Biochimica et Biophysica Acta (BBA) - Gene Structure and Expression*, 1677(1–3), pp. 52–57. doi: 10.1016/j.bbaexp.2003.10.010.

Breuss, M. *et al.* (2012) 'Mutations in the β-Tubulin Gene TUBB5 Cause Microcephaly with Structural Brain Abnormalities', *Cell Reports*, 2(6), pp. 1554–1562. doi: 10.1016/j.celrep.2012.11.017.

de Bruijn, E., Cuppen, E. and Feitsma, H. (2009) 'Highly Efficient ENU Mutagenesis in Zebrafish', in. Humana Press, pp. 3–12. doi: 10.1007/978-1-60327-977-2_1.

Burgess, H. A. and Granato, M. (2007) 'Sensorimotor gating in larval zebrafish.', *The Journal of neuroscience : the official journal of the Society for Neuroscience*. Society for Neuroscience, 27(18), pp. 4984–94. doi: 10.1523/JNEUROSCI.0615-07.2007.

Burket, C. T. *et al.* (2008) 'Generation and characterization of transgenic zebrafish lines using

different ubiquitous promoters.', *Transgenic research*. NIH Public Access, 17(2), pp. 265–79. doi: 10.1007/s11248-007-9152-5.

Caldecott-Hazard, S., Mazziotta, J. and Phelps, M. (1988) 'Cerebral correlates of depressed behavior in rats, visualized using 14C-2-deoxyglucose autoradiography.', *The Journal of neuroscience : the official journal of the Society for Neuroscience*, 8(6), pp. 1951–1961.

Canning, C. A. *et al.* (2007) 'Sustained interactive Wnt and FGF signaling is required to maintain isthmic identity', *Developmental Biology*. Academic Press, 305(1), pp. 276–286. doi: 10.1016/J.YDBIO.2007.02.009.

Carl, M. *et al.* (2007) 'Wnt/Axin1/β-Catenin Signaling Regulates Asymmetric Nodal Activation, Elaboration, and Concordance of CNS Asymmetries', *Neuron*. Elsevier Inc., 55(3), pp. 393–405. doi: 10.1016/j.neuron.2007.07.007.

Carlson, J., Noguchi, K. and Ellison, G. (2001) 'Nicotine produces selective degeneration in the medial habenula and fasciculus retroflexus.', *Brain research*, 906(1–2), pp. 127–34. Available at: http://www.ncbi.nlm.nih.gov/pubmed/11430869 (Accessed: 23 January 2019).

Carper, R. A. *et al.* (2016) 'Reduced Hemispheric Asymmetry of White Matter Microstructure in Autism Spectrum Disorder', *Journal of the American Academy of Child & Adolescent Psychiatry*. Elsevier, 55(12), pp. 1073–1080. doi: 10.1016/j.jaac.2016.09.491.

Catani, M. *et al.* (2007) 'Symmetries in human brain language pathways correlate with verbal recall.', *Proceedings of the National Academy of Sciences of the United States of America*. National Academy of Sciences, 104(43), pp. 17163–8. doi: 10.1073/pnas.0702116104.

Cerda, G. A., Hargrave, M. and Lewis, K. E. (2009) 'RNA profiling of FAC-sorted neurons from the developing zebrafish spinal cord', *Developmental Dynamics*, 238(1), pp. 150–161. doi: 10.1002/dvdy.21818.

Charpentier, M. *et al.* (2018) 'CtIP fusion to Cas9 enhances transgene integration by homology-dependent repair.', *Nature communications*. Nature Publishing Group, 9(1), p. 1133. doi: 10.1038/s41467-018-03475-7.

Chen, Z. *et al.* (2013) 'Primary Neuron Culture for Nerve Growth and Axon Guidance Studies in Zebrafish (Danio rerio)', *PLoS ONE*. Edited by M. Hendricks. Public Library of Science, 8(3), p. e57539. doi: 10.1371/journal.pone.0057539.

Chou, M.-Y. *et al.* (2016) 'Social conflict resolution regulated by two dorsal habenular subregions in zebrafish', *Science*, 352(6281). doi: 10.1126/science.aac9508.

Clanton, J. A., Hope, K. D. and Gamse, J. T. (2013) 'Fgf signaling governs cell fate in the zebrafish pineal complex.', *Development (Cambridge, England)*. Oxford University Press for The Company of Biologists Limited, 140(2), pp. 323–32. doi: 10.1242/dev.083709.

Cohen, J. Y., Amoroso, M. W. and Uchida, N. (2015) 'Serotonergic neurons signal reward and punishment on multiple timescales', *eLife*, 4. doi: 10.7554/eLife.06346.

Collins, J. E. *et al.* (2015) 'High-throughput and quantitative genome-wide messenger RNA

sequencing for molecular phenotyping.', *BMC genomics*. BioMed Central, 16(1), p. 578. doi: 10.1186/s12864-015-1788-6.

Colombo, A. *et al.* (2013) 'Daam1a mediates asymmetric habenular morphogenesis by regulating dendritic and axonal outgrowth.', *Development (Cambridge, England)*, 140(19), pp. 3997–4007. doi: 10.1242/dev.091934.

Colwill, R. M. *et al.* (2005) 'Visual discrimination learning in zebrafish (Danio rerio)', *Behavioural Processes*, 70(1), pp. 19–31. doi: 10.1016/j.beproc.2005.03.001.

Concha, M. L. *et al.* (2000) 'A Nodal signaling pathway regulates the laterality of neuroanatomical asymmetries in the zebrafish forebrain', *Neuron*, 28(2), pp. 399–409. doi: 10.1016/S0896-6273(00)00120-3.

Concha, M. L. *et al.* (2003) 'Local tissue interactions across the dorsal midline of the forebrain establish CNS laterality', *Neuron*, 39(3), pp. 423–438. doi: 10.1016/S0896-6273(03)00437-9.

Concha, M. L., Bianco, I. H. and Wilson, S. W. (2012) 'Encoding asymmetry within neural circuits.', *Nature reviews. Neuroscience*. Nature Publishing Group, 13(12), pp. 832–43. doi: 10.1038/nrn3371.

Concha, M. L. and Wilson, S. W. (2001) 'Asymmetry in the epithalamus of vertebrates', *Journal of anatomy*, 199(Pt 1-2), pp. 63–84. doi: 10.1017/S0021878201008329.

Cui, Y. *et al.* (2018) 'Astroglial Kir4.1 in the lateral habenula drives neuronal bursts in depression', *Nature*. Nature Publishing Group, 554(7692), pp. 323–327. doi: 10.1038/nature25752.

Cunningham, T. J. *et al.* (2013) 'Antagonism between Retinoic Acid and Fibroblast Growth Factor Signaling during Limb Development', *Cell Reports*. Cell Press, 3(5), pp. 1503–1511. doi: 10.1016/J.CELREP.2013.03.036.

D'Aniello, E. *et al.* (2013) 'Depletion of Retinoic Acid Receptors Initiates a Novel Positive Feedback Mechanism that Promotes Teratogenic Increases in Retinoic Acid', *PLoS Genetics*. Edited by M. C. Mullins, 9(8), p. e1003689. doi: 10.1371/journal.pgen.1003689.

Da'as, S. *et al.* (2011) 'Zebrafish mast cells possess an FcεRI-like receptor and participate in innate and adaptive immune responses', *Developmental & Comparative Immunology*, 35(1), pp. 125–134. doi: 10.1016/j.dci.2010.09.001.

Dahlin, J. S. *et al.* (2018) 'A single-cell hematopoietic landscape resolves 8 lineage trajectories and defects in Kit mutant mice', *Blood*, 131(21), pp. e1–e11. doi: 10.1182/blood-2017-12-821413.

Dean, B. J. *et al.* (2014) 'Dbx1b defines the dorsal habenular progenitor domain in the zebrafish epithalamus.', *Neural development*, 9, p. 20. doi: 10.1186/1749-8104-9-20.

Dean, B. J., Gamse, J. T. and Wu, S.-Y. (2018) 'FGF activity asymmetrically regulates the timing of habenular neurogenesis in a Nodal-dependent manner', *bioRxiv*. Cold Spring Harbor Laboratory, p. 261834. doi: 10.1101/261834.

deCarvalho, T. N. *et al.* (2013) 'Aversive cues fail to activate fos expression in the asymmetric olfactory-habenula pathway of zebrafish.', *Frontiers in neural circuits*, 7, p. 98. doi: 10.3389/fncir.2013.00098.

deCarvalho, T. N. *et al.* (2014) 'Neurotransmitter map of the asymmetric dorsal habenular nuclei of zebrafish.', *Genesis (New York, N.Y. : 2000)*, 52(6), pp. 636–55. doi: 10.1002/dvg.22785.

Doll, C. A. *et al.* (2011) 'Subnuclear development of the zebrafish habenular nuclei requires ER translocon function', *Developmental Biology*. Elsevier Inc., 360(1), pp. 44–57. doi: 10.1016/j.ydbio.2011.09.003.

Dreosti, E. *et al.* (2014) 'Left-right asymmetry is required for the habenulae to respond to both visual and olfactory stimuli.', *Current biology : CB*. Elsevier, 24(4), pp. 440–5. doi: 10.1016/j.cub.2014.01.016.

Dronkers, N. F. *et al.* (2007) 'Paul Broca's historic cases: high resolution MR imaging of the brains of Leborgne and Lelong', *Brain*. Oxford University Press, 130(5), pp. 1432–1441. doi: 10.1093/brain/awm042.

Duboué, E. R. *et al.* (2017) 'Left Habenular Activity Attenuates Fear Responses in Larval Zebrafish', *Current Biology*, 27(14), p. 2154–2162.e3. doi: 10.1016/j.cub.2017.06.017.

Elston, T. W., Kalhan, S. and Bilkey, D. K. (2018) 'Conflict and adaptation signals in the anterior cingulate cortex and ventral tegmental area', *Scientific Reports*. Nature Publishing Group, 8(1), p. 11732. doi: 10.1038/s41598-018-30203-4.

Facchin, L., Duboue, E. R. and Halpern, M. E. (2015) 'Disruption of Epithalamic Left-Right Asymmetry Increases Anxiety in Zebrafish', *Journal of Neuroscience*, 35(48). doi: 10.1523/JNEUROSCI.2593-15.2015.

Flinker, A. *et al.* (2015) 'Redefining the role of Broca's area in speech.', *Proceedings of the National Academy of Sciences of the United States of America*. National Academy of Sciences, 112(9), pp. 2871–5. doi: 10.1073/pnas.1414491112.

Fowler, C. D. *et al.* (2011) 'Habenular α5 nicotinic receptor subunit signalling controls nicotine intake', *Nature*, 471(7340), pp. 597–601. doi: 10.1038/nature09797.

Frost, J. A. *et al.* (1999) 'Language processing is strongly left lateralized in both sexes. Evidence from functional MRI.', *Brain : a journal of neurology*, 122 (Pt 2), pp. 199–208. Available at: http://www.ncbi.nlm.nih.gov/pubmed/10071049 (Accessed: 20 January 2019).

Fu, C.-Y. *et al.* (2012) 'Zebrafish Dkk3a protein regulates the activity of myf5 promoter through interaction with membrane receptor integrin α6b.', *The Journal of biological chemistry*. American Society for Biochemistry and Molecular Biology, 287(47), pp. 40031–42. doi: 10.1074/jbc.M112.395012.

Furman, D. J. and Gotlib, I. H. (2016) 'Habenula responses to potential and actual loss in major depression: preliminary evidence for lateralized dysfunction.', *Social cognitive and affective neuroscience*. Oxford University Press, 11(5), pp. 843–51. doi: 10.1093/scan/nsw019.

Gamse, J. T. (2003) ‘The parapineal mediates left-right asymmetry in the zebrafish diencephalon’, *Development*, 130(6), pp. 1059–1068. doi: 10.1242/dev.00270.

Gamse, J. T. *et al.* (2005) ‘Directional asymmetry of the zebrafish epithalamus guides dorsoventral innervation of the midbrain target.’, *Development (Cambridge, England)*. The Company of Biologists Ltd, 132(21), pp. 4869–81. doi: 10.1242/dev.02046.

Garnaas, M. K. *et al.* (2012) ‘Rargb regulates organ laterality in a zebrafish model of right atrial isomerism’, *Developmental Biology*, 372(2), pp. 178–189. doi: 10.1016/j.ydbio.2012.09.001.

Garric, L. *et al.* (2014) ‘Pitx2c ensures habenular asymmetry by restricting parapineal cell number’, *Development*. Oxford University Press for The Company of Biologists Limited, 141(7), pp. 1572–1579.

Garrison, E. and Marth, G. (2012) ‘Haplotype-based variant detection from short-read sequencing’, *arXiv*. Available at: http://arxiv.org/abs/1207.3907 (Accessed: 27 January 2019).

Gilmour, D. T., Maischein, H.-M. and Nüsslein-Volhard, C. (2002) ‘Migration and function of a glial subtype in the vertebrate peripheral nervous system.’, *Neuron*, 34(4), pp. 577–88. Available at: http://www.ncbi.nlm.nih.gov/pubmed/12062041 (Accessed: 23 January 2019).

Goetz, J. J. and Trimarchi, J. M. (2012) ‘Transcriptome sequencing of single cells with Smart-Seq’, *Nature Biotechnology*, 30(8), pp. 763–765. doi: 10.1038/nbt.2325.

Goodwin, S., McPherson, J. D. and McCombie, W. R. (2016) ‘Coming of age: ten years of next-generation sequencing technologies’, *Nature Reviews Genetics*. Nature Publishing Group, a division of Macmillan Publishers Limited. All Rights Reserved., 17(6), pp. 333–351. doi: 10.1038/nrg.2016.49.

Gottesfeld, Z. (1983) ‘Origin and distribution of noradrenergic innervation in the habenula: a neurochemical study.’, *Brain research*, 275(2), pp. 299–304. Available at: http://www.ncbi.nlm.nih.gov/pubmed/6354358 (Accessed: 23 January 2019).

Gutwinski, S. *et al.* (2011) ‘Understanding left-handedness.’, *Deutsches Arzteblatt international*. Deutscher Arzte-Verlag GmbH, 108(50), pp. 849–53. doi: 10.3238/arztebl.2011.0849.

Haesemeyer, M. *et al.* (2015) ‘The Structure and Timescales of Heat Perception in Larval Zebrafish’, *Cell Systems*, 1(5), pp. 338–348. doi: 10.1016/j.cels.2015.10.010.

Haesemeyer, M. *et al.* (2018) ‘A Brain-wide Circuit Model of Heat-Evoked Swimming Behavior in Larval Zebrafish’, *Neuron*. Cell Press, 98(4), p. 817–831.e6. doi: 10.1016/J.NEURON.2018.04.013.

Hama, K. *et al.* (2009) ‘In vivo imaging of zebrafish digestive organ function using multiple quenched fluorescent reporters’, *American Journal of Physiology-Gastrointestinal and Liver Physiology*, 296(2), pp. G445–G453. doi: 10.1152/ajpgi.90513.2008.

Hanson, W. M. *et al.* (2016) ‘Reversible Oligonucleotide Chain Blocking Enables Bead Capture and Amplification of T-Cell Receptor α and β Chain mRNAs’, *Journal of the American Chemical Society*, 138(35), pp. 11073–11076. doi: 10.1021/jacs.6b04465.

He, X. *et al.* (2011) ‘miR-196 regulates axial patterning and pectoral appendage initiation’, *Developmental Biology*, 357(2), pp. 463–477. doi: 10.1016/j.ydbio.2011.07.014.

Hendricks, M. and Jesuthasan, S. (2007) ‘Asymmetric innervation of the habenula in zebrafish.’, *The Journal of comparative neurology*, 502(4), pp. 611–9. doi: 10.1002/cne.21339.

Her, G. M. *et al.* (2003) ‘In vivo studies of liver-type fatty acid binding protein (L-FABP) gene expression in liver of transgenic zebrafish (Danio rerio).’, *FEBS letters*, 538(1–3), pp. 125–33. Available at: http://www.ncbi.nlm.nih.gov/pubmed/12633865 (Accessed: 20 January 2019).

Herbert, M. R. *et al.* (2004) ‘Brain asymmetries in autism and developmental language disorder: a nested whole-brain analysis’, *Brain*. Oxford University Press, 128(1), pp. 213–226. doi: 10.1093/brain/awh330.

Herkenham, M. and Nauta, W. J. H. (1977) ‘Afferent connections of the habenular nuclei in the rat. A horseradish peroxidase study, with a note on the fiber-of-passage problem’, *The Journal of Comparative Neurology*, 173(1), pp. 123–145. doi: 10.1002/cne.901730107.

Hikosaka, O. (2010) ‘The habenula: from stress evasion to value-based decision-making.’, *Nature reviews. Neuroscience*, 11(7), pp. 503–13. doi: 10.1038/nrn2866.

Hong, E. *et al.* (2013) ‘Cholinergic left-right asymmetry in the habenulo-interpeduncular pathway’, *Proceedings of the National Academy of Sciences*, 110(52), pp. 21171–21176. doi: 10.1073/pnas.1319566110.

Hong, S. and Hikosaka, O. (2008) ‘The Globus Pallidus Sends Reward-Related Signals to the Lateral Habenula’, *Neuron*, 60(4), pp. 720–729. doi: 10.1016/j.neuron.2008.09.035.

Hong, S. and Hikosaka, O. (2013) ‘Diverse sources of reward value signals in the basal ganglia nuclei transmitted to the lateral habenula in the monkey.’, *Frontiers in human neuroscience*, 7, p. 778. doi: 10.3389/fnhum.2013.00778.

Hortopan, G. A., Dinday, M. T. and Baraban, S. C. (2010) ‘Spontaneous Seizures and Altered Gene Expression in GABA Signaling Pathways in a mind bomb Mutant Zebrafish’, *Journal of Neuroscience*, 30(41), pp. 13718–13728. doi: 10.1523/JNEUROSCI.1887-10.2010.

Howells, H. *et al.* (2018) ‘Frontoparietal Tracts Linked to Lateralized Hand Preference and Manual Specialization.’, *Cerebral cortex (New York, N.Y. : 1991)*. Oxford University Press, 28(7), pp. 2482–2494. doi: 10.1093/cercor/bhy040.

Hsu, P. D., Lander, E. S. and Zhang, F. (2014) ‘Development and Applications of CRISPR-Cas9 for Genome Engineering’, *Cell*, 157(6), pp. 1262–1278. doi: 10.1016/j.cell.2014.05.010.

Hsu, Y.-C. (2015) ‘Theory and Practice of Lineage Tracing.’, *Stem cells (Dayton, Ohio)*. NIH Public Access, 33(11), pp. 3197–204. doi: 10.1002/stem.2123.

Hüsken, U. *et al.* (2014) ‘Tcf7l2 is required for left-right asymmetric differentiation of habenular neurons.’, *Current biology : CB*, 24(19), pp. 2217–27. doi: 10.1016/j.cub.2014.08.006.

Hüsken, U. and Carl, M. (2013) ‘The Wnt/beta-catenin signaling pathway establishes neuroanatomical asymmetries and their laterality’, *Mechanisms of Development*, 130(6–8), pp.

330–335. doi: 10.1016/j.mod.2012.09.002.

Hyatt, G. A. *et al.* (1992) 'Retinoic acid-induced duplication of the zebrafish retina.', *Proceedings of the National Academy of Sciences of the United States of America*, 89(17), pp. 8293–7. Available at: http://www.ncbi.nlm.nih.gov/pubmed/1518861 (Accessed: 21 January 2019).

Ilicic, T. *et al.* (2016) 'Classification of low quality cells from single-cell RNA-seq data', *Genome Biology*. BioMed Central, 17(1), p. 29. doi: 10.1186/s13059-016-0888-1.

Illumina Inc. (2016) *Optimizing Cluster Density on Illumina Sequencing Systems*. Available at: https://support.illumina.com/content/dam/illumina-marketing/documents/products/other/miseq-overclustering-primer-770-2014-038.pdf (Accessed: 24 January 2019).

Inbal, A. *et al.* (2007) 'Six3 represses nodal activity to establish early brain asymmetry in zebrafish.', *Neuron*. Elsevier, 55(3), pp. 407–15. doi: 10.1016/j.neuron.2007.06.037.

Islam, S. *et al.* (2014) 'Quantitative single-cell RNA-seq with unique molecular identifiers', 11(1). doi: 10.1038/nmeth.2772.

Itoh, M. *et al.* (2003) 'Mind bomb is a ubiquitin ligase that is essential for efficient activation of Notch signaling by Delta.', *Developmental cell*, 4(1), pp. 67–82. Available at: http://www.ncbi.nlm.nih.gov/pubmed/12530964 (Accessed: 18 January 2019).

Jackson, A. *et al.* (2017) 'Varenicline, the clinically effective smoking cessation agent, restores probabilistic response reversal performance during withdrawal from nicotine', *Addiction Biology*. John Wiley & Sons, Ltd (10.1111), 22(5), pp. 1316–1328. doi: 10.1111/adb.12423.

Jetti, S. K., Vendrell-Llopis, N. and Yaksi, E. (2014) 'Spontaneous activity governs olfactory representations in spatially organized habenular microcircuits.', *Current biology : CB*. Elsevier, 24(4), pp. 434–9. doi: 10.1016/j.cub.2014.01.015.

Juárez-Morales, J. L. *et al.* (2016) 'Evx1 and Evx2 specify excitatory neurotransmitter fates and suppress inhibitory fates through a Pax2-independent mechanism', *Neural Development*, 11(1), p. 5. doi: 10.1186/s13064-016-0059-9.

Julius, D. (2013) 'TRP Channels and Pain', *Annual Review of Cell and Developmental Biology*, 29(1), pp. 355–384. doi: 10.1146/annurev-cellbio-101011-155833.

Kasibhatla, S. *et al.* (2006) 'Staining of Suspension Cells with Hoechst 33258 to Detect Apoptosis', *Cold Spring Harbor Protocols*, 2006(21), p. pdb.prot4492-pdb.prot4492. doi: 10.1101/pdb.prot4492.

Kawai, R. *et al.* (2015) 'Motor Cortex Is Required for Learning but Not for Executing a Motor Skill'. doi: 10.1016/j.neuron.2015.03.024.

Kettleborough, R. N. W. *et al.* (2013) 'A systematic genome-wide analysis of zebrafish protein-coding gene function.', *Nature*. Europe PMC Funders, 496(7446), pp. 494–7. doi: 10.1038/nature11992.

Kim, C. H. *et al.* (1996) 'Zebrafish elav/HuC homologue as a very early neuronal marker.', *Neuroscience letters*, 216(2), pp. 109–12. Available at:

http://www.ncbi.nlm.nih.gov/pubmed/8904795 (Accessed: 24 January 2019).

Kim, D., Langmead, B. and Salzberg, S. L. (2015) 'HISAT: a fast spliced aligner with low memory requirements', *Nature Methods*. Nature Publishing Group, 12(4), pp. 357–360. doi: 10.1038/nmeth.3317.

Kivioja, T. *et al.* (2012) 'Counting absolute numbers of molecules using unique molecular identifiers', *Nature Methods*. Nature Publishing Group, 9(1), pp. 72–74. doi: 10.1038/nmeth.1778.

Klein, A. M. *et al.* (2015) 'Droplet Barcoding for Single-Cell Transcriptomics Applied to Embryonic Stem Cells', *Cell*, 161(5), pp. 1187–1201. doi: 10.1016/j.cell.2015.04.044.

Knight, J. and Eagle, A. (no date) *Protease Dissociation - Protocols - ZFIN Community Wiki*. Available at: https://wiki.zfin.org/display/prot/Protease+Dissociation (Accessed: 29 December 2018).

Koide, T., Yabuki, Y. and Yoshihara, Y. (2018) 'Terminal Nerve GnRH3 Neurons Mediate Slow Avoidance of Carbon Dioxide in Larval Zebrafish', *Cell Reports*, 22(5), pp. 1115–1123. doi: 10.1016/j.celrep.2018.01.019.

Kraemer, A. M., Saraiva, L. R. and Korsching, S. I. (2008) 'Structural and functional diversification in the teleost S100 family of calcium-binding proteins', *BMC Evolutionary Biology*, 8(1), p. 48. doi: 10.1186/1471-2148-8-48.

Krishnan, S. *et al.* (2014) 'The Right Dorsal Habenula Limits Attraction to an Odor in Zebrafish', *Current Biology*. Elsevier Ltd, 24(11), pp. 1167–1175. doi: 10.1016/j.cub.2014.03.073.

Kuan, Y.-S. *et al.* (2007) 'Neuropilin asymmetry mediates a left-right difference in habenular connectivity.', *Development (Cambridge, England)*. The Company of Biologists Ltd, 134(5), pp. 857–65. doi: 10.1242/dev.02791.

Kuan, Y.-S. *et al.* (2015) 'Distinct requirements for Wntless in habenular development', *Dev Biol. Dev Biol. October*, 15(4062), pp. 117–128. doi: 10.1016/j.ydbio.2015.06.006.

Kudoh, T., Wilson, S. W. and Dawid, I. B. (2002) 'Distinct roles for Fgf, Wnt and retinoic acid in posteriorizing the neural ectoderm.', *Development (Cambridge, England)*, 129(18), pp. 4335–46. Available at: http://www.ncbi.nlm.nih.gov/pubmed/12183385 (Accessed: 23 December 2018).

Lahti, L. *et al.* (2011) 'FGF signaling gradient maintains symmetrical proliferative divisions of midbrain neuronal progenitors', *Developmental Biology*, 349(2), pp. 270–282. doi: 10.1016/j.ydbio.2010.11.008.

Lammel, S. *et al.* (2012) 'Input-specific control of reward and aversion in the ventral tegmental area', *Nature*. Nature Publishing Group, 491(7423), pp. 212–217. doi: 10.1038/nature11527.

Le, H.-G. T., Dowling, J. E. and Cameron, D. J. (2012) 'Early retinoic acid deprivation in developing zebrafish results in microphthalmia', *Visual Neuroscience*, 29(4–5), pp. 219–228. doi: 10.1017/S0952523812000296.

Lee, A. *et al.* (2010) 'The Habenula Prevents Helpless Behavior in Larval Zebrafish', *Current Biology*. Cell Press, 20(24), pp. 2211–2216. doi: 10.1016/J.CUB.2010.11.025.

Lee, S. *et al.* (2014) 'Kctd12 and Ulk2 Partner to Regulate Dendritogenesis and Behavior in the Habenular Nuclei', *PLoS ONE*. Edited by V. Korzh. Public Library of Science, 9(10), p. e110280. doi: 10.1371/journal.pone.0110280.

Levin, E. D. and Cerutti, D. T. (2009) *Behavioral Neuroscience of Zebrafish*, *Methods of Behavior Analysis in Neuroscience*. CRC Press/Taylor & Francis. Available at: http://www.ncbi.nlm.nih.gov/pubmed/21204325 (Accessed: 15 January 2019).

Li, J. M. (2012) *Identification of an Operant Learning Circuit by Whole Brain Functional Imaging in Larval Zebrafish A dissertation presented*. Available at: https://dash.harvard.edu/bitstream/handle/1/10974703/Li_gsas.harvard_0084L_11032.pdf?sequence=3 (Accessed: 26 January 2019).

Liao, G. *et al.* (2003) 'Regulation of androgen receptor activity by the nuclear receptor corepressor SMRT.', *The Journal of biological chemistry*. American Society for Biochemistry and Molecular Biology, 278(7), pp. 5052–61. doi: 10.1074/jbc.M206374200.

Linville, A. *et al.* (2009) 'Combinatorial roles for zebrafish retinoic acid receptors in the hindbrain, limbs and pharyngeal arches', *Developmental Biology*, 325(1), pp. 60–70. doi: 10.1016/j.ydbio.2008.09.022.

Liu, W.-H. *et al.* (2017) 'Association between habenula dysfunction and motivational symptoms in unmedicated major depressive disorder.', *Social cognitive and affective neuroscience*. Oxford University Press, 12(9), pp. 1520–1533. doi: 10.1093/scan/nsx074.

Llufrio, E. M. *et al.* (2018) 'Sorting cells alters their redox state and cellular metabolome', *Redox Biology*. Elsevier, 16, pp. 381–387. doi: 10.1016/J.REDOX.2018.03.004.

Long, S., Ahmad, N. and Rebagliati, M. (2003) 'The zebrafish nodal-related gene southpaw is required for visceral and diencephalic left-right asymmetry', *Development*. The Company of Biologists Ltd, 127(12), pp. 2583–2592. doi: 10.1242/dev.00270.

Lopes, G. *et al.* (2015) 'Bonsai: an event-based framework for processing and controlling data streams.', *Frontiers in neuroinformatics*. Frontiers, 9, p. 7. doi: 10.3389/fninf.2015.00007.

Lu, H. *et al.* (2013) 'EpCAM Is an Endoderm-Specific Wnt Derepressor that Licenses Hepatic Development', *Developmental Cell*, 24(5), pp. 543–553. doi: 10.1016/j.devcel.2013.01.021.

Lupton, C. *et al.* (2017) 'Loss of the Habenula Intrinsic Neuromodulator Kisspeptin1 Affects Learning in Larval Zebrafish', *eneuro*. Society for Neuroscience, 4(3), p. ENEURO.0326-16.2017. doi: 10.1523/ENEURO.0326-16.2017.

Mathews, M. S., Linskey, M. E. and Binder, D. K. (2008) 'William P. van Wagenen and the first corpus callosotomies for epilepsy', *Journal of Neurosurgery*. American Association of Neurological Surgeons, 108(3), pp. 608–613. doi: 10.3171/JNS/2008/108/3/0608.

Matias, S. *et al.* (2017) 'Activity patterns of serotonin neurons underlying cognitive flexibility',

eLife, 6. doi: 10.7554/eLife.20552.

Matsumoto, M. and Hikosaka, O. (2007) 'Lateral habenula as a source of negative reward signals in dopamine neurons.', *Nature*, 447(7148), pp. 1111–5. doi: 10.1038/nature05860.

Matsumoto, M. and Hikosaka, O. (2009a) 'Representation of negative motivational value in the primate lateral habenula', *Nature Neuroscience*, 12(1), pp. 77–84. doi: 10.1038/nn.2233.

Matsumoto, M. and Hikosaka, O. (2009b) 'Two types of dopamine neuron distinctly convey positive and negative motivational signals', *Nature*, 459(7248), pp. 837–841. doi: 10.1038/nature08028.

McCallum, S. E. *et al.* (2012) 'α3β4 nicotinic acetylcholine receptors in the medial habenula modulate the mesolimbic dopaminergic response to acute nicotine in vivo', *Neuropharmacology*, 63(3), pp. 434–440. doi: 10.1016/j.neuropharm.2012.04.015.

Meeker, N. D. *et al.* (2007) 'Method for isolation of PCR-ready genomic DNA from zebrafish tissues', *BioTechniques*, 43(5), pp. 610–614. doi: 10.2144/000112619.

Minevich, G. *et al.* (2012) 'CloudMap: A Cloud-Based Pipeline for Analysis of Mutant Genome Sequences', *Genetics*, 192(4), pp. 1249–1269. doi: 10.1534/genetics.112.144204.

Miyasaka, N. *et al.* (2009) 'From the Olfactory Bulb to Higher Brain Centers: Genetic Visualization of Secondary Olfactory Pathways in Zebrafish', *Journal of Neuroscience*, 29(15), pp. 4756–4767. doi: 10.1523/JNEUROSCI.0118-09.2009.

Molina, G. A., Watkins, S. C. and Tsang, M. (2007) 'Generation of FGF reporter transgenic zebrafish and their utility in chemical screens', *BMC Developmental Biology*. BioMed Central, 7(1), p. 62. doi: 10.1186/1471-213X-7-62.

Morris, A. C. and Fadool, J. M. (2005) 'Studying rod photoreceptor development in zebrafish.', *Physiology & behavior*. NIH Public Access, 86(3), pp. 306–13. doi: 10.1016/j.physbeh.2005.08.020.

Murayama, E. *et al.* (2015) 'NACA deficiency reveals the crucial role of somite-derived stromal cells in haematopoietic niche formation', *Nature Communications*, 6(1), p. 8375. doi: 10.1038/ncomms9375.

Nawrocki, L. *et al.* (1985) 'Larval and adult visual pigments of the zebrafish, Brachydanio rerio.', *Vision research*, 25(11), pp. 1569–76. Available at: http://www.ncbi.nlm.nih.gov/pubmed/3832580 (Accessed: 26 January 2019).

Neugebauer, J. M. and Yost, H. J. (2014) 'FGF signaling is required for brain left–right asymmetry and brain midline formation', *Developmental Biology*. Academic Press, 386(1), pp. 123–134. doi: 10.1016/J.YDBIO.2013.11.020.

Nguyen, Q. H. *et al.* (2018) 'Profiling human breast epithelial cells using single cell RNA sequencing identifies cell diversity.', *Nature communications*. Nature Publishing Group, 9(1), p. 2028. doi: 10.1038/s41467-018-04334-1.

Ogawa, S. *et al.* (2012) 'Cloning and expression of tachykinins and their association with

kisspeptins in the brains of zebrafish.', *The Journal of comparative neurology*, 520(13), pp. 2991–3012. doi: 10.1002/cne.23103.

Le Pabic, P., Ng, C. and Schilling, T. F. (2014) 'Fat-Dachsous Signaling Coordinates Cartilage Differentiation and Polarity during Craniofacial Development', *PLoS Genetics*. Edited by M. C. Mullins. Public Library of Science, 10(10), p. e1004726. doi: 10.1371/journal.pgen.1004726.

Pama, E. a C., Colzato, L. S. and Hommel, B. (2013) 'Optogenetics as a neuromodulation tool in cognitive neuroscience.', *Frontiers in psychology*, 4(September), p. 610. doi: 10.3389/fpsyg.2013.00610.

Pandey, S. *et al.* (2018) 'Comprehensive Identification and Spatial Mapping of Habenular Neuronal Types Using Single-Cell RNA-Seq', *Current Biology*, 28(7), p. 1052–1065.e7. doi: 10.1016/j.cub.2018.02.040.

Parker, M. O. *et al.* (2012) 'Discrimination reversal and attentional sets in zebrafish (Danio rerio)', *Behavioural Brain Research*. Elsevier, 232(1), pp. 264–268. doi: 10.1016/J.BBR.2012.04.035.

Phillipson, O. T. and Pycock, C. J. (1982) 'Dopamine neurones of the ventral tegmentum project to both medial and lateral habenula. Some implications for habenular function.', *Experimental brain research*, 45(1–2), pp. 89–94. Available at: http://www.ncbi.nlm.nih.gov/pubmed/6799315 (Accessed: 23 January 2019).

Picelli, S. *et al.* (2013) 'Smart-seq2 for sensitive full-length transcriptome profiling in single cells', *Nature Methods*, 10(11), pp. 1096–1098. doi: 10.1038/nmeth.2639.

Picelli, S. *et al.* (2014) 'Full-length RNA-seq from single cells using Smart-seq2', *Nature Protocols*, 9(1), pp. 171–181. doi: 10.1038/nprot.2014.006.

Plaster, N. *et al.* (2007) 'REREa/Atrophin-2 interacts with histone deacetylase and Fgf8 signaling to regulate multiple processes of zebrafish development.', *Developmental dynamics : an official publication of the American Association of Anatomists*, 236(7), pp. 1891–904. doi: 10.1002/dvdy.21196.

Poole, R. J. and Hobert, O. (2006) 'Early Embryonic Programming of Neuronal Left/Right Asymmetry in C. elegans', *Current Biology*, 16(23), pp. 2279–2292. doi: 10.1016/j.cub.2006.09.041.

Portugues, R. and Engert, F. (2011) 'Adaptive Locomotor Behavior in Larval Zebrafish', *Frontiers in Systems Neuroscience*. Frontiers, 5, p. 72. doi: 10.3389/fnsys.2011.00072.

Qin, C. and Luo, M. (2009) 'Neurochemical phenotypes of the afferent and efferent projections of the mouse medial habenula', *Neuroscience*, 161(3), pp. 827–837. doi: 10.1016/j.neuroscience.2009.03.085.

Rauch, G. J. *et al.* (2003) *Submission and Curation of Gene Expression Data*, *ZFIN Direct Data Submission*.

Raymond, M. *et al.* (1996) 'Frequency-dependent maintenance of left handedness in humans',

Proceedings of the Royal Society of London. Series B: Biological Sciences, 263(1377), pp. 1627–1633. doi: 10.1098/rspb.1996.0238.

Rebagliati, M. R. *et al.* (1998) 'cyclops encodes a nodal-related factor involved in midline signaling.', *Proceedings of the National Academy of Sciences of the United States of America*. National Academy of Sciences, 95(17), pp. 9932–7. doi: 10.1073/PNAS.95.17.9932.

Rebagliati, M. R. *et al.* (1998) 'Zebrafish Nodal-Related Genes Are Implicated in Axial Patterning and Establishing Left–Right Asymmetry', *Developmental Biology*, 199(2), pp. 261–272. doi: 10.1006/dbio.1998.8935.

Reddy, L. F. *et al.* (2016) 'Probabilistic Reversal Learning in Schizophrenia: Stability of Deficits and Potential Causal Mechanisms', *Schizophrenia Bulletin*, 42(4), pp. 942–951. doi: 10.1093/schbul/sbv226.

Regan, J. C. *et al.* (2009) 'An Fgf8-dependent bistable cell migratory event establishes CNS asymmetry.', *Neuron*. Elsevier, 61(1), pp. 27–34. doi: 10.1016/j.neuron.2008.11.030.

Reifers, F. *et al.* (1998) 'Fgf8 is mutated in zebrafish acerebellar (ace) mutants and is required for maintenance of midbrain-hindbrain boundary development and somitogenesis.', *Development (Cambridge, England)*, 125(13), pp. 2381–95. Available at: http://www.ncbi.nlm.nih.gov/pubmed/9609821 (Accessed: 22 December 2018).

Richardson, G. M., Lannigan, J. and Macara, I. G. (2015) 'Does FACS perturb gene expression?', *Cytometry Part A*, 87(2), pp. 166–175. doi: 10.1002/cyto.a.22608.

Roberson, S. and Halpern, M. E. (2017a) 'Convergence of signaling pathways underlying habenular formation and axonal outgrowth in zebrafish', *Development*, 144(14), pp. 2652–2662. doi: 10.1242/dev.147751.

Roberson, S. and Halpern, M. E. (2017b) 'Development and connectivity of the habenular nuclei', *Seminars in Cell and Developmental Biology*. Elsevier Ltd. doi: 10.1016/j.semcdb.2017.10.007.

Rønnekleiv, O. K. and Møller, M. (1979) 'Brain-pineal nervous connections in the rat: an ultrastructure study following habenular lesion.', *Experimental brain research*, 37(3), pp. 551–62. Available at: http://www.ncbi.nlm.nih.gov/pubmed/520442 (Accessed: 23 January 2019).

Roussigné, M. *et al.* (2009) 'Nodal signalling imposes left-right asymmetry upon neurogenesis in the habenular nuclei.', *Development (Cambridge, England)*, 136(9), pp. 1549–57. doi: 10.1242/dev.034793.

Roussigné, M. *et al.* (2018) 'Left/right asymmetric collective migration of parapineal cells is mediated by focal FGF signaling activity in leading cells', *Proceedings of the National Academy of Sciences*, 115(42), pp. E9812–E9821. doi: 10.1073/pnas.1812016115.

Ruhl, T. *et al.* (2015) 'The endocannabinoid system and associative learning and memory in zebrafish', *Behavioural Brain Research*. Elsevier, 290, pp. 61–69. doi: 10.1016/J.BBR.2015.04.046.

Sacks, O. (1986) *The man who mistook his wife for a hat*. 2nd edn. London: Picador.

Salas, R. *et al.* (2009) 'Nicotinic Receptors in the Habenulo-Interpeduncular System Are Necessary for Nicotine Withdrawal in Mice', *Journal of Neuroscience*, 29(10), pp. 3014–3018. doi: 10.1523/JNEUROSCI.4934-08.2009.

Samarut, E. *et al.* (2014) 'Retinoic Acid Receptor Subtype-Specific Transcriptotypes in the Early Zebrafish Embryo', *Molecular Endocrinology*, 28(2), pp. 260–272. doi: 10.1210/me.2013-1358.

Samarut, É., Lissouba, A. and Drapeau, P. (2016) 'A simplified method for identifying early CRISPR-induced indels in zebrafish embryos using High Resolution Melting analysis', *BMC Genomics*. BioMed Central, 17(1), p. 547. doi: 10.1186/s12864-016-2881-1.

Sartorius, A. *et al.* (2010) 'Remission of Major Depression Under Deep Brain Stimulation of the Lateral Habenula in a Therapy-Refractory Patient', *Biological Psychiatry*. Elsevier, 67(2), pp. e9–e11. doi: 10.1016/j.biopsych.2009.08.027.

Sartorius, A. and Henn, F. A. (2007) 'Deep brain stimulation of the lateral habenula in treatment resistant major depression', *Medical Hypotheses*. Churchill Livingstone, 69(6), pp. 1305–1308. doi: 10.1016/J.MEHY.2007.03.021.

Sassen, W. A. *et al.* (2017) 'Embryonic zebrafish primary cell culture for transfection and live cellular and subcellular imaging', *Developmental Biology*. Academic Press, 430(1), pp. 18–31. doi: 10.1016/J.YDBIO.2017.07.014.

Satija, R. *et al.* (2015) 'Spatial reconstruction of single-cell gene expression data', *Nature Biotechnology*, 33(5), pp. 495–502. doi: 10.1038/nbt.3192.

Schredelseker, T. and Driever, W. (2018) 'Bsx controls pineal complex development', *Development*, 145(13), p. dev163477. doi: 10.1242/dev.163477.

Schumacher, J. A. *et al.* (2014) 'Two-color fluorescent in situ hybridization using chromogenic substrates in zebrafish', *BioTechniques*, 57(5), pp. 254–6. doi: 10.2144/000114229.

Schuster, V. *et al.* (2017) 'Comparison of fMRI paradigms assessing visuospatial processing: Robustness and reproducibility.', *PloS one*. Public Library of Science, 12(10), p. e0186344. doi: 10.1371/journal.pone.0186344.

Sena, J. A. *et al.* (2018) 'Unique Molecular Identifiers reveal a novel sequencing artefact with implications for RNA-Seq based gene expression analysis', *Scientific Reports*. Nature Publishing Group, 8(1), p. 13121. doi: 10.1038/s41598-018-31064-7.

Sever, R. and Glass, C. K. (2013) 'Signaling by nuclear receptors.', *Cold Spring Harbor perspectives in biology*. Cold Spring Harbor Laboratory Press, 5(3), p. a016709. doi: 10.1101/cshperspect.a016709.

Sheffield, E. B., Quick, M. W. and Lester, R. A. (2000) 'Nicotinic acetylcholine receptor subunit mRNA expression and channel function in medial habenula neurons.', *Neuropharmacology*, 39(13), pp. 2591–603. Available at: http://www.ncbi.nlm.nih.gov/pubmed/11044729 (Accessed: 23 January 2019).

Shen, Y. *et al.* (2007) 'Functional architecture of atrophins.', *The Journal of biological chemistry*. American Society for Biochemistry and Molecular Biology, 282(7), pp. 5037–44. doi: 10.1074/jbc.M610274200.

Shepard, P. D., Holcomb, H. H. and Gold, J. M. (2006) 'Schizophrenia in translation: the presence of absence: habenular regulation of dopamine neurons and the encoding of negative outcomes.', *Schizophrenia bulletin*, 32(3), pp. 417–21. doi: 10.1093/schbul/sbj083.

Shih, P.-Y., McIntosh, J. M. and Drenan, R. M. (2015) 'Nicotine Dependence Reveals Distinct Responses from Neurons and Their Resident Nicotinic Receptors in Medial Habenula.', *Molecular pharmacology*. American Society for Pharmacology and Experimental Therapeutics, 88(6), pp. 1035–44. doi: 10.1124/mol.115.101444.

Shumake, J., Edwards, E. and Gonzalez-Lima, F. (2003) 'Opposite metabolic changes in the habenula and ventral tegmental area of a genetic model of helpless behavior.', *Brain research*, 963(1–2), pp. 274–81. Available at: http://www.ncbi.nlm.nih.gov/pubmed/12560133 (Accessed: 23 January 2019).

Simbolo, M. *et al.* (2013) 'DNA Qualification Workflow for Next Generation Sequencing of Histopathological Samples', *PLoS ONE*. Edited by J. D. Hoheisel, 8(6), p. e62692. doi: 10.1371/journal.pone.0062692.

Snelson, C. D. *et al.* (2008) 'Tbx2b is required for the development of the parapineal organ.', *Development (Cambridge, England)*. NIH Public Access, 135(9), pp. 1693–702. doi: 10.1242/dev.016576.

Snelson, C. D., Burkart, J. T. and Gamse, J. T. (2008) 'Formation of the asymmetric pineal complex in zebrafish requires two independently acting transcription factors.', *Developmental dynamics : an official publication of the American Association of Anatomists*. NIH Public Access, 237(12), pp. 3538–44. doi: 10.1002/dvdy.21607.

Sperry, R. W. (1968) 'Hemisphere deconnection and unity in conscious awareness.', *The American psychologist*, 23(10), pp. 723–33. Available at: http://www.ncbi.nlm.nih.gov/pubmed/5682831 (Accessed: 22 January 2019).

Spring, S. *et al.* (2010) 'Cerebral asymmetries in 12-week-old C57Bl/6J mice measured by magnetic resonance imaging', *NeuroImage*, 50(2), pp. 409–415. doi: 10.1016/j.neuroimage.2009.12.043.

Steinmetz, H. *et al.* (1991) 'Anatomical left-right asymmetry of language-related temporal cortex is different in left- and right-handers', *Annals of Neurology*, 29(3), pp. 315–319. doi: 10.1002/ana.410290314.

Stephenson-Jones, M. *et al.* (2012) 'Evolutionary conservation of the habenular nuclei and their circuitry controlling the dopamine and 5-hydroxytryptophan (5-HT) systems', *Proceedings of the National Academy of Sciences*, 109(3), pp. E164–E173. doi: 10.1073/pnas.1119348109.

Stephenson-Jones, M. *et al.* (2016) 'A basal ganglia circuit for evaluating action outcomes', *Nature*. Nature Research, 539(7628), pp. 289–293. doi: 10.1038/nature19845.

Strober, W. (2001) 'Trypan Blue Exclusion Test of Cell Viability', in *Current Protocols in Immunology*. Hoboken, NJ, USA: John Wiley & Sons, Inc., p. Appendix 3B. doi: 10.1002/0471142735.ima03bs21.

Stulberg, M. J. *et al.* (2012) 'Crosstalk between Fgf and Wnt signaling in the zebrafish tailbud.', *Developmental biology*. NIH Public Access, 369(2), pp. 298–307. doi: 10.1016/j.ydbio.2012.07.003.

Tan, H., Onichtchouk, D. and Winata, C. (2016) 'DANIO-CODE: Toward an Encyclopedia of DNA Elements in Zebrafish.', *Zebrafish*, 13(1), pp. 54–60. doi: 10.1089/zeb.2015.1179.

Tarifeño-Saldivia, E. *et al.* (2017) 'Transcriptome analysis of pancreatic cells across distant species highlights novel important regulator genes', *BMC Biology*, 15(1), p. 21. doi: 10.1186/s12915-017-0362-x.

Taylor, R. W. *et al.* (2011) 'Asymmetric inhibition of Ulk2 causes left-right differences in habenular neuropil formation.', *The Journal of neuroscience : the official journal of the Society for Neuroscience*, 31(27), pp. 9869–78. doi: 10.1523/JNEUROSCI.0435-11.2011.

Teh, C. *et al.* (2010) 'Optogenetic in vivo cell manipulation in KillerRed-expressing zebrafish transgenics.', *BMC developmental biology*. BioMed Central, 10, p. 110. doi: 10.1186/1471-213X-10-110.

Thermo Fisher Scientific (no date) *B-27 Supplement (50X), serum free*. Available at: https://www.thermofisher.com/order/catalog/product/17504044?SID=srch-hj-17504044 (Accessed: 29 December 2018).

Thisse, B. and Thisse, C. (2004) *Fast Release Clones: A High Throughput Expression Analysis*, *ZFIN Direct Data Submission*. Available at: https://zfin.org/ZDB-PUB-040907-1 (Accessed: 2 June 2016).

Thisse, B. and Thisse, C. (2014) *In Situ Hybridization on Whole-Mount Zebrafish Embryos and Young Larvae.*, *Methods Molecular Biology*. Available at: https://zfin.org/cgi-bin/webdriver (Accessed: 2 June 2016).

Turner, K. J. *et al.* (2016) 'Afferent Connectivity of the Zebrafish Habenulae', *Frontiers in Neural Circuits*. Frontiers, 10. doi: 10.3389/fncir.2016.00030.

Ullsperger, M. and von Cramon, D. Y. (2003) 'Error monitoring using external feedback: specific roles of the habenular complex, the reward system, and the cingulate motor area revealed by functional magnetic resonance imaging.', *The Journal of neuroscience : the official journal of the Society for Neuroscience*. Society for Neuroscience, 23(10), pp. 4308–14. doi: 10.1523/JNEUROSCI.23-10-04308.2003.

Valerius, G. *et al.* (2008) 'Reversal Learning as a Neuropsychological Indicator for the Neuropathology of Obsessive Compulsive Disorder? A Behavioral Study', *The Journal of Neuropsychiatry and Clinical Neurosciences*, 20(2), pp. 210–218. doi: 10.1176/jnp.2008.20.2.210.

Vallortigara, G. and Rogers, L. J. (2005) 'Survival with an asymmetrical brain: Advantages and

disadvantages of cerebral lateralization', *Behavioral and Brain Sciences*, 28(04), pp. 575-89; discussion 589-633. doi: 10.1017/S0140525X05000105.

Varshney, G. K. *et al.* (2015) 'High-throughput gene targeting and phenotyping in zebrafish using CRISPR/Cas9.', *Genome research*. Cold Spring Harbor Laboratory Press, 25(7), pp. 1030–42. doi: 10.1101/gr.186379.114.

Velasquez, K. M., Molfese, D. L. and Salas, R. (2014) 'The role of the habenula in drug addiction', *Frontiers in Human Neuroscience*, 8. doi: 10.3389/fnhum.2014.00174.

Vilhais-Neto, G. C. *et al.* (2010) 'Rere controls retinoic acid signalling and somite bilateral symmetry.', *Nature*. Macmillan Publishers Limited. All rights reserved, 463(7283), pp. 953–7. doi: 10.1038/nature08763.

Viswanath, H. *et al.* (2014) 'The medial habenula: still neglected', *Frontiers in Human Neuroscience*, 7. doi: 10.3389/fnhum.2013.00931.

Wagner, F., French, L. and Veh, R. W. (2016) 'Transcriptomic-anatomic analysis of the mouse habenula uncovers a high molecular heterogeneity among neurons in the lateral complex, while gene expression in the medial complex largely obeys subnuclear boundaries.', *Brain structure & function*, 221(1), pp. 39–58. doi: 10.1007/s00429-014-0891-9.

Wagner, F., Stroh, T. and Veh, R. W. (2014) 'Correlating habenular subnuclei in rat and mouse by using topographic, morphological, and cytochemical criteria', *Journal of Comparative Neurology*, 522(11), pp. 2650–2662. doi: 10.1002/cne.23554.

Wang, L. *et al.* (2006) 'Histone deacetylase-associating Atrophin proteins are nuclear receptor corepressors.', *Genes & development*. Cold Spring Harbor Laboratory Press, 20(5), pp. 525–30. doi: 10.1101/gad.1393506.

Wang, Y. Y., Chang, R. B. and Liman, E. R. (2010) 'TRPA1 is a component of the nociceptive response to CO2.', *The Journal of neuroscience : the official journal of the Society for Neuroscience*. NIH Public Access, 30(39), pp. 12958–63. doi: 10.1523/JNEUROSCI.2715-10.2010.

Wang, Z., Gerstein, M. and Snyder, M. (2009) 'RNA-Seq: a revolutionary tool for transcriptomics.', *Nature reviews. Genetics*, 10(1), pp. 57–63. doi: 10.1038/nrg2484.

Wen, L. *et al.* (2008) 'Visualization of monoaminergic neurons and neurotoxicity of MPTP in live transgenic zebrafish', *Developmental Biology*, 314(1), pp. 84–92. doi: 10.1016/j.ydbio.2007.11.012.

Wittling, R. A. *et al.* (2009) 'A simple method for measuring brain asymmetry in children: Application to autism', *Behavior Research Methods*. Springer-Verlag, 41(3), pp. 812–819. doi: 10.3758/BRM.41.3.812.

Wolman, D. (2012) 'The split brain: A tale of two halves', *Nature*, 483(7389), pp. 260–263. doi: 10.1038/483260a.

Worthington Biochemical Corporation (no date) *Worthington Tissue Dissociation Guide*.

Available at: http://www.worthington-biochem.com/tissuedissociation/default.html (Accessed: 29 December 2018).

Wu, S. Y. *et al.* (2014) 'Mediator subunit 12 coordinates intrinsic and extrinsic control of epithalamic development', *Developmental Biology*. Elsevier, 385(1), pp. 13–22. doi: 10.1016/j.ydbio.2013.10.023.

Xu, X. *et al.* (2007) 'Active avoidance conditioning in zebrafish (Danio rerio)', *Neurobiology of Learning and Memory*, 87(1), pp. 72–77. doi: 10.1016/j.nlm.2006.06.002.

Yanagisawa, H. *et al.* (2000) 'Protein binding of a DRPLA family through arginine-glutamic acid dipeptide repeats is enhanced by extended polyglutamine.', *Human molecular genetics*, 9(9), pp. 1433–42. Available at: http://www.ncbi.nlm.nih.gov/pubmed/10814707 (Accessed: 28 January 2019).

Yang, Y. *et al.* (2018) 'Lateral habenula in the pathophysiology of depression', *Current Opinion in Neurobiology*. Elsevier Current Trends, 48, pp. 90–96. doi: 10.1016/J.CONB.2017.10.024.

Zeisel, A. *et al.* (2018) 'Molecular Architecture of the Mouse Nervous System Resource Molecular Architecture of the Mouse Nervous System', *Cell*, 174, p. 999–1014.e22. doi: 10.1016/j.cell.2018.06.021.

Zhang, B. *et al.* (2017) 'Left Habenula Mediates Light-Preference Behavior in Zebrafish via an Asymmetrical Visual Pathway', *Neuron*. Cell Press, 93(4), p. 914–928.e4. doi: 10.1016/J.NEURON.2017.01.011.

Zhang, S. *et al.* (2002) 'Drosophila atrophin homolog functions as a transcriptional corepressor in multiple developmental processes.', *Cell*, 108(1), pp. 45–56. Available at: http://www.ncbi.nlm.nih.gov/pubmed/11792320 (Accessed: 21 January 2019).

Zhao, Q. *et al.* (2002) 'A mitochondrial specific stress response in mammalian cells.', *The EMBO journal*. European Molecular Biology Organization, 21(17), pp. 4411–9. doi: 10.1093/EMBOJ/CDF445.

Zhao, X. and Duester, G. (2009) 'Effect of retinoic acid signaling on Wnt/beta-catenin and FGF signaling during body axis extension.', *Gene expression patterns : GEP*. NIH Public Access, 9(6), pp. 430–5. doi: 10.1016/j.gep.2009.06.003.

Zuo, W. *et al.* (2016) 'Nicotine regulates activity of lateral habenula neurons via presynaptic and postsynaptic mechanisms.', *Scientific reports*. Nature Publishing Group, 6, p. 32937. doi: 10.1038/srep32937.